LA-11096-MS
(ISPO-281)

Rec'd w/LTR DTD
9309220161 930913

Safeguarding LWR Spent Fuel with the Fork Detector

102

UNITED STATES PROGRAM
FOR TECHNICAL ASSISTANCE TO IAEA SAFEGUARDS

POTAS

DEPARTMENT OF STATE
DEPARTMENT OF ENERGY
ARMS CONTROL AND DISARMAMENT AGENCY
NUCLEAR REGULATORY COMMISSION

Los Alamos

Los Alamos National Laboratory is operated by the University of California for the United States Department of Energy under contract W-7405-ENG-36.

9309220321 930913
PDR WASTE
WM-11 PDR

CONTENTS

ABSTRACT 1
I. INTRODUCTION 2
A. Overview 2
B. Importance of Spent Fuel Safeguards 2
1. Safeguards Goals 2
2. Safeguards Techniques and Diversion Strategies 3
C. The Fork Detector System 4
1. The Equipment 4
a. Purpose 4
b. Description 5
c. Characterization Studies 5
2. The Nature of the Data 5
a. Types of Data 5
b. Uncertainties and Scatter 6
(1) Counting Statistics 6
(2) Mispositioning 6
(3) Short-Lived Isotopes 7
(4) Errors in the ^{244}Cm Fraction . . . 7
(5) Gamma-Ray Interference with Neutron Counts 7
c. Reproducibility 8
(1) At One Facility 8
(a) Vermont Yankee 8
(b) Tihange 9
(c) General Electric-Morris Operations 10
(d) Loviisa 10
(2) Different Facilities 10
(3) Summary 11
3. Adjustments to the Data 11
4. Sensitivity to Missing Fuel 12
5. Sensitivity to Added Fuel 22
6. The Standard Assembly 23
D. Notation 25

II. SMALL-SCALE DIVERSION DETECTION 26
A. Assumptions 26
B. Data Imprecisions 33
1. Practical Sources of Uncertainties 33
2. Tolerance Limits 34
C. Diversion Concealment Strategies 36
1. Correctly Declared E and T 36
a. First Inspection. 36
b. Subsequent Inspections 41
2. Falsely Declared T 43

a. First Inspection 43
b. Subsequent Inspections 46
(1) Neutron Curve 46
(2) Gamma-Ray Curve 47
(3) Neutron-Gamma Curve 50
3. Falsely Declared E 51
a. Neutron-Exposure Equation 51
b. Gamma-Time Equation 52
(1) Decreased γ/E 52
(2) Increased γ/E 54
(3) Diversion Limitations 55
c. Neutron-Gamma Equation 55
d. Subsequent Inspections 56
4. Falsely Declared E and T 57
a. Decreased n 59
b. Increased γ/E 59
c. Decreased γ/E 61
d. Standard Assembly Examples 61
e. Subsequent Inspections 61
(1) Neutron Data 62
(2) Gamma-Ray Data 64
(3) Neutron-Gamma Equation 64
5. Summary of Problems for Diverters 64

III. CONCLUSIONS 67

APPENDIX A. "DIVFRAC.BAS" 70

APPENDIX B. UNCERTAINTIES OF PARAMETERS IN POWER-LAW RELATIONS 74

APPENDIX C. NEWTON-RAPHSON SOLUTION FOR A ROOT 77

REFERENCES 79

SAFEGUARDING LWR SPENT FUEL WITH THE FORK DETECTOR

by

P. M. Rinard and G. E. Bosler

ABSTRACT

The fork detector measures passive neutron and gamma-ray emissions from irradiated fuel assemblies for safeguards purposes. The detector is transportable, takes data rapidly, and requires only partial removal of the assemblies from the storage racks.

After describing the detector and the nature of the data taken with it, this report will concentrate on the sensitivity of the detector to missing fuel pins. The interactions between the analyses of the neutron and gamma-ray data place severe restrictions on potential diverters.

From the most recent exercises using calculated adjustments to the neutron data, neutron count rates are correlated with declared exposures with about a 10% scatter about the average. A diverter could thus remove a small number of pins from an assembly (about 5 from the 204 pins in a PWR assembly) with little chance of being detected. However, this would have to be repeated with 65 assemblies to reach a significant quantity of plutonium (or 1020 assemblies for a significant quantity of ^{235}U). This large effort would have to be performed in view of other applied safeguards (for example, surveillance cameras, underwater cameras, seals, and night-vision devices).

By falsifying the declared exposure and cooling time, a diverter might try to expand the size of the diversion per assembly. A carefully reduced exposure could be used to conceal a reduced neutron count rate, but this strongly affects the analysis of the gamma-ray data point. To control the new gamma-ray data point, the cooling time could be altered; however, cooling times must match known refueling dates and cannot be chosen at will. If the cooling time is falsified, a subsequent remeasurement will eventually reveal the diversion. Falsifying exposures and cooling times is quite complex because of the interactions between the neutron and gamma-ray data analyses.

The fork detector essentially forces a potential diverter into either foregoing a diversion or making a large diversion that could be readily detected. A diversion that would escape detection by the fork would require the removal of a few pins from a large number of assemblies, enhancing the detection probability by other safeguards techniques.

I. INTRODUCTION

A. Overview

The fork detector is one of several means to safeguard spent fuel assemblies. The detector measures passive neutron and gamma-ray emissions, is transportable, and takes measurements rapidly. In this report, we analyze the sensitivity of the detector to missing fuel while the diverter may be attempting to conceal the action with false declarations. Other safeguards techniques will be mentioned briefly where interactions with the fork detector could arise.

After reviewing the safeguards problem for spent fuel and the nature of the fork detector, this report will concentrate on the data analysis techniques and their effect on detecting diversions. Several techniques have been used somewhat individually in the past; an important purpose of this report is to demonstrate how the coordinated application of two or more of these analyses severely limit a diverter's options.

B. Importance of Spent Fuel Safeguards

1. Safeguards Goals. The objective of safeguards efforts by the International Atomic Energy Agency (IAEA) is the "timely detection of diversion of significant quantities of nuclear material from peaceful nuclear activities to the manufacture of nuclear weapons or of other nuclear explosive devices or for purposes unknown, and deterrence of such diversion by the risk of early detection."[1]

The materials of most concern with spent fuel are ^{235}U and ^{239}Pu. A significant quantity of plutonium is defined as a mass of at least 8 kg. The amount of ^{235}U that is significant depends on the enrichment; at least 25 kg of ^{235}U for more than 20% enrichment, and at least 75 kg of ^{235}U for less than 20% enrichment.[2,3]

Timeliness in detecting a diversion also varies with the isotope. For a pure compound of plutonium (such as PuO_2) or mixed oxide (MOX), the estimated minimum time required to convert the material to a finished metal is 1 month; for plutonium in an irradiated fuel assembly, the minimum time is 1 to 3 months. For uranium containing less than 20% ^{235}U, the minimum conversion time is about 1 year.[2-4]

Not many light-water reactor (LWR) assemblies are required to provide significant quantities of ^{235}U and plutonium. A pressurized-water reactor (PWR) assembly with a ^{235}U enrichment of 2.75% contains about 11 kg of ^{235}U initially; after an exposure of 30 gigawatt days per ton of uranium (GWd/tU), only about 3 kg of ^{235}U will remain, but 2 to 3 kg of ^{239}Pu will be present (among about 4 to 6 kg of plutonium).

2. Safeguards Techniques and Diversion Strategies. Many safeguards techniques can be applied to fuel at a reactor site.[2] Book auditing and item counting are common. Fresh fuel can be verified just before it is loaded in the core by measuring its enrichment and amount of fissile material. Seals can be applied to the reactor vessel and a power monitor placed near the core to verify the operating history of the reactor. Seals might also be applied to individual fuel assemblies. Cameras can record activities in storage areas. Night-vision viewing devices, underwater television cameras, and periscopes have been used at spent fuel ponds to remotely examine irradiated assemblies.[5] The fork detector measures radiations from assemblies stored under water; in this report, we analyze the data from this system.

Diversion possibilities listed in Ref. 2 consist of substituting whole dummy assemblies for real assemblies or possibly only removing some of the fuel pins from an assembly. Cumbersome shielding is expected to be necessary in any diversion of spent fuel. Very complex diversion strategies can be postulated that would pass virtually any inspection, but it is quite another matter to achieve them in practice. This report does not try to consider all possible diversion strategies; they are limited to the removal of whole pins after an irradiation cycle and substitution with dummy pins that are not radioactive.

An alternative strategy of adding fissile materials within assemblies for breeding purposes (for example, using PWR "control rod" clusters of uranium) is related but not discussed in detail here (see Sec. I.C.5).

It is a daunting task to successfully falsify the records, move assemblies (and their shielding) without detection by a surveillance system, remove fuel from highly radioactive assemblies, return the real or substitute assemblies to the storage pond without being observed, maintain the integrity of any seals, and finally have the assemblies produce the proper radiations to pass examinations by the night-vision device and fork detector.

The use of a completely nonradioactive dummy assembly is simple to detect with the fork detector, and it need not be considered further. The construction of a dummy assembly with the proper mixture of neutron and gamma-ray emissions requires sophistication and materials that may be beyond the capability or interest of a diverter.

The diversions considered here illuminate the sensitivities and capabilities of the fork detector. It is assumed that only a few of any one assembly's pins are removed and that a small fraction of the assemblies in a storage pond are modified to obtain a significant quantity of plutonium. For example, removing 15 PWR pins (out of 204 per assembly) from each of 30 assemblies (out of perhaps 1000 in a pond) could yield one significant quantity of plutonium. This will be referred to as a "small-scale" diversion.

Under these conditions, the parameters in the consistency equations introduced later are insignificantly affected by the diversions. Data from assemblies in the pond will generally seem normal, but data from the modified assemblies will appear out of bounds.

Only the effect of the fork detector on a diverter will be considered in detail here; further restrictions, for example, from surveillance devices, will only be mentioned casually where appropriate.

C. The Fork Detector System

1. The Equipment

a. Purpose. The fork detector system (consisting of the detector head and associated electronics) was developed in response to an IAEA request for a transportable detector that could quickly verify assemblies in a spent fuel pond. This detector and its variants have been used at many nuclear facilities around the world since 1982 by various national and international agencies.

The detector cannot measure directly the uranium and plutonium content of spent fuel assemblies. The neutron emissions are dominated by transuranic isotopes (most often curium isotopes), and fission product gamma rays make it impossible to see gamma rays from the fuel isotopes. Rather, the intent of the detector is to verify that the assemblies are legitimate spent fuel assemblies that have not been modified since their removal from the core.

b. Description. The detector head, called the fork, is a U-shaped piece of polyethylene with the arms containing fission chambers and ionization chambers. The fork is supported by a watertight pipe that travels vertically to the bridge spanning the pond; electrical cables run through the pipe connecting the detectors in the fork with the electronics on the bridge.

An electronics unit, the ION-1, was developed at Los Alamos for use with the fork detector head. A commercial version, called the GRAND-I, is now available from D. S. Davidson and Co. The GRAND-I provides the high voltages for the detector tubes, counts the neutron pulses, and measures the current through the ionization chambers. The user interface with the equipment is through a keypad and display on the ION-1. A computer or printer may be attached to either the ION-1 or GRAND-I for data logging or online data analysis.

More details on the detector are in Refs. 6 and 7.

c. Characterization Studies. Applications of the fork detector to actual assemblies have been described elsewhere.[5-14] Laboratory and calculational studies have also been conducted to aid understanding of the responses from the detector.[15-19]

2. The Nature of the Data

a. Types of Data. Data from a fork detector consist of neutron count rates and electric currents induced in ionization chambers by gamma rays. These radiation measurements are taken from opposite sides of the assemblies (either pair of opposite sides may be used[6,13]) and from one or more axial heights.

The fork contains two sets of fission chambers that differ only in that one is enveloped by cadmium-wrapped polyetheylene and the other is left "bare" inside the fork body; this configuration allows the inspector to estimate the boron content of the water (which can affect the measurement count rates) without recourse to an operator's declaration.[6,11] The neutron count rates used in the data analysis are generally from the cadmium-wrapped fission chambers because they are less affected by boron in the water. The bare fission chambers, however, give more uniform responses to distribution of neutron sources within an assembly,[18,19] so the choice of which fission chambers to use is not a simple one.

b. Uncertainties and Scatter

(1) Counting Statistics. Well-understood uncertainties are introduced in the data through counting statistics in the neutron pulses and time-dependent fluctuations in the ionization chamber currents. An LWR assembly with more than 20 GWd/tU exposure is a strong emitter of neutrons,[15] and counting statistics uncertainties can easily be reduced to less than 1% by counting for less than 1 min. Exposures of only 10 GWd/tU might require 8 min to reach the same precision; at such low exposures, the plutonium production is also low,[15] and 1% precision in the count rate (and the time required to get it) may not be warranted. After 30 GWd/tU exposure, the 1% precision can be obtained in about 10 s.

(2) Mispositioning. Variations in the data are introduced through axial or transverse mispositioning of the fork about the assemblies, although these variations are quite small.

If an axial scan along the length of an assembly is not done, the typical measurement position is near the midpoint of the assembly. Axial positioning has been done quite accurately with gauges on operators' fuel-handling devices or with marks specially placed on the devices.[6] Radiation readings from a PWR assembly vary slowly along the middle three-fourths of its length,[13,14] so even an implausibly large mispositioning has inconsequential effects. Radiation profiles for boiling-water reactor (BWR) assemblies are less uniform and can even have minima at the center position.[6,14] One-position measurements with BWR assemblies could introduce large errors into the data analysis, and generally multiposition measurements should be used (as was done in Ref. 6).

A fork fits closely about an assembly; different size forks are used for BWR and PWR assemblies and polyethylene sleeves can be placed around the fork tines to tighten the fit even further.[6] Some gap must exist between the fork and the assembly, of course, and this is the largest possible transverse positioning variation. It is only 1 to 3 cm, however, and the assembly can be placed anywhere within the fork with only small or no effect on the data.[6,7,11] One exception, with a 3-cm gap and the bare fission chambers, produced a 10% variation.[11]

A large error can arise, however, if the back of the fork is not held in contact with the assembly. At a BWR facility, a 5-cm gap lowered the neutron

count rate by about 7% and the gamma-ray reading by about 5%. A 10-cm gap reduced both the neutron count rate and the gamma-ray reading by about 13%. It is simple to maintain the contact, and even cursory attention to the data should alert the inspector to the drift.

In general, mispositioning of the fork is not a major source of variations in the data. If BWR assemblies are being examined, however, it may be necessary to take data at several (five or more) axial positions and calculate integrated values to avoid serious errors arising from the different possible profile shapes.

(3) Short-Lived Isotopes. Other variations arise from the presence of short-lived isotopes in assemblies, particularly gamma-emitting isotopes. Initial enrichment and ^{242}Cm production complicate the interpretation of neutron count rates in reasonably understood ways, and adjustments for them are being developed.[8,20,21] However, scatter in gamma-ray data during the first few months of cooling have yet to be explained adequately.

(4) Errors in the ^{244}Cm Fraction. The fraction of the neutron count rate from ^{244}Cm can be calculated[8,20,21] and used to adjust the neutron count rates. The calculation itself introduces some uncertainty but gives an overall improvement in the data.

(5) Gamma-Ray Interference with Neutron Counts. The original preamplifier used with the fork detector has been found to poorly distinguish fission chamber pulses caused by gamma rays from pulses caused by neutrons.[22] Fortunately, the gamma-ray intensity must be about that from the center of a spent fuel assembly with a short cooling time, so nearly all of the data taken with this preamplifier should be valid. Nevertheless, some of the scatter in some neutron data might result from this interference.

The interference has been essentially eliminated by use of a newer preamplifier.[22] The gamma-ray pulses are lowered into the voltage region where pulses from the uranium alpha particles are found and away from the high-voltage pulses caused by neutrons.

c. Reproducibility

(1) At One Facility. With the same detector used at the same facility, data taken at different times should be commensurate (accounting for the effects of cooling time). Such data are available from three facilities.

(a) Vermont Yankee. At the Vermont Yankee Power Station, data were taken in April and June 1982. In April, fourteen 8-by-8 BWR assemblies were measured (ignoring for now two assemblies that had been reconstituted and were missing pins); the gamma-ray data are not useful because of equipment problems. In June, 33 assemblies were measured.

Table I compares the neutron count rates for assemblies measured on both dates; the small correction for the difference in cooling time has been made (assuming that all the neutrons were emitted by ^{244}Cm). The average ratio of June-to-April data (and its standard deviation) is 1.060 ± 0.098, which is consistent with exactly one.

The usual consistency analysis of neutron data assumes that $n = \alpha E^{\beta}$, where n is the neutron count rate (corrected for the cooling of ^{244}Cm) and E is the declared exposure. From least-square fits of all the April and June data, the values of α are 0.00198 and 0.00184, respectively; the values of β are 3.73 and 3.76, respectively.

In general, these data taken 2 months apart are essentially identical.

TABLE I

NEUTRON COUNT RATES AT VERMONT YANKEE

Assembly	Neutron Count Rates April 1982	Neutron Count Rates June 1982	Ratio June/April
VT215	8.9	11.0	1.236
VT161	10.7	11.4	1.065
GED003	81.8	79.3	0.969
LJ7140	458.0	502.0	1.096
LJ3991	65.7	65.5	0.997
LJ3949	88.1	87.9	0.998

(b) Tihange. During a joint exercise at Tihange, data were taken by EURATOM personnel using their own fork detector and by IAEA personnel using another fork and electronics unit. The assemblies were of the 15-by-15 PWR type. References 8 and 9 present all the data and their analyses. Neutron count rates were taken for 20 assemblies; gamma-ray readings were measured for 19 of the same assemblies (the assembly left out had a cooling time of only 36 days and produced ionization chamber currents that gave off-scale ION-1 gamma-ray readings; the extended range of the GRAND-I should not have this problem).

During the 3-day measurement campaign, an assembly was measured 22 times with the IAEA detector and 13 times with the EURATOM detector. The relative standard deviation of the neutron count rates was about 1.2% for the two fork detectors; the relative standard deviation for the gamma-ray rates were 0.81% and 0.90%. Both detector systems were judged very stable.

From the data in Table 3 of Ref. 8, the average ratio of the two sets of neutron count rates (IAEA/EURATOM) is 0.910 ± 0.068. These data were taken with two completely separate fork detectors and electronic units. The lower IAEA values could result from fission chambers that are a little less efficient or from a slightly higher lower-level discriminator setting in their ION-1. Nevertheless, the two sets of neutron count rates are quite similar.

The same ratio for the gamma-ray data is 0.929 ± 0.028 with the IAEA data again being a little lower than the EURATOM data. The IAEA's ionization chambers could have been less efficient than those of EURATOM's fork.

Although matching the fission chambers and ionization chambers that go into a single fork has always been attempted, matching the chambers among different forks has not been possible. This alone could account for the differences.

The parameters in the power-law relation $n = \alpha E^{\beta}$ were computed for the two sets of data and are given in Table 7a of Ref. 9 for the 20 assemblies (using megawatt days per ton of uranium). The values of α were 5.86×10^{-13} and 4.51×10^{-13}; the β's were 3.30 and 3.32.

The gamma-ray data were fitted to a similar power law: $\gamma/E = aT^{-b}$, where γ is the gamma-ray reading, E is the declared exposure (gigawatt days per ton of uranium), and T is the declared cooling time (days). Table 18 of Ref. 15 shows the IAEA and EURATOM parameter values. The values of a were 9.44×10^3 and 9.81×10^3; the values of b were 0.869 and 0.883.

The exercise at Tihange was a fine opportunity to compare two fork detectors on the same assemblies on the same day. These two detectors gave very much the same results. Small differences were probably due to not matching the fission and ionization chambers between the two forks. A detector efficiency correction should be applied to data from different forks.

Of particular note with the Tihange data are the beneficial effects of corrections for the irradiation histories. Calculations estimated the fractions of the neutron count rates that were due to ^{244}Cm (with the rest from ^{242}Cm and plutonium isotopes) and normalization factors for different initial enrichments. Later we will present some plots of data, including Fig. 12(b), which show how these corrections brought the data in Fig. 12(a) more in agreement with the power-law relation. The importance of making these corrections will be emphasized in Sec. II.

(c) General Electric-Morris Operations. A fork was used at the General Electric-Morris Operations for 1 year to measure BWR 7-by-7 assemblies. The fork spent the total time under water without a problem; the ION-1 electronics unit underwent a modification during a break in the measurements and necessitated a normalization correction to the later data. The work is reported in Ref. 6.

Assembly CZ331 was selected as a reference assembly because it had the longest cooling time and was measured eight times over 8 months. The data from CZ331 show a gradual cooling, as expected, but otherwise are quite consistent over these 8 months. The cooling effects are larger for the other assemblies, but even without a quantitative correction for cooling, the excellent neutron and gamma-ray data reproducibility is evident over the 8-month time span (Tables II and IV of Ref. 6).

(d) Loviisa. A Los Alamos fork was used on Soviet (WWER) fuel at the Loviisa Nuclear Power Station in Finland[21] in conjunction with the IAEA. An assembly was measured repeatedly on different days by different IAEA inspectors; the variations in the neutron data were about 2%, whereas the variations were 3% to 4% for the gamma-ray data.

(2) Different Facilities. Comparing fork data among different facilities has not been simple for at least three reasons. The detector design was

under development until about 1982 and minor changes were still made for another year or so. Spent fuel ponds for PWR facilities contain boron in the water, and the concentration affects the neutron count rates; corrections are not routinely made to the fork data for boron (an exception is in Ref. 10), although the effects of boron have been investigated.[11] Furthermore, the relative efficiencies of the fission and ionization chambers placed in different forks have not always been determined.

Given all these problems, it is not surprising to find a wide range of ß's, for example. Most of the reported ß's are between 3 and 4, but the full range has been from 2 to 5.4. Most of the values of b in the gamma-ray cooling expression have been between 0.8 and 0.9, but the full range is from 0.49 to 1.04.

(3) Summary. The work at Tihange showed that two similar detectors give comparable results. The data from Vermont Yankee and General Electric-Morris Operations demonstrated reproducibility with one fork over time.

An obvious need exists for a procedure to compare the efficiencies of different forks and to correct for boron concentrations. When these two fairly simple corrections are routinely applied, it will be practical to compare data among different facilities, to reliably use absolute count rates, and to establish calibration curves that apply to any fork detector and facility.

3. Adjustments to the Data. Backgrounds are, of course, subtracted from the neutron count rates and the gamma-ray readings, although, in practice, they have been insignificant in almost all cases. An assembly to be measured is pulled from its storage rack only far enough to put the measurement point about 50 cm above the neighboring assemblies; this is sufficient to shield the fork from radiations produced by neighboring assemblies. In this report, measured values include background subtraction.

No adjustments beyond background subtraction are currently made to the gamma-ray readings, although they are needed at cooling times less than 1 year, as mentioned in Sec. I.C.2.b.4.

Several additional adjustments are performed on the measured neutron count rates. When the exposure is greater than 12 GWd/tU and the cooling time

is greater than 2 years, nearly all the neutrons originate from the spontaneous fissioning of ^{244}Cm. By multiplying by $e^{\lambda T}$, where λ is the decay constant of ^{244}Cm and T is the cooling time, the neutron count rate is adjusted to the time of discharge. Although this simple adjustment can be fairly effective, it is now becoming practical to first multiply the count rate by the calculated ^{244}Cm fraction of the neutron source strength,[8,12,20,21] written as f(E,T) (as mentioned in Sec. I.C.2.c.1.b), where E is the exposure and T is again the cooling time. This is an especially important adjustment for short cooling times when the ^{242}Cm isotope is present in very important amounts. This fraction also depends on the initial enrichment but will not be so indicated in this report where the only application will be to assemblies of one enrichment. It is necessary to know the power history of the reactor to calculate f(E,T), but the results have been well worth the effort (especially for the case of Ref. 12 where initial enrichments were very different).

The neutron count rate n used in the data analysis is thus related to the measured count rate n_m by $n = n_m\, f(E,T)\, e^{\lambda T}$.

A third adjustment is expected in the future that will account for differing concentrations of boron in the water of storage ponds. The concentration can be estimated with the fission chambers in the fork.[6,11]

4. Sensitivity to Missing Fuel. If a fraction of an assembly is removed and replaced with nonradioactive material (or not replaced at all), what is the effect on the neutron and gamma-ray measurements with the fork detector? The answer is complex and depends on the characteristics of the specific assembly, the distribution within the assembly of the material removed, the boron concentration in the water, and the characteristics of the fork head itself.

So far there has not been an opportunity to take measurements on an irradiated assembly before and after some pins were removed. Three BWR assemblies at Vermont Yankee had already been reconstituted and were left with two or three pins missing. However, the nature of the reconstitution is unknown and thus how much of the reduced count rates is due to the missing pins is also unclear.

The best that can be done at the moment is to use the information in Refs. 11 and 17. Both of those studies dealt with a 15-by-15 PWR assembly with 204 pins (and 21 water-filled guide tubes). The geometry is shown in Fig. 1, along with row and column assignments relative to a fork. The neutron

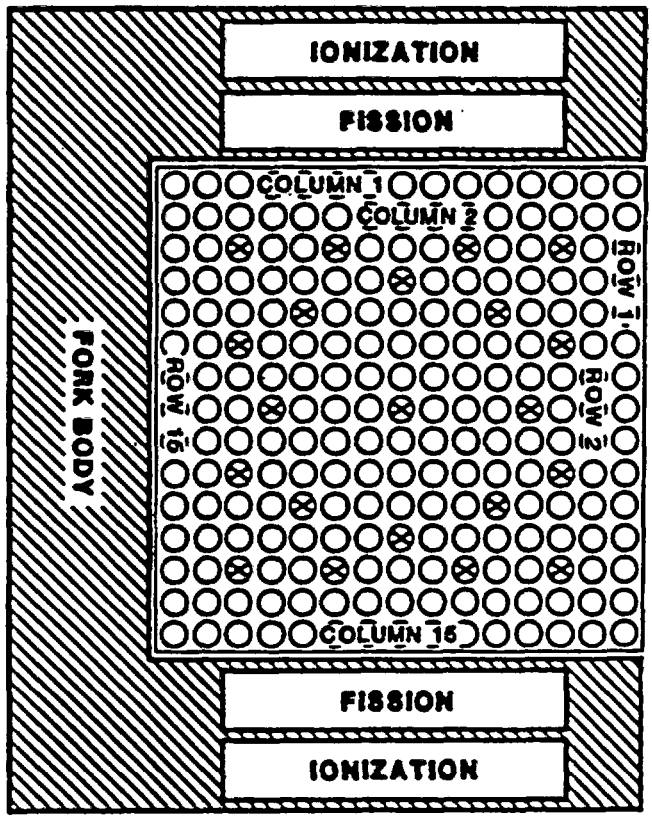

Fig. 1. A 15-by-15 PWR assembly (8.5 in. on a side) is shown within the tines of a fork; the view is from the top. The general locations of the fission and ionization chambers are indicated; they both had active lengths of 6 in. The definition of rows and columns used in the text is shown. Water channels have a large "X" in them; the row and column labels do not obscure any water channels.

measurements in Ref. 11 were made on a fresh fuel assembly, so the multiplication was higher than for a spent fuel assembly. A ^{252}Cf source was moved from one pin position to another. The gamma-ray calculations in Ref. 17 were made with the assumption that a long air-filled collimator tube was between the assembly and the detector, unlike the ionization chambers separated from the assembly by water and polyethylene. Neither of these studies is ideal for the case at hand, but they are the best available. A hexagonal WWER fresh fuel assembly has been similarly studied[18,19] to determine the contributions of individual pins to the neutron and gamma-ray data; the conclusions were much the same as those below for a PWR assembly.

The data in Ref. 11 can be used to correlate the change in neutron count rate with the change in mass of an assembly. The count rate from each pin was measured for cadmium-wrapped and bare fission chambers at different boron concentrations. In this report, only the cadmium-wrapped detectors with boron concentrations of 0 and 2000 ppm will be considered (Tables I and IX of Ref. 11). It is assumed that the irradiation throughout a cross section of the assembly is uniform, so no weighting factors need be applied to the data from Ref. 11. Under these conditions, the amount of uranium and plutonium

removed is proportional to the number of pins removed; the change in neutron count rate is simply the sum of the rates in the tables of Ref. 11 for the pins removed. Removing pins from a spent fuel assembly would affect the multiplication, reducing the count rate a little more than expected from the fraction of the mass taken away. The multiplication of this fresh fuel assembly is constant because the count rates in Ref. 11 were taken when all pins were present.

Applying the results of Ref. 17 is much harder. Contributions from whole rows of pins are presented in Tables II and III of Ref. 17 for seven different gamma-ray energies. The 661-keV gamma ray from ^{137}Cs dominates the spent fuel emissions in most cases,[23] so only that energy was used here. The weighting factors assigned to pins for use here are shown in Table II of this report. The values for rows 1, 2, 14, and 15 were reduced to simulate end effects with the ionization chambers.

TABLE II

GAMMA-RAY WEIGHTING FACTORS

Columns	Rows	Weight
1 and 15	1,2,14,15	0.316
	3-13	0.633
2 and 14	1,2,14,15	0.116
	3-13	0.233
3 and 13	1,2,14,15	0.043
	3-13	0.086
4 and 12	1,2,14,15	0.015
	3-13	0.031
5 and 11	1,2,14,15	0.009
	3-13	0.018
6 and 10	1,2,14,15	0.003
	3-13	0.005
7-9	1-15	0.000

With all this information it is easy to calculate approximate effects of removing pins from the assembly. The reader may prefer to make other assumptions or assign different weighting to the pins, so the computer code used is given in Appendix A. It is written in a fairly generic BASIC. The data in the code can be modified to reflect other opinions on the importance of individual pins.

The code as given was used to compare count rates before and after pins are removed. The results for a variety of removal schemes are shown in Figs. 2-10.

The fractional drop in neutron count rate is fairly close to the fractional drop in mass (or equivalently, the number of pins), regardless of where the mass is removed from within the assembly. In other words, the count rate is approximately proportional to the mass of the assembly. (This relation also was found for a WWER assembly.[18,19]) This will be a convenient correlation to use throughout this report.

The short range of the gamma rays, however, does not allow such a simple correspondence between mass and gamma-ray response. Material removed from the center of the assembly does not change the response, whereas the same amount removed from an edge near the fork has a large effect.

The neutron count rate shows the amount of material removed and the gamma-ray response indicates the general location of the diversion within the assembly. An assembly whose neutron count rate is suspiciously low could be rotated 90° within the fork to give two "views" of the gamma-ray emissions to better estimate where the diversion occurred.

One aspect of the sensitivity to missing pins is the reproducibility of data from a given assembly, which indicates the precision of the detector. Data are reproducible to within about 1% (which corresponds to 2 or 3 pins of a 204-pin PWR assembly). Because this is such a low figure, it is not the limiting factor in the sensitivity. Scatter in the data beyond the fork's precision is due to errors in the declared exposure, effects of different core locations, and (for gamma rays) short-lived isotopes.

In Sec. II tolerance intervals will be used extensively to allow for scatter about average values. Current data analysis makes it seem likely that tolerance intervals that are 5% of the averages are reasonable. In that case, the sensitivity to missing pins can be estimated.

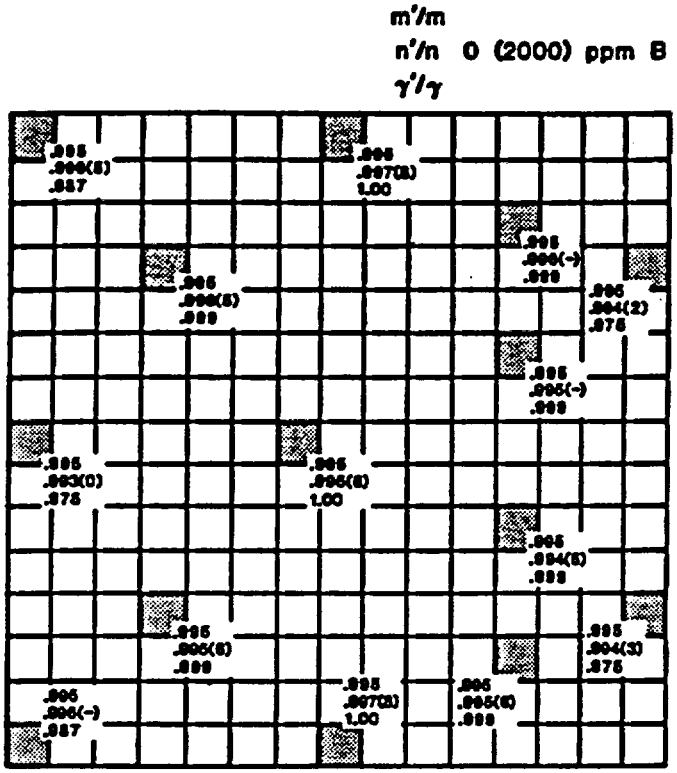

Fig. 2. The effect of removing one single pin or another on the assembly's mass (m), neutron count rate (n), and gamma-ray reading (γ) is indicated at several locations. The assembly and its orientation is the same as in Fig. 1. The three lines of numbers near a pin location show the ratios m'/m, n'/n, and γ'/γ (in that order) after the removal of that single pin. The n'/n number is for no boron in the water. The number in parenthesis after n'/n shows how the last digit of n'/n should be written when the boron concentration is 2000 ppm. For example, when the pin in row 1, column 1 (the upper left-hand corner) is removed, the value of n'/n with no boron present is 0.996; with 2000 ppm boron, the new value of n'/n is 0.995. When a dash is inside the parenthesis, the two ratios are the same at both boron concentrations. Because of the left-right symmetry about the center column, each result also applies to a second location also (for example, location row 12, column 4 and location row 12, column 12 are mirror images).

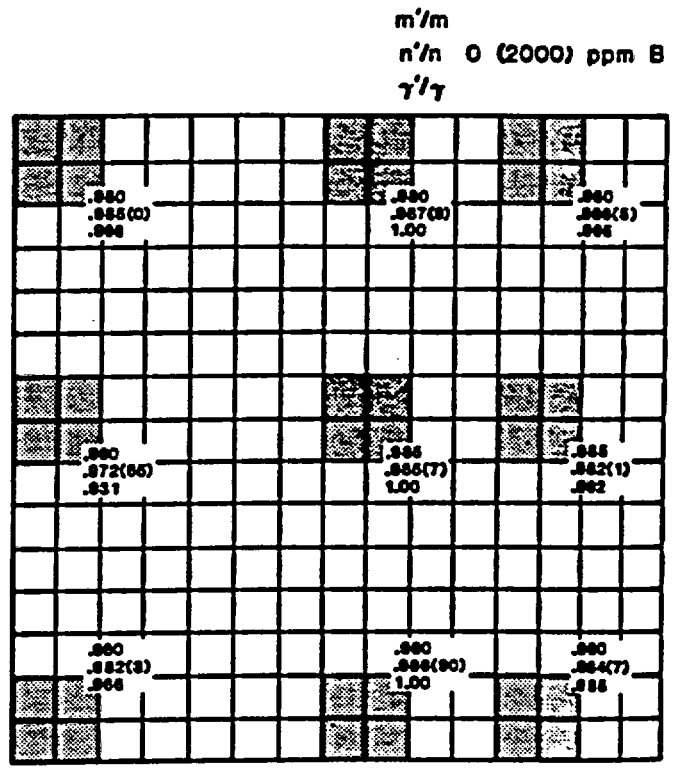

Fig. 3. The effect of removing a square of four pins (or three pins around a guide tube) is indicated at several locations. The values of m'/m, n'/n (at 0 and 2000 ppm boron), and γ'/γ are shown near each location of a set of missing pins, as explained in the caption to Fig. 2. When two digits are inside parenthesis, they replace the last two digits of n'/n for the 2000 ppm boron case. Because of the left-right symmetry about the center column, each result also applies to a second location.

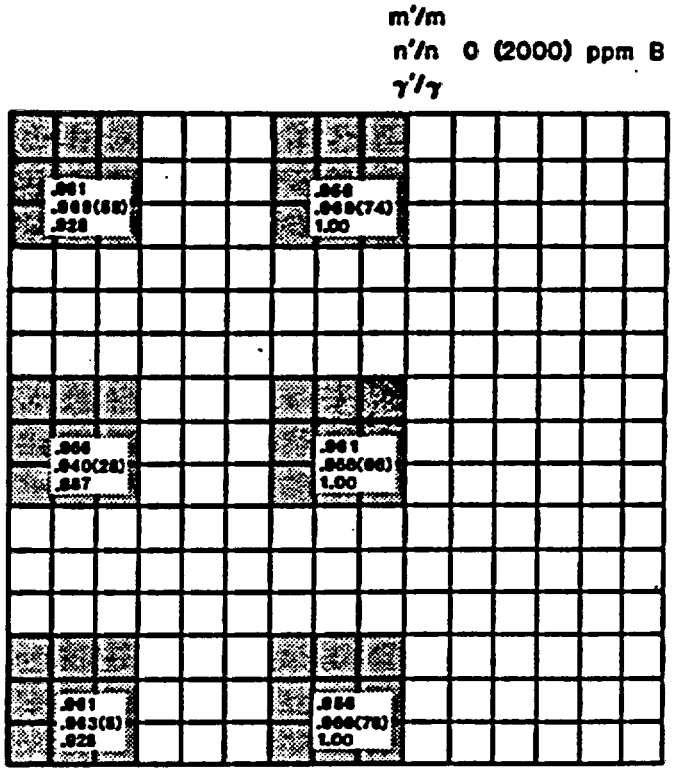

Fig. 4. The effect of removing a square of 9 pins (or 8 pins around a guide tube) is indicated at several locations. The values of m'/m, n'/n (at 0 and 2000 ppm boron), and γ'/γ are shown inside each location of a set of missing pins, as explained in the captions to Figs. 2 and 3. Because of the left-right symmetry about the center column, each result also applies to a second location.

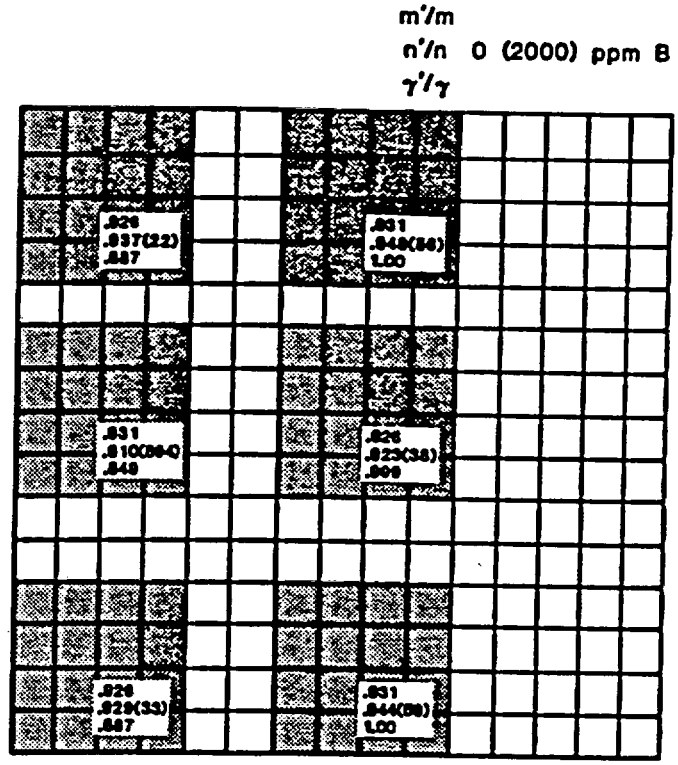

Fig. 5. The effect of removing a square of 16 pins (or 15 pins around a guide tube) is indicated at several locations. The values of m'/m, n'/n (at 0 and 2000 ppm boron), and γ'/γ are shown inside the location of each set of missing pins, as explained in the captions to Figs. 2 and 3. Because of the left-right symmetry about the center column, each result also applies to a second location.

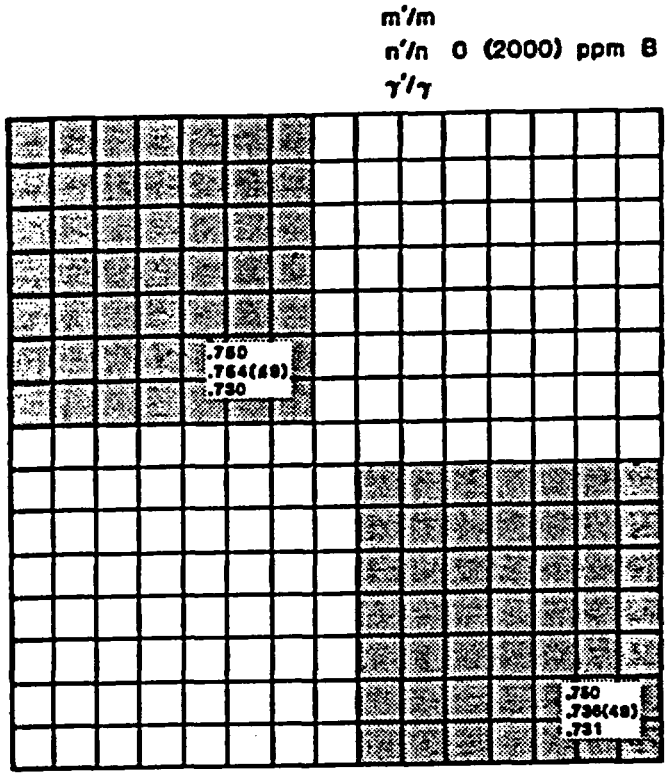

6(a)

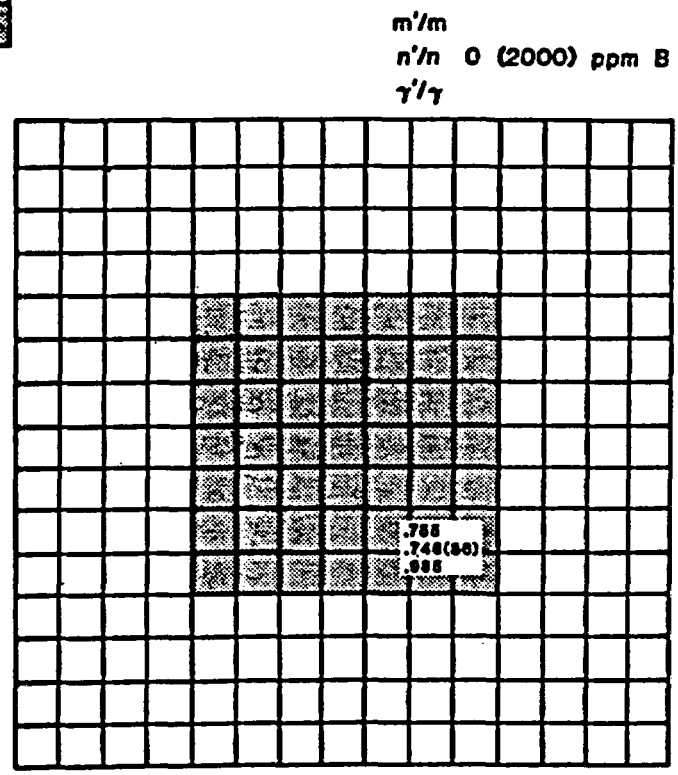

6(b)

Fig. 6. The effect of removing pins from a square of 7 pins on a side is indicated at three locations. The values of m'/m, n'/n (at 0 and 2000 ppm boron), and γ'/γ are shown inside the location of each set of missing pins, as explained in the captions to Figs. 2 and 3. Because of the left-right symmetry about the center column, each result also applies to a second location.

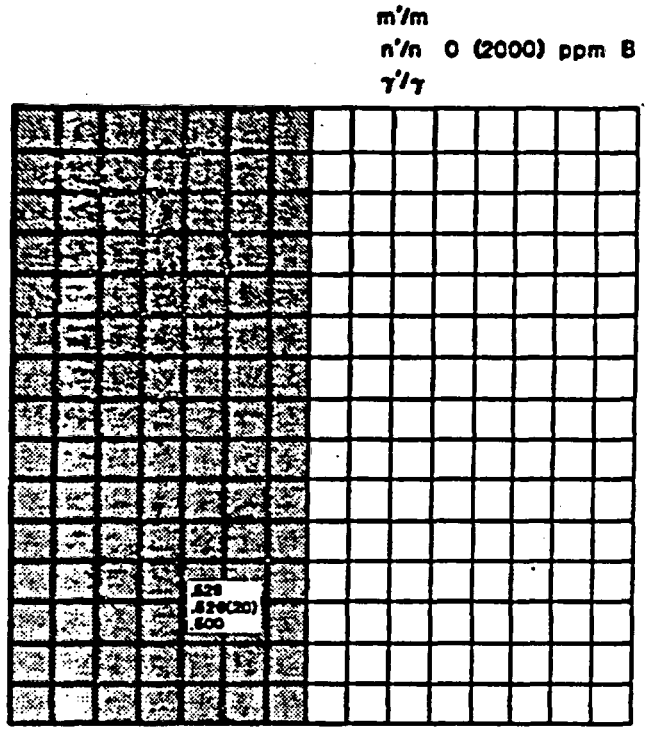

7(a)

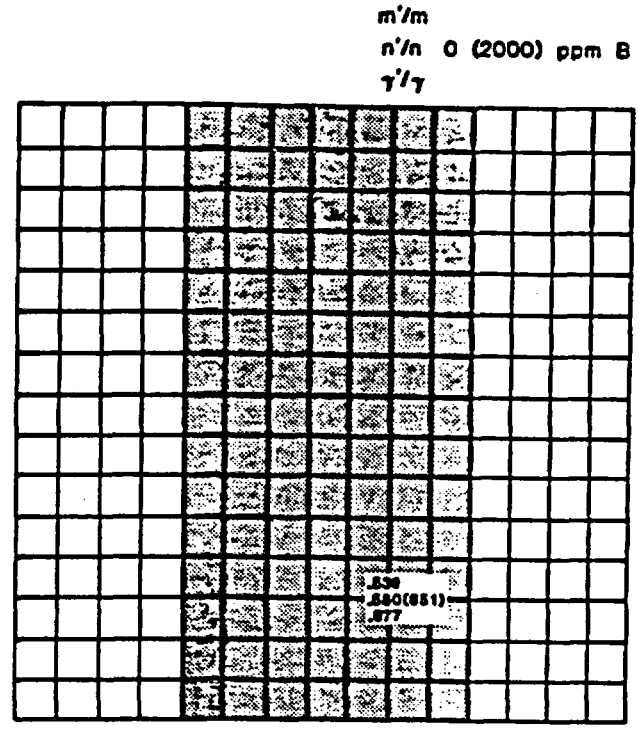

7(b)

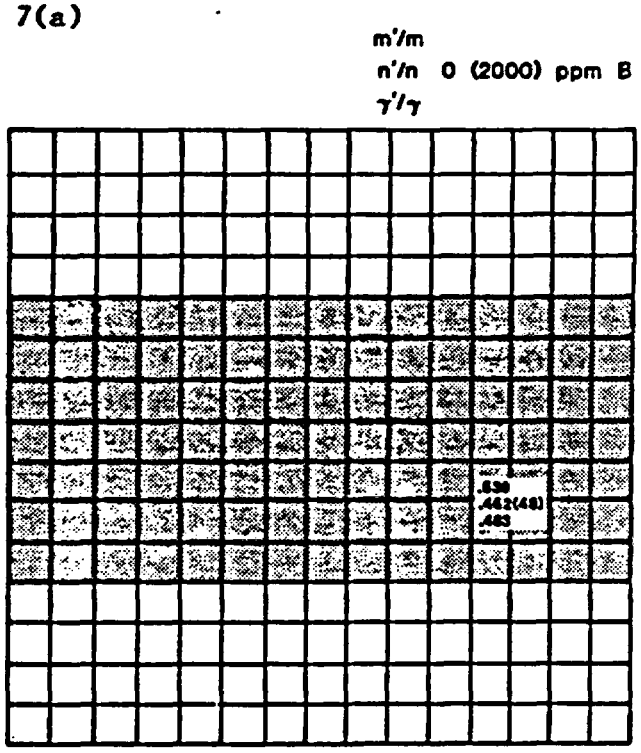

7(c)

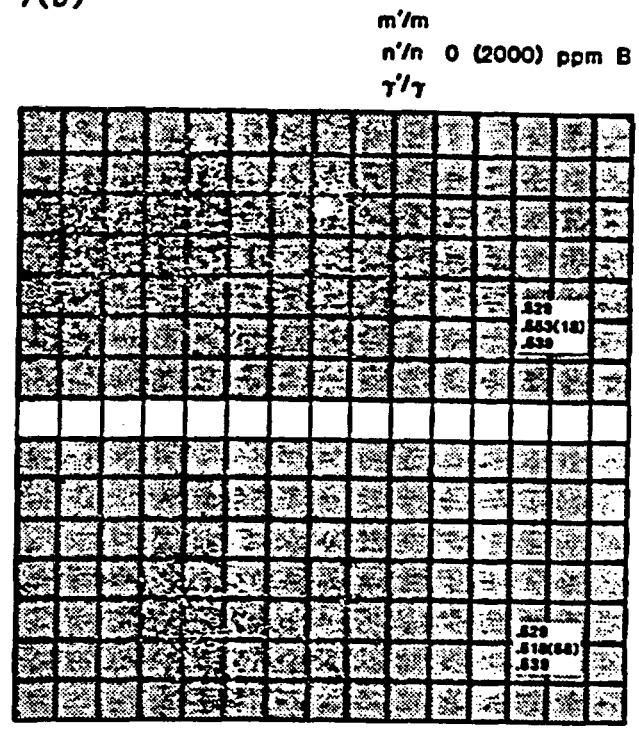

7(d)

Fig. 7. The effect of removing pins from a rectangle of 7 by 15 pins is indicated at five locations. The values of m'/m, n'/n (at 0 and 2000 ppm boron), and γ'/γ are shown inside each of the sets of missings pins, as explained in the captions to Figs. 2 and 3. Because of the left-right symmetry about the center column, each result also applies to a second location.

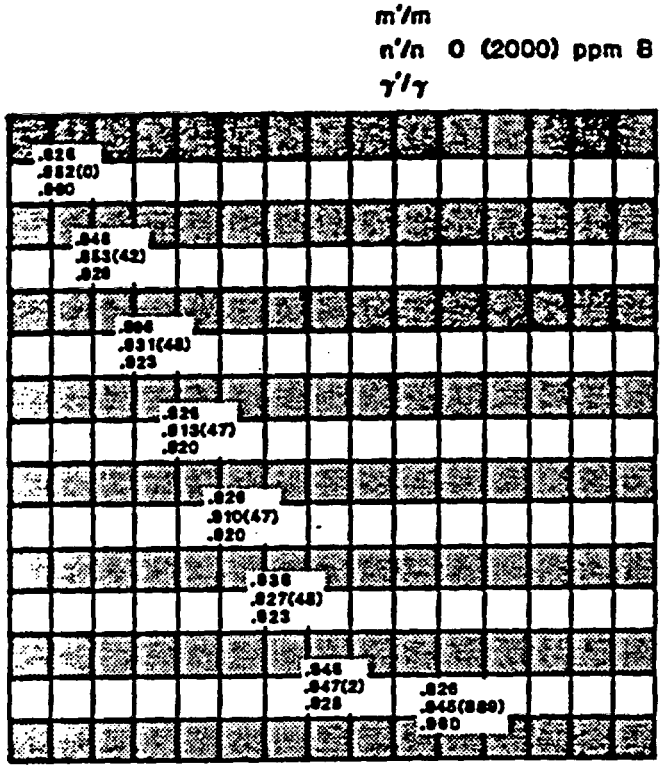

8(a)

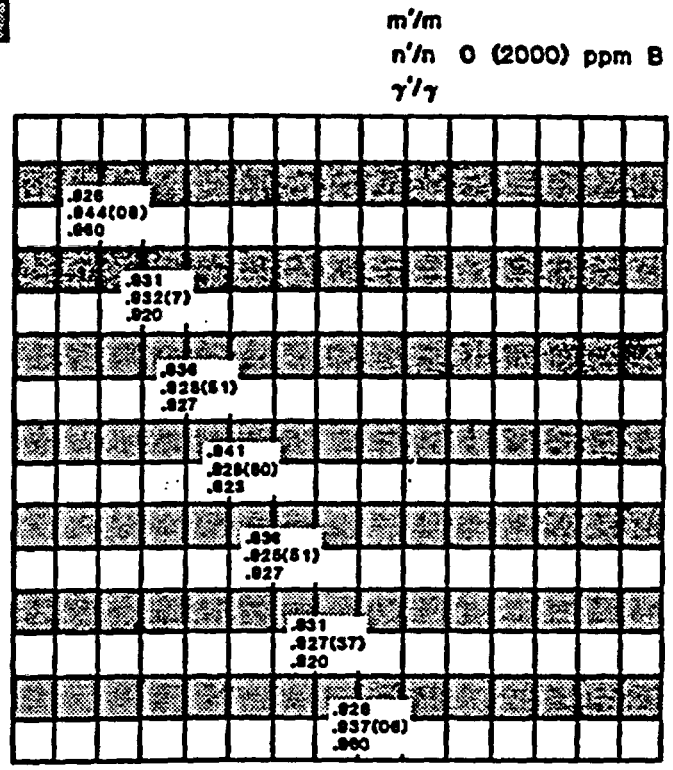

8(b)

Fig. 8. The effect of removing pins from a whole row is indicated for each row. The values of m'/m, n'/n (at 0 and 2000 ppm boron), and γ'/γ are shown near the location of each row of missing pins, as explained in the captions to Figs. 2 and 3.

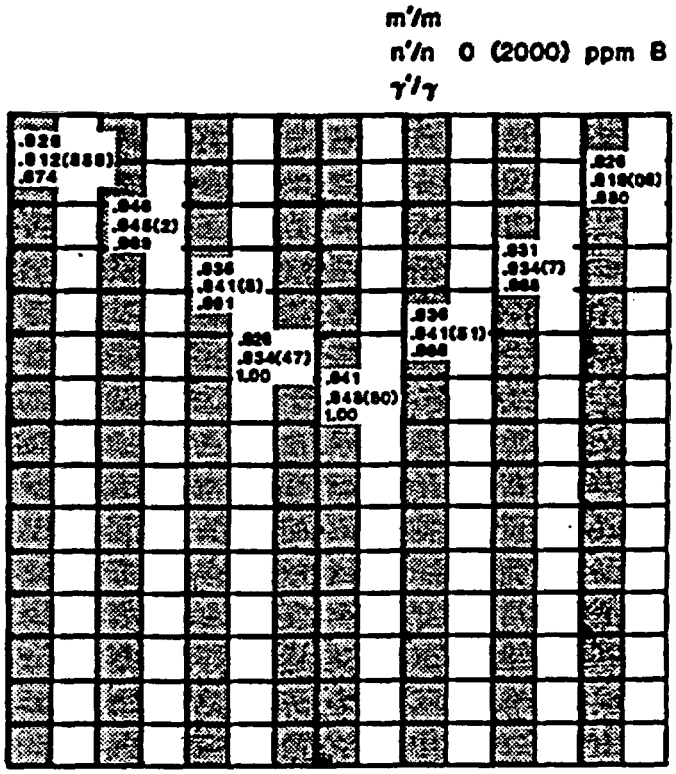

Fig. 9. The effect of removing pins from a whole column is indicated for each column. The values of m'/m, n'/n (at 0 and 2000 ppm boron), and γ'/γ are shown inside the location of each column of missing pins, as explained in the captions to Figs. 2 and 3. Because of the left-right symmetry about the center column, each result also applies to a second location.

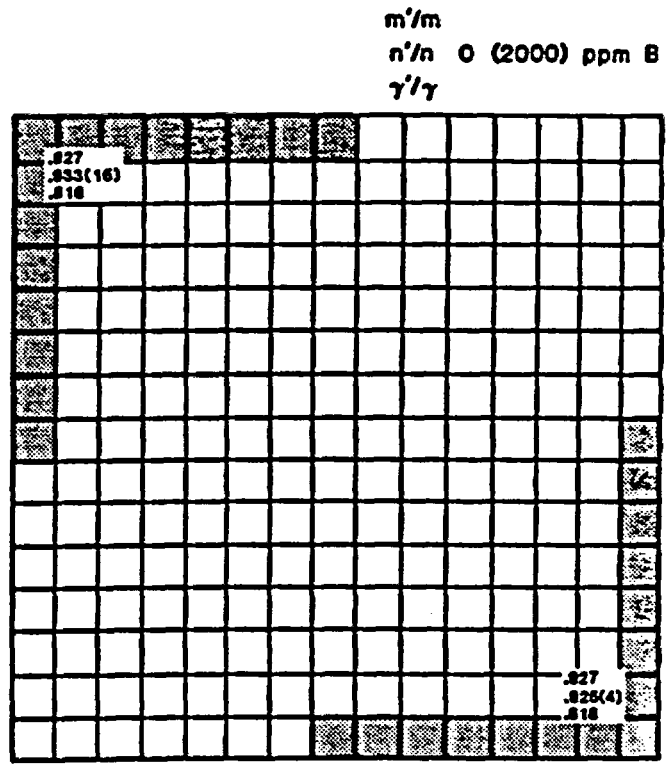

Fig. 10. The effect of removing a corner array of 15 pins is indicated. The values of m'/m, n'/n (at 0 and 2000 ppm boron), and γ'/γ are shown near the location of each set of missing pins, as explained in the captions to Figs. 2 and 3. Because of the left-right symmetry about the center column, each result also applies to a second location.

If data points are distributed uniformly throughout the tolerance limit and a diverter selects randomly from them, the diverter's goal is to avoid moving the data points outside the tolerance interval. Consider the case of neutron data. If it were known that an undiverted data point would be near the upper tolerance limit, 10% of an assembly could be removed and the new data point would be on the lower tolerance limit.

However, it will not be known in advance where an undiverted data point will fall, so diversions must be much smaller. A 1% diversion (2 or 3 pins out of 204 pins in a PWR assembly) still has a 10% chance of leading to a new data point below the lower limit. To obtain a significant quantity requires removal of 2 or 3 pins from about 130 assemblies, so about 13 of these new data points might lie outside the tolerance interval.

The IAEA has indicated a sensitivity goal of detecting a 50% diversion at the 4σ measurement level; presumably this means a 99.99% probability of detecting such a diversion. The diversion of half the pins from an assembly will produce approximately half the neutron count rate (the reduced multiplication within the assembly will probably make the count rate even less than half the rate from the full assembly); the precise effect on the gamma-ray data depends on the geometrical pattern of removal. During some measurement exercises, large deviations from the curve fitted to the neutron data were readily attributed to differences in initial enrichments or power histories. With the ability to correct for these effects, such outliers should no longer arise. Data points that are about half the values expected from the fitted curve will be far outside a 99.99% confidence curve that contains that percentage of the data points from complete assemblies.

The detection of an assembly with half the pins missing also depends on the declared exposure and cooling time. If the declared values are not falsified, the inspection will detect such a large diversion. It will be seen in Sec. II that the diverter of half an assembly will be severely challenged to find false values that will withstand scrutiny.

5. Sensitivity to Added Fuel. Instead of removing fuel from an irradiated assembly, someone may add breeding material to a normal assembly and later remove it for processing. The material could be introduced into the guide tubes of PWR assemblies, for example, in place of the normal control rods.

With the additional fuel still in the assembly, a fork detector should produce an enhanced neutron count rate for the declared exposure and cooling time. To the first approximation, an extra rod can be assumed to increase the count rate by the same amount a missing rod diminishes the count rate; better approximations would include effects on the multiplication, although they may be small.

The presence of fuel inside control rods for the guide tubes could be detected with a neutron coincidence collar[24-30] just before a fresh fuel assembly is loaded into a core. The loading would have to be witnessed to ensure that the control rod cluster was not changed after the measurement.

No measurements have been made on assemblies with extra fuel, and this report will concentrate on the case of missing fuel. The arguments presented can be adapted to the case of added fuel.

6. The Standard Assembly. To allow some numerical examples to be given throughout this report, a standard assembly is defined to be a 15-by-15 PWR assembly (as in Fig. 1) with an initial ^{235}U enrichment of 3% and a UO_2 density of 10.2 g/cm^3.

The assembly is assumed to have received an exposure of 30 GWd/tU after experiencing a power level of 276.75 W/cm^2 for three consecutive reactor cycles; each cycle consists of 335 days at full power followed by 30 days of shutdown. The cooling time will often be taken as 800 days after the start of the third shutdown.

It is further assumed that after the 30 GWd/tU irradiation, the assembly contains 3 kg of ^{235}U and 5 kg of plutonium, as mentioned in Sec. I.A.1. It would thus take all the ^{235}U from 25 such assemblies to reach the significant quantity of 75 kg, but it would take only two assemblies to exceed the significant quantity of 8 kg of plutonium.

Under these conditions, we used a CINDER code[31-34] adapted for a personal computer to calculate the fraction of the source neutrons within the assembly that is due to ^{244}Cm spontaneous fissions to be 0.9465; this fraction will be written f(E,T) in general and as f(30,800) = 0.9465 in particular. An earlier code called BUNECO, written for a small computer, apparently overestimates the ^{244}Cm fraction when the exposure and cooling time are small.[20] This CINDER code was written for a larger personal computer and may be more accurate.

When false declarations are made about the exposure and cooling time, the ^{244}Cm neutron fraction f(E',T') must be redetermined with the declared parameters (the primes indicate falsely declared values). Even though such a fraction would be incorrect, it is the value that would be used by an inspector.

For the limited purposes of this report, an analytical expression for f(E,T) has been devised from many calculations to allow flexibility. This expression assumes that a diverter would not risk declaring a false exposure more than 25% below the actual value and that a declared false cooling time would be between 400 and 1500 days (flanking the 800-day cooling time). The expression is

$$f(E,T) = A(E)\ T^2 + B(E)\ T + C(E) \quad , \tag{1}$$

where

$$A(E) = 0.000000026588\ E - 0.0000012315 \quad , \tag{2}$$

$$B(E) = -0.00006113\ E + 0.0026950 \quad , \text{ and} \tag{3}$$

$$C(E) = -0.0011333\ E^2 + .099569\ E - 1.4332 \quad . \tag{4}$$

As stated above,

$$22 < E < 30 \text{ GWd/tU, and } 400 < T < 1500 \text{ days} \quad .$$

Equations (1)-(4) should <u>only</u> be applied to the standard assembly described in this section. They do not have general validity for all assemblies.

Figure 11 is a plot of Eq. (1). It is generally a slowly changing function and reproduces the values calculated with the CINDER code to within 1%.

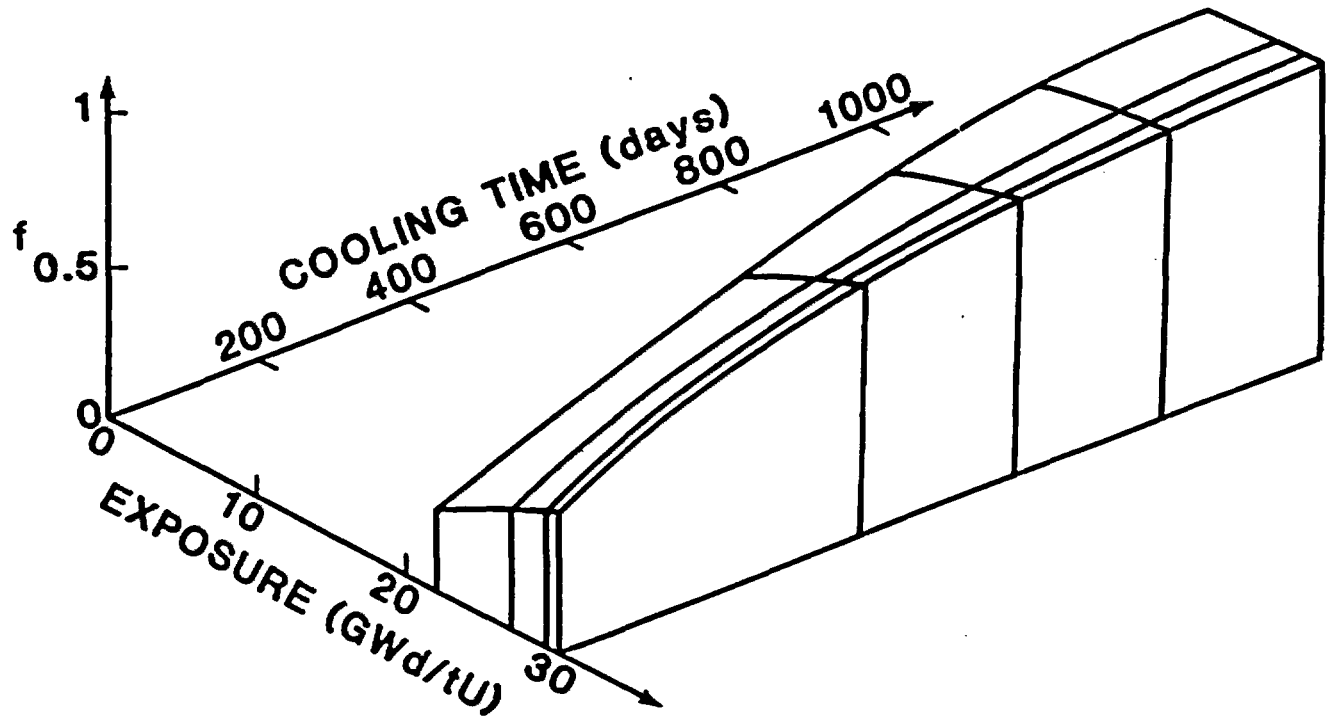

Fig. 11. A fraction f of the source neutrons within an assembly is due to spontaneous fissions of ^{244}Cm. This fraction depends on several parameters, two of which are shown here: exposure and cooling time. These fractions were calculated with a CINDER-type code for this report's standard PWR assembly (15- by 15-pin array) with an initial enrichment of 3% and a UO_2 density of 10.2 g/cm^3. The power level was 276.75 W/cm^2 for three consecutive reactor cycles (consisting of 335 days of constant power separated by 30 days of shutdown). Because of the relatively long half life of ^{244}Cm, the fraction increases with cooling time regardless of the exposure. For short cooling times, there is a strong sensitivity to the exposure.

D. Notation

The main variables in this report are these:

n_m = measured neutron count rate after background subtraction;

n = neutron count rate after background subtraction, corrected for the decay of ^{244}Cm back to the discharge date, with the contribution from ^{242}Cm (and other isotopes) subtracted, and adjusted to a standard boron concentration;

γ = measured gamma-ray reading;

E = an assembly's exposure;

T = an assembly's cooling time;

r = relative tolerance width;

λ = decay constant of ^{244}Cm;

= 0.0001048 day^{-1} = 0.003190 $month^{-1}$ = 0.03827 $year^{-1}$;

$f(E,T)$ = fraction of the source neutrons from ^{244}Cm after an exposure E and cooling time T;

c = concentration of boron in a storage pond's water;

$B(c)$ = multiplier of the measured neutron count rate that normalizes the data with a boron concentration c to a standard boron concentration.

When one of these variables is falsified or has been affected by a falsified variable, a prime will be placed after its symbol. For example, a modified assembly will give a corrected neutron count rate of n' instead of n and may be given a declared exposure of E' rather than E. The n' is the result of a measurement and a ^{244}Cm cooling time correction using the declared cooling time, which may be the true time T or a falsified time T'.

In Sec. II average values of some of the variables will be used; they will be denoted with an asterisk (*), as with n*.

II. SMALL-SCALE DIVERSION DETECTION

A. Assumptions

A small-scale diversion here means that less than half the plutonium is removed from any one assembly and the number of assemblies affected is a small fraction of the number in the pond.

There are three major assumptions in this section.

Assumption (1). Neutron and gamma-ray measurements made with the fork system produce data that on the average follow these relations, with an asterisk (*) meaning an average:

$$n^* = \alpha E^{\beta} \quad \text{and} \tag{5}$$

$$\gamma^*/E = a T^{-b} \quad . \tag{6}$$

(E* and T* are not used, as will be explained in Sec. II.B.1.) The validity of these relations can be judged from the data shown in Figs. 12-20. Only the neutron data in Fig. 12(b) have been adjusted for the ^{244}Cm fraction and its cooling; the other neutron data show much more scatter about the fitted curve. Plots of additional data are in Refs. 5, 6, 10, 12-14, and 21.

It is assumed that the average values n* and γ* are not affected significantly by any diversions; this means that the curve fitted to the data points is essentially the same as would be found had there been no diversion. The fraction of modified assemblies could be too small to affect the averages or the averages might have been established before any diversions took place.

With similar inspection equipment applied to similar reactors, the data obtained should also be similar. If all the assemblies in one pond were identically modified, the values of the parameters in Eqs. (37) and (38) would be affected and could differ significantly from the values found with the equipment at similar reactor facilities. The source of any unusual values of the parameters should be investigated; if the equipment is working properly, the integrity of the fuel could be suspect.

An assembly will be classified as an outlier if its data are not within certain tolerance limits about the calibration curves. The tolerance limits will be defined in Sec. II.B.3.

<u>Assumption (2)</u> When fissile material is removed from an assembly, (a) it is done once and (b) proportional amounts of ^{244}Cm and fission product isotopes (primarily ^{134}Cs and ^{137}Cs) are also removed with no radiation-emitting materials put in their places.

<u>Assumption (3)</u> Cooling times are not completely arbitrary; their starting times must coincide with a reactor refueling date. Surveillance cameras and inspections that check assembly identifications would give assurance that the assemblies had not been replaced in the core.

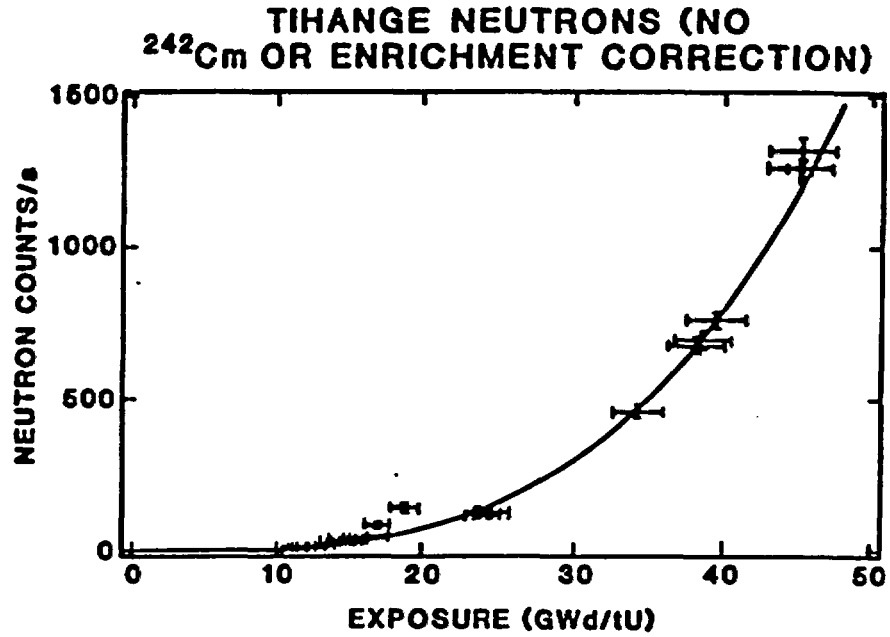

Fig. 12(a). The IAEA neutron data from Refs. 8 and 9 (Tihange) are shown here. A least-squares fit of Eq. (5) to the data is drawn through the data.

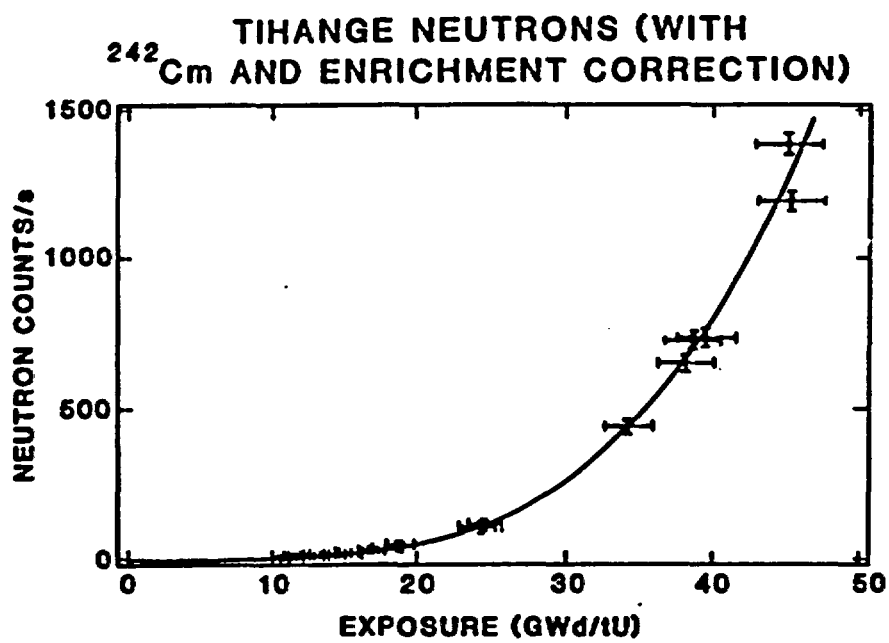

Fig. 12(b). The data in Fig. 1(a) have been corrected for ^{242}Cm neutron count rates and another fit to Eq. (5) is shown.

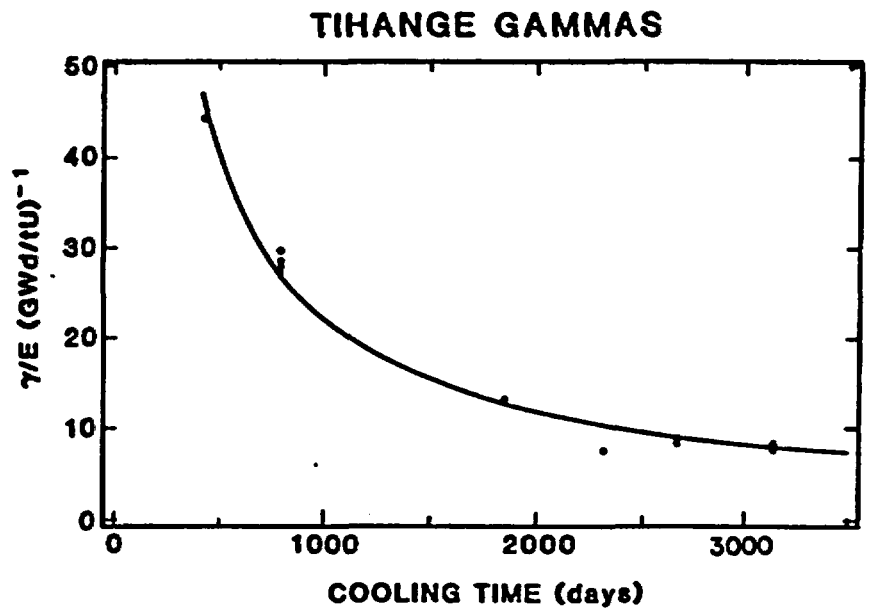

Fig. 13. The IAEA gamma-ray data from Refs. 8 and 9 (Tihange) are shown along with a least-squares fit of Eq. (6) to the data.

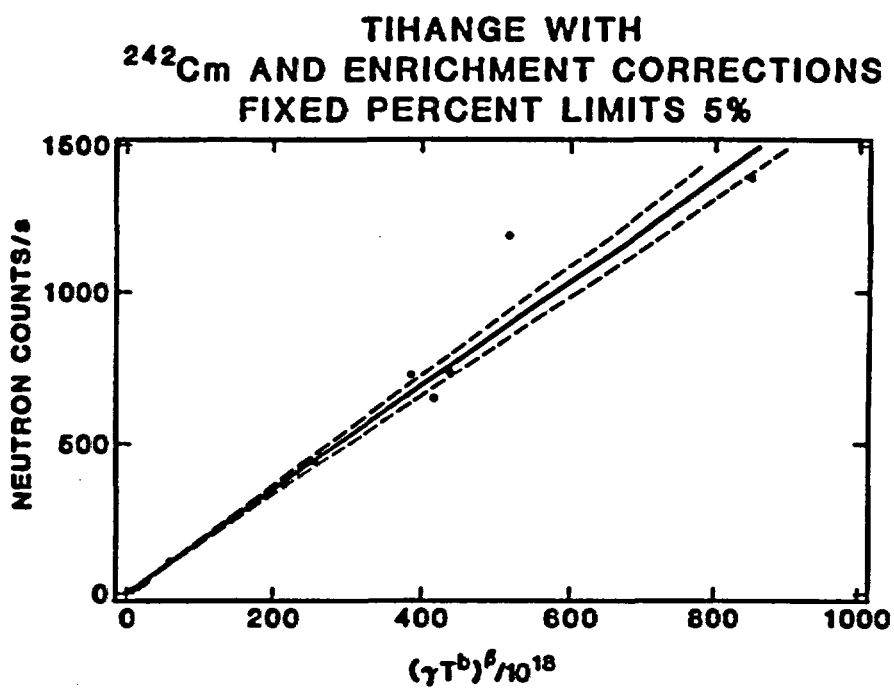

Fig. 14. The IAEA neutron and gamma-ray data from Refs. 8 and 9 (Tihange) are plotted along with the curve resulting from a least-squares fit of Eq. (7).

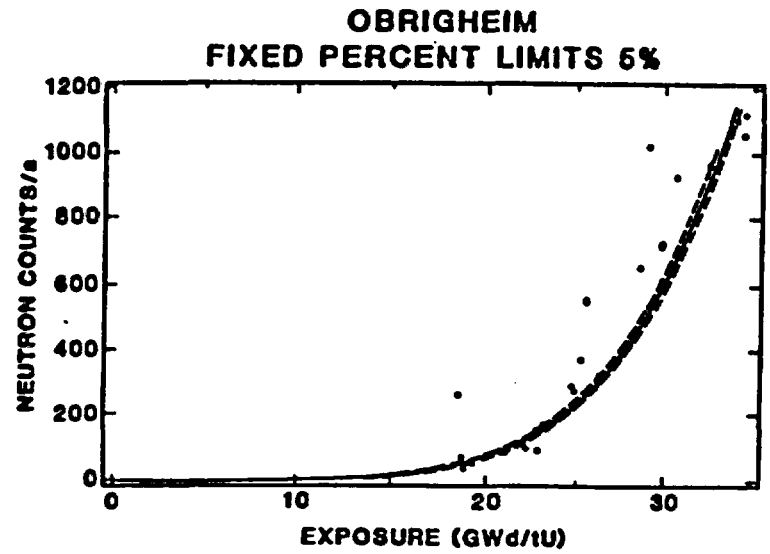

Fig. 15. The neutron data from Ref. 7 (Obrigheim) are plotted, with different symbols to indicate the irradiation histories. The curve of Eq. (5) was fitted to only the data points for assemblies that were irradiated continuously for two or three cycles. These data are not adjusted for the effects of different initial enrichments and reactor power histories; these items affect the fraction of the neutrons that are due to ^{244}Cm.

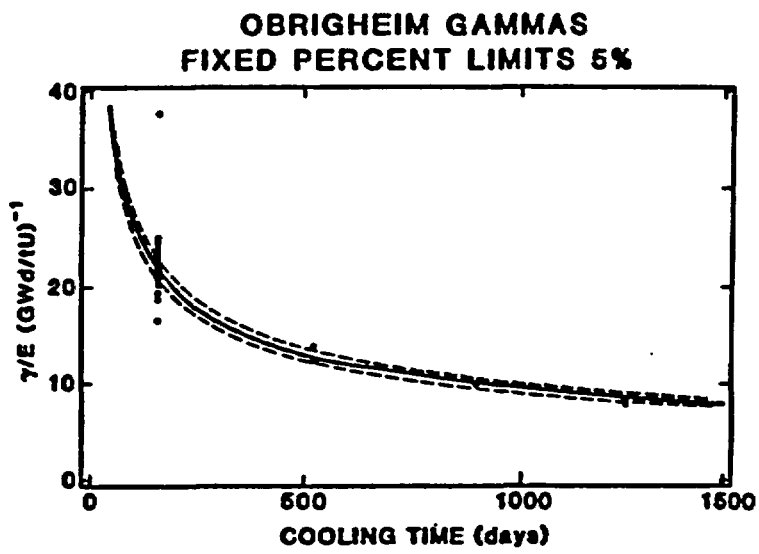

Fig. 16. The gamma-ray data from Ref. 7 (Obrigheim) are shown here with different symbols to indicate the irradiation histories. All points were used to fit Eq. (6). The large scatter in the data at 160 days of cooling is due to short-lived isotopes whose amounts depend on detailed irradiations of the assemblies; they disappear within about a year of cooling.

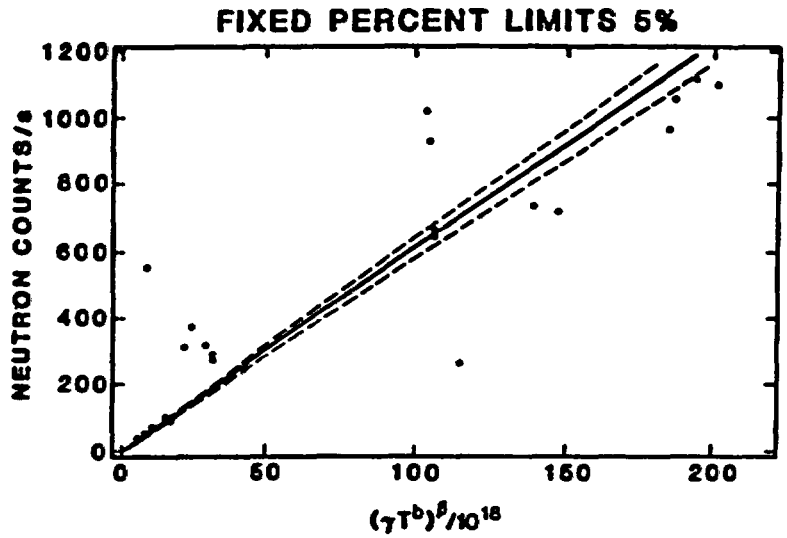

Fig. 17. The neutron and gamma-ray data of Ref. 7 (Obrigheim) are combined in this plot, according to Eq. (7). The neutron data are not adjusted for the effects of different initial enrichments and reactor power histories; these items affect the fraction of the neutrons that are due to ^{244}Cm.

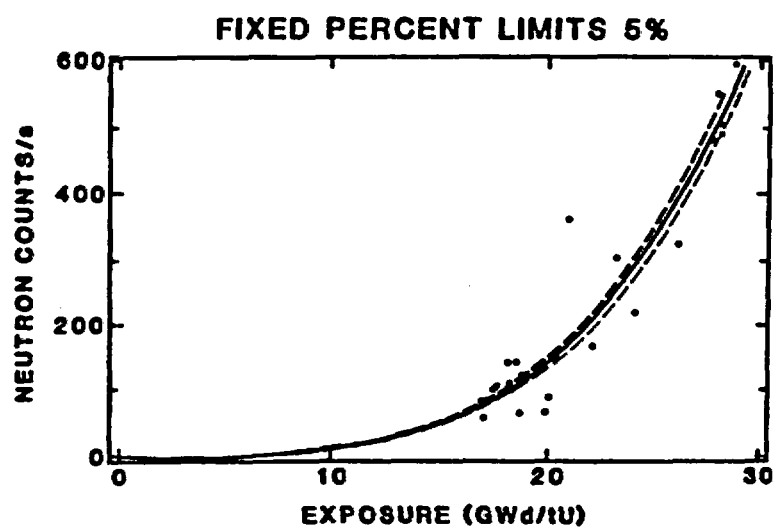

Fig. 18. The neutron data from unpublished measurements at Vermont Yankee are shown. Three assemblies had been reconstituted and had one or two pins missing. Another assembly had an interrupted irradiation history that led to an extra amount of ^{242}Cm that had not decayed away at the time of the measurement. These data are not adjusted for the effects of different initial enrichments and reactor power histories; these items affect the fraction of the neutrons that are due to ^{244}Cm.

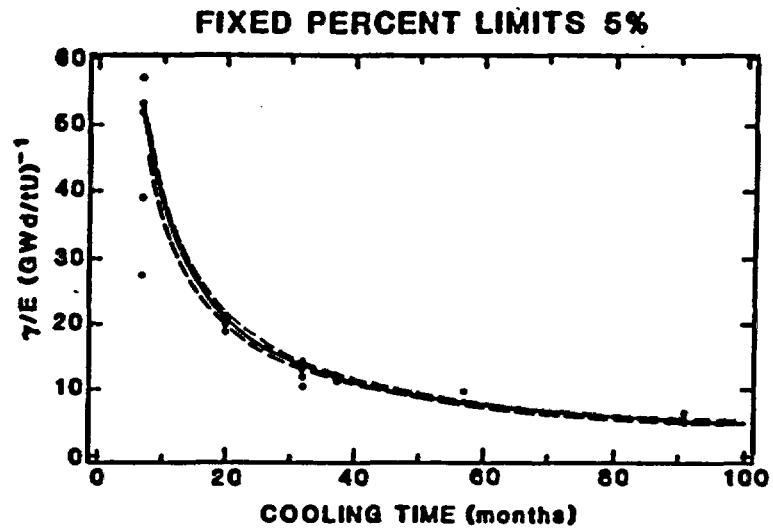

Fig. 19. The gamma-ray data from unpublished measurements at Vermont Yankee are presented here. The reconstituted assemblies with missing pins are not remarkable in this case, although the assembly with an interrupted irradiation history is again quite different from the others.

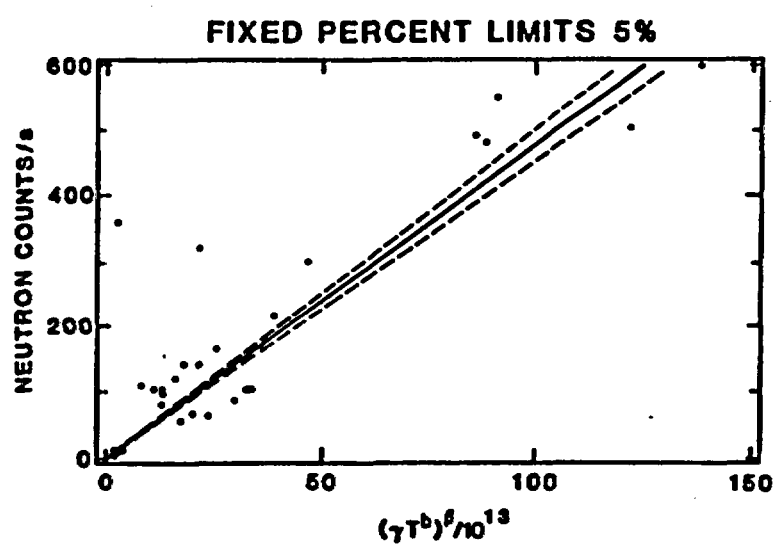

Fig. 20. The neutron and gamma-ray data from unpublished work at Vermont Yankee are combined according to Eq. (7). The reconstituted assemblies are outside the trend of the data, as is the data point from the assembly with an interrupted irradiation history. The neutron data are not adjusted for the effects of different initial enrichments and reactor power histories; these items affect the fraction of the neutrons that are due to ^{244}Cm.

The third assumption severely restricts the values of falsified cooling times, but a diverter has more flexibility in the declared exposures. By eliminating E between Eqs. (5) and (6), a verification can be made that is much less dependent on the declared exposures:

$$n^* = (\alpha/a^{\beta})\ (\gamma^* T^b)^{\beta} \quad . \tag{7}$$

If the parameters α, β, a, and b are obtained from Eqs. (5) and (6), they can be used with Eq. (7) to form a straight-line plot of n^* vs $(\gamma^* T^b)^{\beta}$; however, this procedure uses the declared exposures. Equation (7) could be used alone with α/a^{β} treated as one parameter and with β and b as two other parameters; these "new" parameters are thus determined without direct use of the exposures. A weak dependence on declared exposures can enter through the correction of the neutron count rate for the contributions from isotopes other than ^{244}Cm when such an adjustment is made.

On occasion, correlations have been sought between n and γ using the relation $n = k\gamma^c$. Equation (7) shows that this is useful for the special case of uniform cooling times. The value of c should then be β and the value of k should be $(\alpha/a^{\beta})T^{b\beta}$.

B. Data Imprecisions

1. Practical Sources of Uncertainties. During an inspection n and γ are measured with a fork detector; both of these quantities are assigned measurement uncertainties.

Uncertainties in the cooling times are not significant for this study. The times are known to within a day and the correction for ^{244}Cm decay is not sensitive to such a small time uncertainty; a single day's effect on the rate of gamma-ray production is hardly measurable.

The uncertainties in the declared exposures are difficult to ascertain. One report[35] recommends using 5%, whereas another work[36] found a bias of about 3% between operator and measured exposures; the operator's predictions of plutonium contents (which depend on the exposure) were biased[37] relative to measured amounts by less than 1%. Some of the scatter about the curve in

Fig. 12(b) is no doubt due to errors in the exposures, but given the agreement between the fit and the data, the errors must be less than 1% in this case.

Uncertainties in the exposures will not be considered in this study. Neither the operator nor the inspector can know the true exposures; they both use the declared exposures as exact values. The scatter introduced into the data points by this process cannot be eliminated. When the power-law curve is fitted to the data, uncertainties in the exposures may be stated, but their only function will be to help generate weighting factors for the data points.

In summary, uncertainties will only be attributed to the measured quantities of neutron count rate and gamma-ray rate, not to operator-declared exposures and cooling times.

2. Tolerance Limits. Associated with the plots of Eqs. (5) and (6) are tolerance limits above and below the curves. A data point outside the tolerance limits is considered an outlier and might represent a diversion (among other explanations, as seen in Figs. 15 and 18-20). Data that do not satisfy the following inequalities will be investigated as outliers:

$$n^* (1 - r_n) < n < n^* (1 + r_n) \tag{8}$$

and

$$\gamma^*/E (1 - r_\gamma) < \gamma/E < \gamma^*/E (1 + r_\gamma) \quad . \tag{9}$$

Although r_n and r_γ need not be independent of such parameters as E and T, it is a likely condition in practice; they will be treated as such in this report.

The relationships between the measurement distributions and the tolerance limits are shown in Figs. 21 and 22.

The width of the tolerance limits for Eq. (7) is related to the widths for the other two equations. Unlike Eqs. (5) and (6), both variables in Eq. (7)

Fig. 21. The curve of Eq. (5) is plotted in the vertical plane with error limits shown as dashed lines on either side. At each exposure there can be visualized a normal distribution centered on the curve, as shown at two exposures here. The standard deviation of the distribution is related to the width of the error limits.

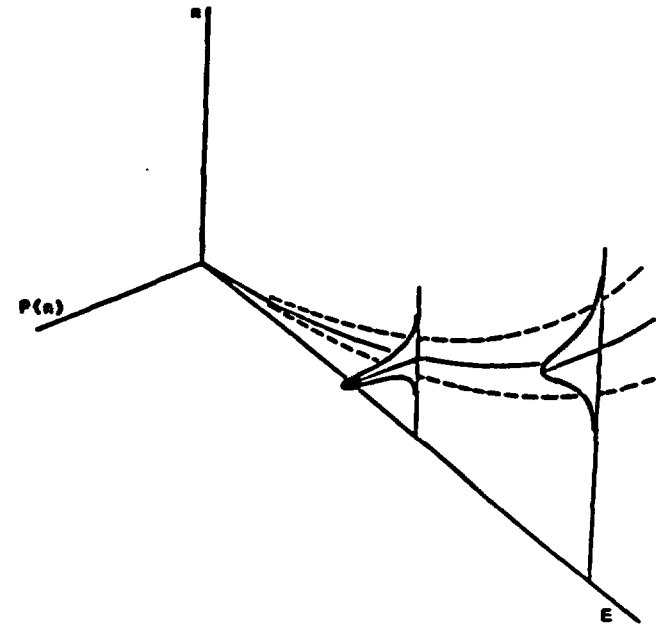

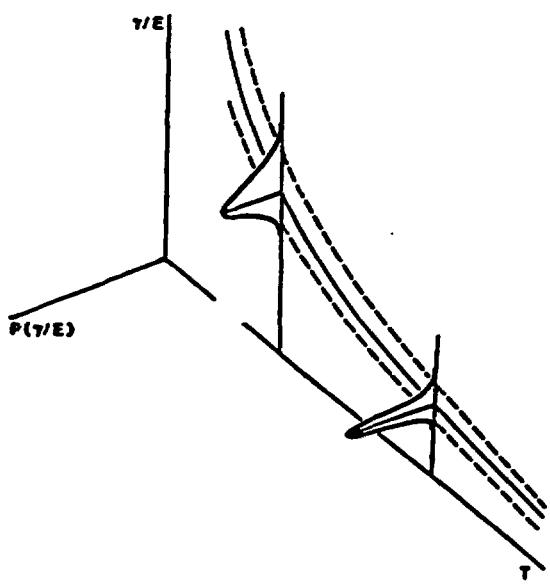

Fig. 22. The curve of Eq. (6) is plotted in the vertical plane with error limits shown as dashed lines on either side. At each cooling time there can be visualized a normal distribution centered on the curve, as shown at two exposures here. The standard deviation of the distribution is related to the width of the error limits.

have nonzero uncertainties. The symbol r_3 will be used to express the width of the tolerance limits for Eq. (7). The three different r's can be related through the standard deviations of the variables; each r could be a multiple of a corresponding standard deviation. A standard deviation of n can be calculated from Eq. (7) that should not be confused with the measured σ_n:

$$(\sigma_n/n)^2 = (\sigma_\gamma/\gamma)^2\beta^2 + (\sigma_\alpha/\alpha)^2$$

$$+ \sigma_\beta^2[\ln(\gamma T^b/a)]^2 + (\sigma_a/a)^2\beta^2 + \sigma_b^2[\ln T^\beta]^2 \quad . \tag{10}$$

Although the relative uncertainty of α may be greater than that of β, it does not necessarily dominate the expression in Eq. (10) (see Appendix B).

The r_3 is some multiplier times the σ_n/n of Eq. (10). A valid data point will thus also satisfy this relation:

$$n^* (1 - r_3) < n < n^* (1 + r_3) \quad . \tag{11}$$

The values of r_3 could easily be two or three times larger than r_n, reducing the usefulness of Eq. (7) somewhat.

C. Diversion Concealment Strategies

1. Correctly Declared E and T

a. First Inspection. If a diversion is made and no action is taken to conceal it, how detectable is the diversion? With nonzero tolerance limit widths, the diverter has some flexibility through the declared exposures and cooling times. However, the exposures and cooling times cannot be bent beyond reason without being obviously false even without any fork measurements.

The optimum diversion strategy would be to pick an assembly whose data points fall on the upper tolerance limits and divert enough material so that the new data points fall on the lower tolerance limits (Figs. 23-25). This procedure extracts the most material (without immediate detection) from the

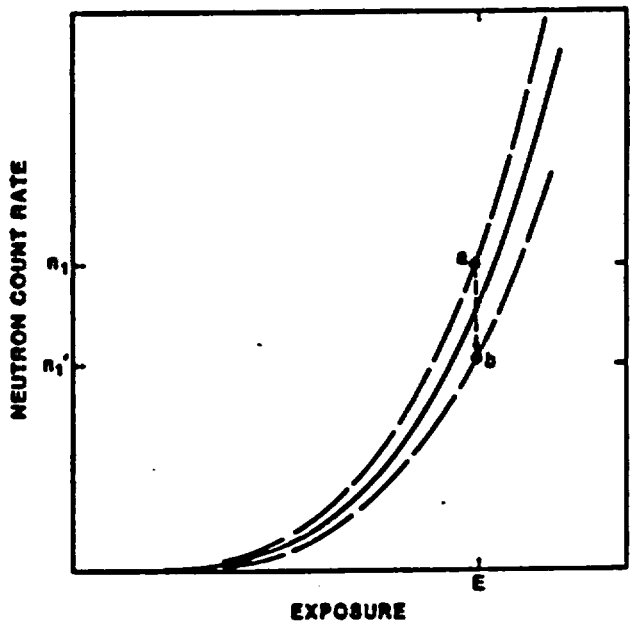

Fig. 23. If a diversion reduces the neutron count rate by an amount that keeps n_1' within the tolerance limits, the diversion will not be detected. Points "a" and "b" show the worst case from a safeguards viewpoint; the diverter has somehow been able to select an assembly whose data should just fall on the upper tolerance limit and then removed just the right amount of material to have the new data point rest on the lower limit.

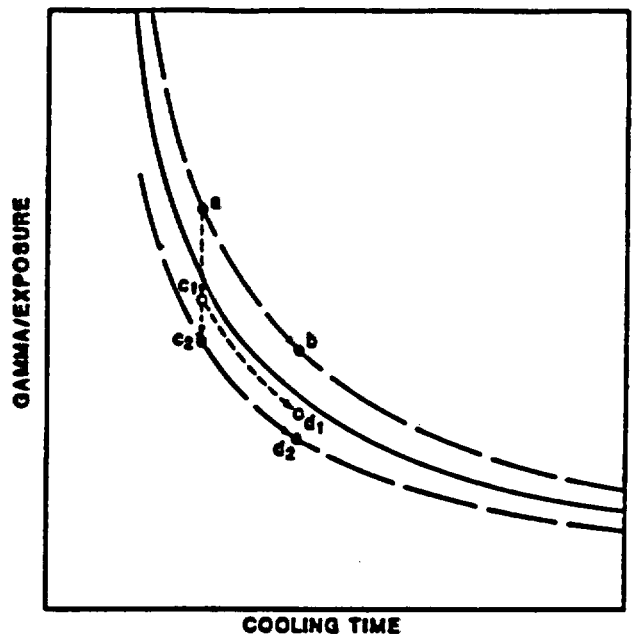

Fig. 24. The diversion of Fig. 23 also affects the gamma-ray reading and reduces it to γ_1'. A diverter might try to find an assembly and diverted amount that would take data point "a" to "c_1" within the tolerance limits or "c_2" on the lower tolerance limit. In either case, the diversion will not be detected by later measurements.

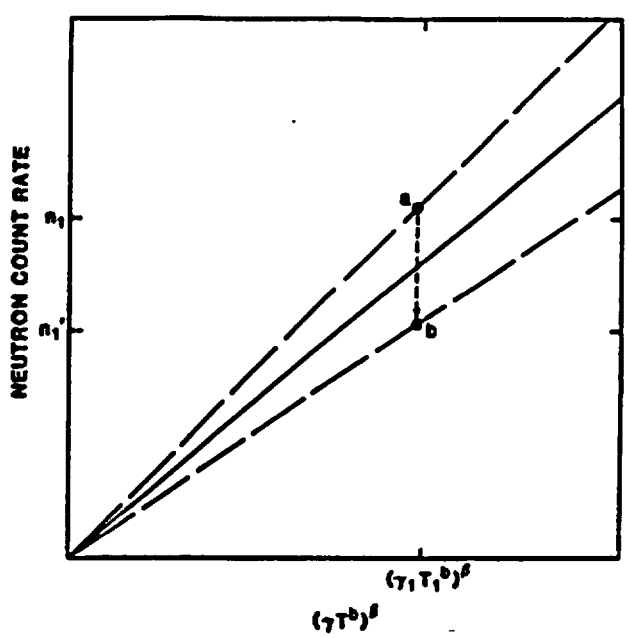

Fig. 25. The diversion of Figs. 23 and 24 is seen from the view of Eq. (7). The range by which point "a" can be shifted to "b" by the diversion depends on the width of the tolerance limits.

fewest number of assemblies, reducing the work of the diverter. It is unlikely that a diversion would actually move both neutron and gamma-ray data points from upper tolerance limits to lower tolerance limits, as shown in Figs. 23-24. It is more likely that if Fig. 23 were achieved (although this would not be easy), the lower data point in Fig. 24 would be somewhere between the tolerance limits; a careless diverter could produce a new data point in Fig. 24 below the lower tolerance limit.

A conservative assumption from the safeguards point of view is that a diverter can somehow select assemblies whose data will fall on upper tolerance limits and perform the diversion of Fig. 23, although how he might gain this knowledge and skill is unclear. A rational diverter would remove much less from assemblies than indicated by Figs. 23-24.

At a cooling time T_1, the ratios of the falsified and true measurements for neutron count rates follow from Eq. (5) for the average count rates:

$$n_1 = \alpha E^{\beta} (1 + r_n) \quad , \tag{12}$$

$$n_1' = \alpha E^{\beta} (1 - r_r) \quad , \text{ and} \tag{13}$$

$$n_1'/n_1 = (1 - r_n)/(1 + r_n) \quad . \tag{14}$$

A similar expression for gamma-ray ratio is deduced from Eq. (6):

$$\gamma_1'/\gamma_1 = (1 - r_\gamma)/(1 + r_\gamma) \quad . \tag{15}$$

When many assemblies are examined, as at a spent fuel pond, the probability of detection of one or more assemblies from an aggregate is important. It is assumed that for a given exposure the (adjusted) neutron data points from many different assemblies form a normal distribution. The probability that a diversion from a single assembly will be detected depends on the position of

the data point before the diversion, the size of the diversion, and the width of the normal distribution. The probabilities of detecting diversions of different sizes are given in Table III for 4σ (relative to the average neutron count rate n) from 16% to 28%.

The first column shows the size of the diversion relative to 1σ; the mass diverted is assumed to be proportional to the change in neutron count rate.

The second column gives four options of 4σ; they are shown as percentages of the average n (at any exposure).

The diversion fraction in column 3 is $\Delta n/n = (\Delta n/\sigma)(4\sigma/n)/4$.

The number of assemblies that must undergo the partial diversion before a significant quantity of plutonium (8 kg) is obtained is given in the fourth column. It is assumed here that typical PWR assemblies with about 30-GWd/tU exposure are being considered.

The last three columns, labeled PD(N), give probabilities of detection under three conditions. PD(1) is the probability that a diversion on a single assembly will lead to a neutron data point below the lower 4σ limit. After diversions are performed on the necessary number of assemblies to reach a significant quantity, the probability that one or more of these assemblies will produce a neutron data point below the lower 4σ limit is PD(all). If only one-fifth of the diverted assemblies are selected in a measurement plan, the probability that one or more of these assemblies will produce a neutron data point below the lower 4σ limit is PD(all/5).

Very small diversions with $\Delta n/\sigma < 1$ require many assemblies to get a significant quantity, but the overall detection probability with the fork detection is <1%.

Large diversions with $\Delta n/\sigma > 5$ are virtually (if not actually) guaranteed to be detected by the fork as long as the measurement plan includes at least one of the assemblies. These diversions remove 20% to 35% of each assembly. [The last row ($\Delta n/\sigma = 7$) is included for reference later in this report.]

A diverter would probably first consider making relatively large diversions from only a few assemblies. This procedure minimizes the diverter's effort, presents the fewest number of assemblies that could generate outliers by the fork detector, and presents fewer problems with some other safeguards techniques (for example, surveillance cameras). However, if even only about

TABLE III

DETECTION PROBABILITIES OF DIVERSIONS OF VARIOUS SIZES

$\Delta n/\sigma$	$4\sigma/n$ (%)	$\Delta n/n$ (%)	No. Assemblies for 1 SQ[a]	PD(1)[b] (%)	PD(all) (%)	PD(all/5) (%)
1	16	4	41	0.14	5	1
	20	5	33	0.14	4	1
	24	6	27	0.14	4	1
	28	7	23	0.14	3	1
2	16	8	20	2.3	37	9
	20	10	16	2.3	31	7
	24	12	14	2.3	28	7
	28	14	12	2.3	24	5
3	16	12	14	16	91	40
	20	15	11	16	85	29
	24	18	9	16	79	29
	28	21	8	16	75	29
4	16	16	10	50	99.9	75
	20	20	8	50	99.6	75
	24	24	7	50	99.2	50
	28	28	6	50	98.4	50
5	16	20	8	84	100	97
	20	25	7	84	100	84
	24	30	6	84	100	84
	28	35	5	84	100	84
7	28	49	4	99.9	100	99.9

[a] SQ = Significant quantity of plutonium (8 kg).
[b] PD(N) = Probability of detection after measuring N of the assemblies used to gain the significant quantity.

20% of the pins in an assembly were removed with $\Delta n/\sigma = 3$, the probability that the new data point would show the diversion is 16%. This must be repeated for eight or nine assemblies to gain a significant quantity. The probability that one or more of these eight assemblies will reveal the diversion is about 75%; if only two of these assemblies are included in the measurement plan, the probability that one or more of them will indicate a diversion is still about 29%.

Diverting 50% from a few assemblies has a very high probability of detection by the fork (Table III, $\Delta n/\sigma = 7$). Although only four assemblies are needed to gain a significant quantity (with $4\sigma/n = 28\%$), fork measurements on these four assemblies have essentially a 100% chance of finding an outlier. A measurement on only one of these assemblies still has a 99.9% chance of generating an outlier.

The alternative diversion scheme is many small diversions, which reduces the risk of detection by the fork but increases the effectiveness of other safeguards techniques. Consider the smaller diversion with $\Delta n/\sigma = 2$. After 10% of the pins are removed from 16 assemblies, only a 2.3% chance may exist that any one of the assemblies will produce a data point outside the 4σ limits. However, if all 16 assemblies were measured, the chance of one or more of them revealing a diversion is 31%. If only four of these assemblies were included in a measurement plan, the probability of at least one of them revealing the diversion is about 7%.

A diversion will be detected with Eq. (7) only if the diversion exceeds a certain limit. Figure 25 shows the effect of a diversion. The following inequality must be met if detection is to be avoided:

$$n_1' > (\alpha/a^{\beta})\,(\gamma_1'\,T_1^{b})^{\beta}\,(1 - r_3) \quad . \tag{16}$$

<u>b. Subsequent Inspections</u>. If another inspection is performed at cooling time T_2, the diversion accomplished before time T_1 will still not be apparent from the neutron data. The count rates corrected for the ^{244}Cm fraction and its decay are naturally not affected by additional cooling time; the purpose of the corrections is to make the count rate independent of cooling time

and proportional to the amount of ^{244}Cm present. As long as the correct E and T are declared, αE^{β} is a constant and the neutron data will remain within the tolerance interval, although at a smaller count rate than it would without the diversion. The equation is

$$\alpha\ E^{\beta} = n_{m1}'\ f(E;T_1)\ e^{\lambda T_1} = n_{m2}'\ f(E,T_2)\ e^{\lambda T_2}\ , \tag{17}$$

or

$$n_1' = n_2'\ . \tag{18}$$

The gamma-ray data at T_2 will not indicate a diversion either. The correct data point "a" in Fig. 24 would be found at "c" after a diversion; this false point is expressed as

$$\gamma_1'/E = p\ a\ T_1^{-b}\ . \tag{19}$$

If detection is to be avoided, p must be greater than $(1 - r_\gamma)$. Without the substitution of other gamma-ray emitting material, this point will cool to point "d" of Fig. 24 in agreement with Eq. (6):

$$\gamma_2'/E = p\ a\ T_2^{-b}\ . \tag{20}$$

If the data point starts within the tolerance limits, it stays there.

At a later time with Eq. (7), $n_2' = n_1'$ [as in Eq. (18)] and $(\gamma_2'\ T_2^b) = (\gamma_1'\ T_1^b)$ from Eqs. (19) and (20), so a diversion that is undetectable at T_1 is not detectable later.

2. Falsely Declared T

a. First Inspection. If the declared cooling time is increased from T_1 to $T_1' = T_1 + \Delta T$, the diverter may temporarily improve on the diversion. The worst safeguards scenario again starts with an assembly's data on the upper tolerance limits. Material is diverted so that the new data points are within the limits, as shown in Figs. 26-28.

If the end point on the neutron plot is on the lower limit, the value of T_1' is obtained from Eq. (5):

$$n_1'/n_1 = (n_{m1}'/n_{m1})\ [f(E,T_1')/f(E,T_1)]\ e^{\lambda(T_1'-T_1)}$$

$$= (1 - r_n)/(1 + r_n) \quad ; \tag{21}$$

$$f(E,T_1')\ e^{\lambda T_1'} = (n_{m1}/n_{m1}')\ f(E,T_1)\ e^{\lambda T_1}\ [(1 - r_n)/(1 + r_n)] \quad . \tag{22}$$

This equation must be solved numerically for T_1'; the Newton-Raphson method of Appendix C is a good technique.

For the end point to be on the upper neutron limit at T_1', a different required time is found from this equation:

$$f(E,T_1')\ e^{\lambda T_1'} = (n_{m1}/n_{m1}')\ f(E,T_1)\ e^{\lambda T_1} \quad . \tag{23}$$

If the end point on the gamma-ray plot is to be on the lower limit, another T_1' is required by Eq. (6):

$$(\gamma_1'/\gamma_1)\ (T_1'/T_1)^b = (1 - r_\gamma)/(1 + r_\gamma) \quad ; \tag{24}$$

$$T_1' = T_1\ [(\gamma_1/\gamma_1')\ (1 - r_\gamma)/(1 - r_\gamma)]^{1/b} \quad . \tag{25}$$

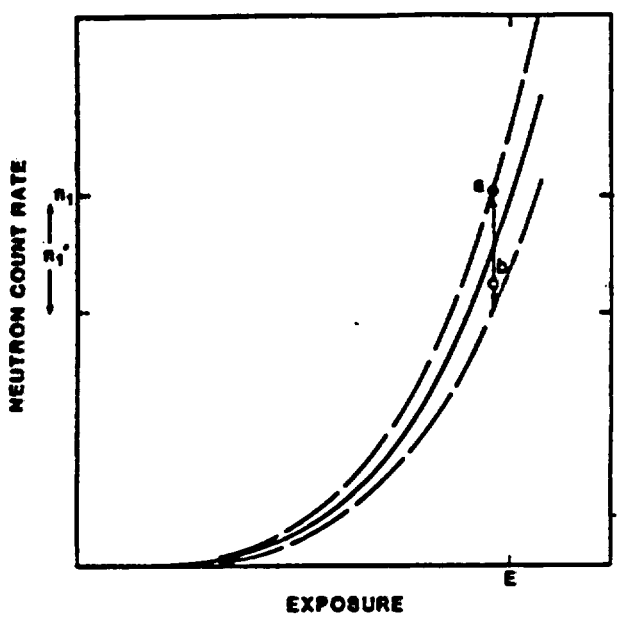

Fig. 26. A diverter can falsify the cooling time, resulting in a correct data point at "a" moving to any place between the tolerance limits (such as "b"). The most material could be removed by having "b" on the lower limit, as in Fig. 23.

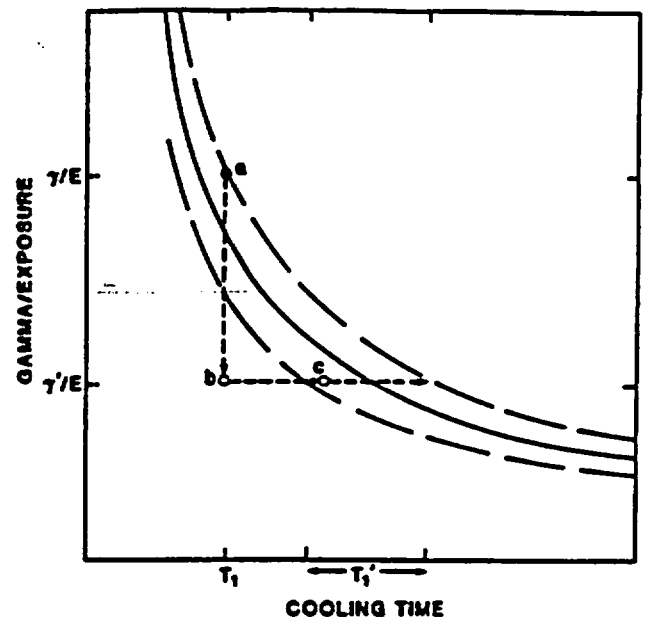

Fig. 27. The diversion with a false cooling time of Fig. 26 affects the gamma-ray curve as shown here. The correct point "a" is reduced to "b," then moved between the tolerance limits (as at "c") with a properly selected false cooling time.

Fig. 28. The diversion of Figs. 26 and 27 seen from Eq. (7). A range of $(\gamma_1' T_1'^{b})^{\beta}$ is available for the false point "b."

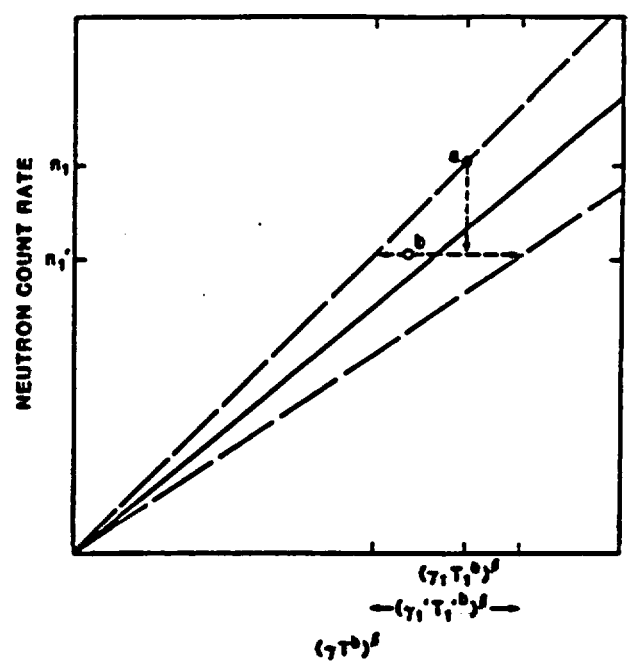

For the gamma-ray end point to fall on the upper limit, a fourth T_1' is necessary:

$$T_1' = T_1 \, (\gamma_1/\gamma_1')^{1/b} \quad . \tag{26}$$

The smallest $(\gamma_1' T_1')^b$ that will escape detection with Eq. (7) is seen from Fig. 28 to satisfy

$$n_1' = n_{m1}' \, f(E,T_1') \, e^{\lambda T_1'} \tag{27}$$

$$= (\alpha/a)^{\beta} \, (\gamma_1' T_1'^{\,b})^{\beta} \tag{28}$$

$$= (\alpha/a)^{\beta} \, (\gamma_1' T_1'^{\,b})_{min}^{\beta} \, (1 + r_3) \quad . \tag{29}$$

For a given n_1' and γ_1', a value of T_1' can be found from Eqs. (27) and (29).

The maximum false time uses the other tolerance limit:

$$n_{m1}' \, f(E,T_1') \, e^{\lambda T_1'} \tag{30}$$

$$= (\alpha/a)^{\beta} \, (\gamma_1' T_1'^{\,b})_{max}^{\beta} \, (1 - r_3) \quad . \tag{31}$$

If detection is to be avoided, the declared T_1' must be greater than the biggest minimum time and less than the smallest maximum time from Eqs. (22)-(31):

$$\max[\text{Eqs. (22), (25), (29)}] < T_1' < \min[\text{Eqs. (23), (26), (31)}] \quad . \tag{32}$$

b. Subsequent Inspections. A diversion may succeed at T_1' but may be found at T_2' with Eqs. (6) and (7).

(1) Neutron Curve. Had there been no diversion, the adjusted neutron count rate n_1 at cooling time T_1 would not change with cooling time: $n_2 = n_1$.

The adjusted data point at T_1' is n_1' and will not equal n_2' at T_2' because incorrect times are used in computing the adjusted count rate. An inspector will find this ratio of count rates (that is less than one):

$$(n_2'/n_1') = (n_{m2}'/n_{m1}')\ [f(E,T_2')/f(E,T_1')]\ e^{\lambda(T_2' - T_1')} \quad . \tag{33}$$

Study of the behavior of this ratio requires that the ratio of measured count rates be eliminated. They are related through the use of the correct cooling times and the adjusted count rate n_t that would have been calculated had the cooling times not been falsified. The n_{t1} and n_{t2} rates are equal because the correct cooling times are used:

$$(n_{t2}/n_{t1}) = 1 = (n_{m2}'/n_{m1}')\ [f(E,T_2)/f(E,T_1)]\ e^{\lambda(T_2 - T_1)} \quad . \tag{34}$$

This equation can be solved for the ratio of measured count rates:

$$(n_{m2}'/n_{m1}') = [f(E,T_1)/f(E,T_2)]\ e^{-\lambda(T_2 - T_1)} \quad . \tag{35}$$

Placing Eq. (35) into (33), with ΔT being the falsified time interval, shows the ratio of inspection count rates to be

$$(n_2'/n_1') = [f(E,T_1)/f(E,T_1 + \Delta T)]/[f(E,T_2)/f(E,T_2 + \Delta T)] \quad . \tag{36}$$

All these ^{244}Cm fractions have the same exposure E. The fraction increases toward 1 as cooling time increases. The quantities in brackets on the right-hand side of Eq. (36) are thus both less than one, but the one in the denominator is the larger of the two because T_2 is greater than T_1, and its ratio will be more nearly equal to one. Using false cooling times thus means that the adjusted neutron count rate will decrease with time instead of staying constant.

Eventually there will be some T_2' at which n_2' is below the lower tolerance limit and detection will be possible. If the diversion places n_1' on the lower tolerance limit to maximize the amount removed, detection will be possible at any future inspection. There will be some delay before detection if n_1' is above the lower tolerance limit. To find the delay, n_1' is set equal to $q\alpha E^{\beta}$ and n_2' to $(1-r_n)\alpha E^{\beta}$:

$$(1 - r_n)/q = [f(E,T_1)/f(E,T_1 + \Delta T)]/[f(E,T_2)/f(E,T_2 + \Delta T)] \quad . \qquad (37)$$

Numerical solutions for the delay T_2-T_1 are given in Table IV for the standard assembly; it is assumed that the cooling times have been falsified by 1 year. With relaxed tolerance intervals and n_1' near the upper limit, a substantial delay occurs before detection is possible. With 5% limits and n_1' near the lower tolerance limit, detection would be possible in about a month.

The delay strongly depends on where the diversion leaves the first count rate n_1'. The diverter would like to remove as much of an assembly as possible, but this produces a lower n_1' that will be detected sooner. The diverter cannot know exactly where his actions will place n_1'. To avoid immediate detection at T_1' and to postpone detection at T_2' as long as possible, the diverter is forced to withdraw only a small fraction of an assembly.

(2) Gamma-Ray Curve. Figure 29 shows the data point "a" that might be found for an undiverted assembly at T_1; at T_2, this assembly would generate the data point "b" as point "d" slides along a curve proportional to the cooling curve:

TABLE IV

DETECTION DELAYS WITH NEUTRONS AFTER FALSIFIED COOLING TIME

$E = 30$ GWd/tU, $T_1 = 800$ days, $\Delta T = 365$ days

r_n	q	T_2 (d)	$T_2 - T_1$ (d)
0.02	1.01	900	100
	1.00	870	70
	0.99	840	40
0.05	1.04	1072	272
	1.00	961	161
	0.96	841	41
0.10	1.09	1314	514
	1.00	1111	311
	0.95	970	170
	0.91	842	42

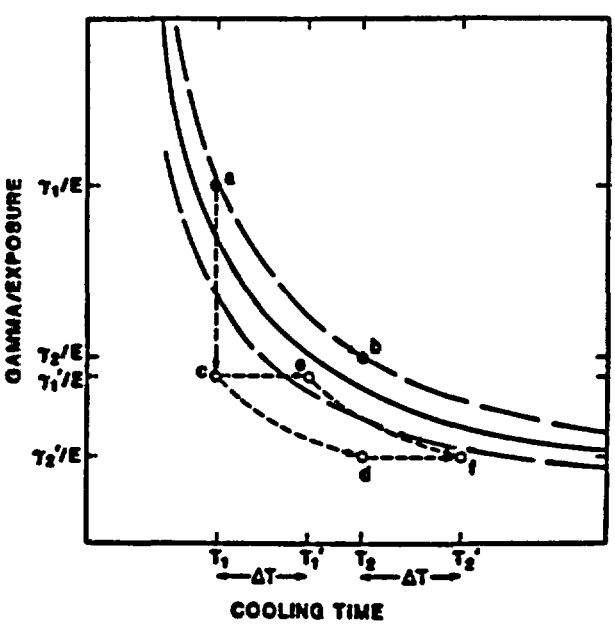

Fig. 29. The diversion of Figs. 26 to 28 are considered at a later inspection time T_2. Figure 26 does not change with time, but the points of Fig. 27 move as shown here. If no diversion had been performed, the true data point "a" would have become point "b." Because of the diversion, "a" became "c," which was then shifted to "e" by the false cooling time T_1'. At the later inspection time, "c" would have been found at "d," but the ΔT shift places "d" at "f." It appears that point "e" drifted to "f"; the drift does not follow the form of Eq. (6) and will eventually cross the lower tolerance limit, as has already happened in this drawing.

$$\gamma_1/E = p\ a\ T_1^{-b}\ ,\quad (1 - r_\gamma) < p < (1 + r_\gamma)\ . \tag{38}$$

After a diversion, point "a" drops to point "c":

$$\gamma_1'/E = q\ p\ a\ T_1^{-b}\ ,\quad q < 1\ . \tag{39}$$

The gamma-ray reading is reduced to $\gamma_1' = q\gamma_1$ by the diversion.

To disguise the diversion, the diverter moves point "c" within the tolerance interval by declaring a longer cooling time, T_1', producing point "e." An inspection will thus not detect the diversion at T_1'.

At some later time T_2, point "c" would move to point "d," following a curve proportional to the true cooling curve. Point "e" will slide to point "f" along a curve that is not proportional to the true cooling curve because the times being used are incorrect. At some time T_2' point "f" will intersect the lower tolerance limit and detection becomes possible (the value of γ_2'/E is obtained from point "d"):

$$\gamma_2'/E = q\ p\ a\ T_2^{-b} = (1 - r_\gamma)\ a\ T_2'^{-b}\ . \tag{40}$$

An equation for T_2 can be deduced with $\Delta T = T_2' - T_2$:

$$(T_2 + \Delta T) = T_2\ [(1 - r_\gamma)/(q\ p)]^{(1/b)}\ . \tag{41}$$

The time during which the diversion was hidden is $T_2 - T_1 = T_2' - T_1' = \Delta T$. Some possible values of the delay from Eq. (41) for the standard assembly show that this detection process by itself is not adequately sensitive; even large changes in the gamma-ray reading (qp) require many months or years to detect. However, the diverter must be concerned about matching the fraction

diverted with the change in cooling time, keeping the change in time equal to some multiple of the core loading interval.

In principle, detection could be made earlier than T_2' if one observes that point "e" does not drift along a curve proportional to the average cooling curve. In practice, it may be difficult to confidently determine the drift curve where there are measurement uncertainties.

If a small diversion is made so that point "c" of Fig. 29 is within the tolerance limits and point "e" is kept within the tolerance limits by declaration of a sufficiently small cooling time, then point "f" will stay within the limits for all time; point "f" will approach point "d" as the cooling time increases. This small diversion will be undetectable if ΔT matches reactor core loading time intervals and point "e" is within the tolerance limits.

(c) Neutron-Gamma Curve. If Eq. (7) is used at T_2', the data point from T_1' will have drifted. For an assembly with correctly declared E and T, n and γT^b are constants. After a diversion and falsified times, n' and $\gamma' T'^b$ are not constant. Whether n' increases or decreases depends on the assembly; $f(E,T')$ and $e^{\lambda T'}$ both increase, but n_m' decreases. To show that $\gamma' T'^b$ is not constant either, assume that it is constant and find a contradiction. The ratio γ'/γ is set to ε:

$$\gamma_2' = \gamma_1' \ (T_1'/T_2')^b \quad , \tag{42}$$

$$\varepsilon \ \gamma_2 = \varepsilon \ \gamma_1 \ [(T_1 + \Delta T)/(T_2 + \Delta T)]^b \quad , \tag{43}$$

$$\gamma_2 (T_2 + \Delta T)^b = \gamma_1 (T_1 + \Delta T)^b \quad , \tag{44}$$

which is not consistent with $\gamma_2 \ T_2^b = \gamma_1 \ T_1^b$.

With no diversion, this drifting should not occur; the mere fact that the point shifts would be suspicious.

3. Falsely Declared E

a. Neutron-Exposure Equation. If a diversion is to be masked by an incorrect declared exposure, the maximum material could be removed by somehow selecting an assembly whose neutron data point originally falls on the upper tolerance curve. The amount of material removed could produce a neutron count rate that is even below the lower tolerance curve at E because a reduced declared exposure E' could move the new data point within the tolerance curves (Fig. 30). (The operator is again granted great skill in performing this diversion scenario.) Assume that the data point for the undiverted assembly would be on the upper limit:

$$n_1 = n_{m1}\, f(E,T_1)\, e^{\lambda T_1} = \alpha\, E^{\beta}\, (1 + r_n) \quad . \tag{45}$$

The range of plausible new exposures after a diversion producing n_1' can be calculated from the intersections of n_1' with the upper and lower tolerance curves:

$$n_1' = n_{m1}'\, f(E'_{max},T_1)\, e^{\lambda T_1} = \alpha\, E'^{\beta}_{max}\, (1 - r_n) \quad ; \tag{46}$$

$$n_1' = n_{m1}'\, f(E'_{min},T_1)\, e^{\lambda T_1} = \alpha\, E'^{\beta}_{min}\, (1 + r_n) \quad . \tag{47}$$

With Eq. (45), α can be eliminated from each of these two equations:

$$(E'_{max}/E)^{\beta} = (n_1'/n_1)\, [(1 + r_n)/(1 - r_n)] \quad \text{and} \tag{48}$$

$$(E'_{min}/E)^{\beta} = (n_1'/n_1) \quad . \tag{49}$$

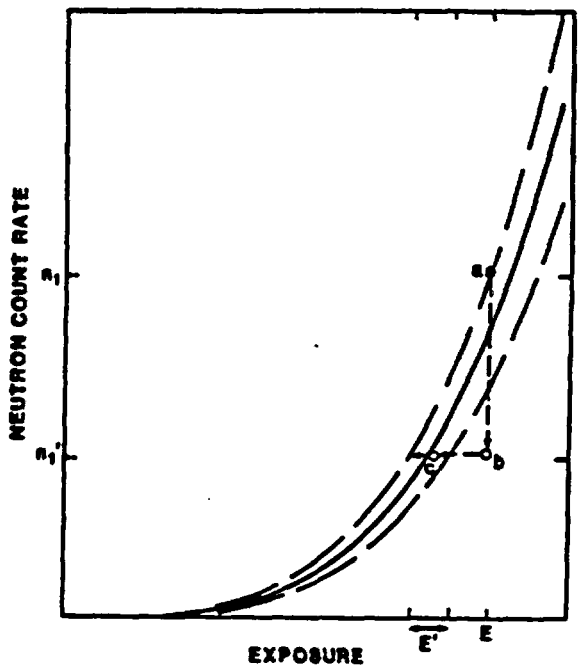

Fig. 30. A diversion might be concealed by falsifying the declared exposure. This drawing shows how a well-informed diverter might maximize the amount removed from an assembly. Point "a" is from the true assembly. After the diversion, the reduced neutron count rate moves "a" to point "b." To avoid detection, a range of exposures E' may be declared (point "c"), although E' must still seem reasonable for the reactor's operating history.

Equations (48) and (49) have been evaluated for $\beta = 3.33$ and selected n_1'/n_1 values; the results in Table V show that the range of E' is generally small. If the undiverted data point had been below the upper tolerance limit (as would have to be assumed by a diverter), the amount that could be diverted is reduced for the same range of E'.

b. Gamma-Time Equation. The gamma-ray data point will also be affected by the diversion and falsely declared exposure. The value of γ/E could either increase or decrease. These cases are now considered separately.

(1) Decreased γ/E. If γ/E decreases, a diverter would want the value of γ_1'/E' to be on or above the lower tolerance limit; the worst safeguards case is to assume the data point was originally on the upper tolerance limit (Fig. 31):

$$\gamma_1/E = a\, T_1^{-b}\, (1 + r_\gamma) \quad , \tag{50}$$

$$\gamma_1'/E' > a\, T_1^{-b}\, (1 - r_\gamma) \quad , \text{ and} \tag{51}$$

TABLE V

RANGE OF FALSE EXPOSURES AFTER A DIVERSION

$\beta = 3.33$, $E = 30$ GWd/tU.

n_1'/n_1	E'_{min}	r_n	E'_{max}	Fig. No.	No. Assemblies for 8 kg Pu
0.995	29.95	0.01	30.14	2	327
		0.02	30.32		
		0.04	30.68		
		0.05	30.87		
		0.10	31.82		
		0.20	33.83		
		0.40	38.63		
0.960	29.63	0.01	29.81	4	36
		0.02	29.99		
		0.04	30.36		
		0.05	30.54		
		0.10	31.48		
		0.20	33.47		
		0.40	38.22		
0.750	27.52	0.01	27.68	6	6
		0.02	27.85		
		0.04	28.19		
		0.05	28.36		
		0.10	29.23		
		0.20	31.08		
		0.40	35.59		
0.53	24.79	0.01	24.94	7	4
		0.02	25.09		
		0.04	25.40		
		0.05	25.55		
		0.10	26.33		
		0.20	28.00		
		0.40	32.00		

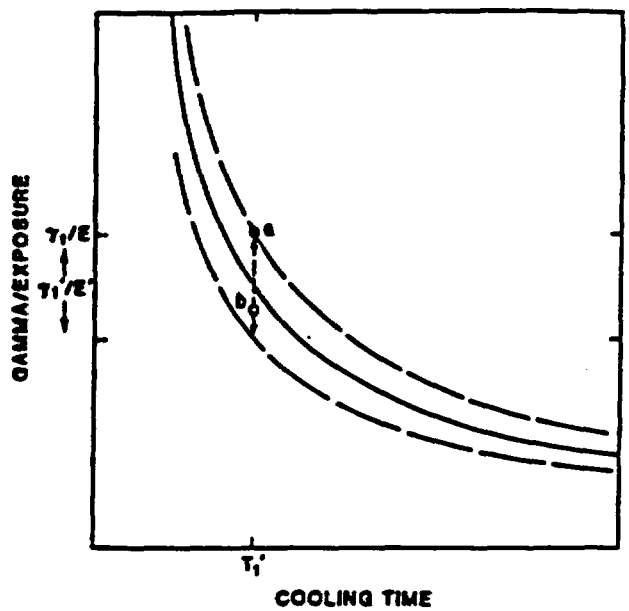

Fig. 31. The diversion of Fig. 30 affects γ_1 also. If detection is to be avoided, the true data point "a" must move to "b" with γ_1/E' within the tolerance limits, as shown here. In this case, "a" was on the upper tolerance limit.

$$E' < E\,(\gamma_1'/\gamma_1)\,(1 + r_\gamma)/(1 - r_\gamma) \quad . \tag{52}$$

If the point is to be kept at or below the upper tolerance limit, E' cannot be too small:

$$E' > E\,(\gamma_1'/\gamma_1) \quad . \tag{53}$$

<u>(2) Increased γ/E</u>. If γ changes less than E, γ/E will increase to γ'/E' after a diversion. The diverter would then prefer to start with a data point on the lower tolerance limit (Fig. 32). This produces restrictions on E' similar to those of Eqs. (52) and (53):

$$E' > E\,(\gamma_1'/\gamma_1)\,(1 - r_\gamma)/(1 + r_\gamma) \quad \text{and} \tag{54}$$

$$E' < E\,(\gamma_1'/\gamma_1) \quad . \tag{55}$$

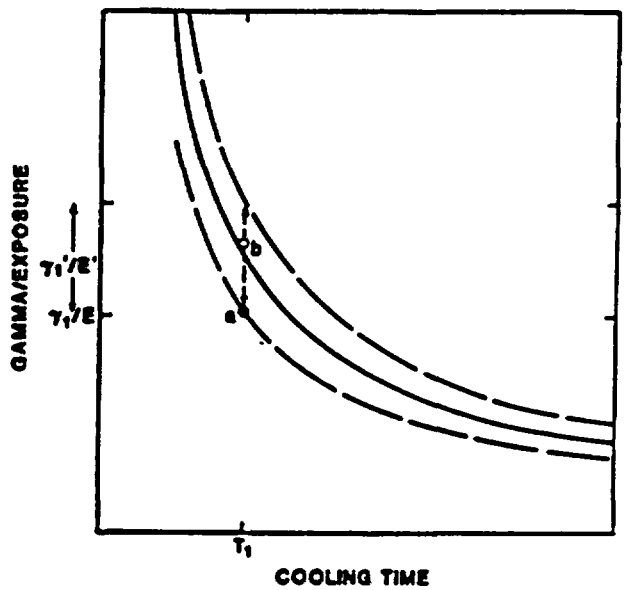

Fig. 32. The diversion of Fig. 30 affects γ_1 also. If detection is to be avoided, the true data point "a" must move to "b" with γ_1/E' within the tolerance limits, as shown here. In this case, "a" was on the lower tolerance limit.

(3) Diversion Limitations. The diverter would not want to declare exposures that are implausibly different from those expected from the reactor's operating history. Therefore, he should keep E'/E close to one. The ratio γ_1'/γ_1 is less than one (if no substitute radioactive substance is introduced into the assembly); the ratios involving r_γ in Eqs. (52) and (54) are greater than one and less than one, respectively. To keep E'/E nearly one, the diverter is best advised to decrease γ/E so that Eq. (52) applies where there are two ratios changing in opposite directions.

The diverter must again find a balance among these neutron and gamma-ray equations. There is some range of small diversions per assembly that will be undetectable, but it forces the diverter to remove only a few pins from each of many assemblies.

c. Neutron-Gamma Equation. Equation (7) places limits on n_1' more directly because E' has little effect in that case (Fig. 28 again). If n_1 is on the upper tolerance limit and n_1' is on the lower limit, the smallest ratio of n_1'/n_1 that would not be detected as a diversion is

$$n_1'/n_1 = [f(E',T_1)/f(E,T_1)]\ [(1 - r_3)/(1 + r_3)] \quad . \tag{56}$$

This expression has been evaluated for the standard assembly, and the results presented in Table VI show the importance of keeping the value of r_3 as small as possible.

d. Subsequent Inspections. At a later inspection, the declared exposure must still be E'. The lengthened cooling time affects the calculated ^{244}Cm fractions f(E',T).

For the standard assembly, the ratio of f's in Eq. (56) is hardly changed by additional cooling. Waiting a year after the initial 800-day cooling has only a 2% effect on the ratio. The usefulness of the neutron data is not significantly altered at subsequent inspections.

TABLE VI

DIVERSION RANGE WITH THE NEUTRON-GAMMA EQUATION WITH A FALSE EXPOSURE

E = 30 GWd/tU, T = 800 days.

r_3	E' (GWd/tU)	n_1'/n_1
0.05	25	0.879
	26	0.889
	27	0.896
	28	0.901
	29	0.904
	30	0.905
0.10	25	0.795
	26	0.804
	27	0.810
	28	0.815
	29	0.817
	30	0.818
0.20	25	0.648
	26	0.655
	27	0.660
	28	0.664
	29	0.666
	30	0.667

A gamma-ray data point that was initially within the tolerance intervals will remain there at all subsequent cooling times. The fission products remaining in the assembly will continue to cool normally and the false exposure is not changed, so the data point will maintain its position relative to the average curve and the tolerance limit. Figure 33 shows such a case. Points "a" and "b" would be found had there been no diversion; points "c" and "d" result from a diversion and a false declared exposure.

Subsequent inspections thus offer little safeguards advantages when small diversions are disguised with falsely declared exposures. The slight change in f(E,T) with time is of only marginal benefit. With narrow tolerance intervals, the diverter is forced into diverting very small quantities from each of many assemblies; this increased activity would enhance detection by containment and surveillance techniques.

4. Falsely Declared E and T. At first glance a diverter seems to have a great deal of flexibility when both the exposure and cooling time are falsified. However, restrictions still exist on the exposure and cooling time, and it will be seen below that diversions can be detected with subsequent measurements. In the short term, falsifying both E and T allows larger diversions, but in the long run the false T makes detection inevitable.

The largest diversion that can be hidden within the tolerance limits would follow these actions: (a) The neutron data point starts on the upper tolerance limit and the diversion drops it below the lower limit; a smaller exposure is declared to just place the new data point within the tolerance limits again (Fig. 30). (b) If γ/E decreases after the diversion, the data point is assumed to be on the upper tolerance limit before the diversion and the declared cooling time is increased to bring the new data point within the tolerance limits (Fig. 27 with γ'/E replaced by γ'/E'). (c) If γ/E increases after the diversion, an assembly is chosen (as a worst safeguards case) for which the gamma-ray data point starts on the lower tolerance limit, then a reduced cooling time is declared to position the new data point on the lower limit again (Fig. 34 with c_1 or c_2 as far left as possible); this delays the detection for the longest possible time.

Although extremes of these actions would maximize the amount of material that could be diverted, they have to be restrained to avoid declaration of patently implausible values of exposure and cooling time.

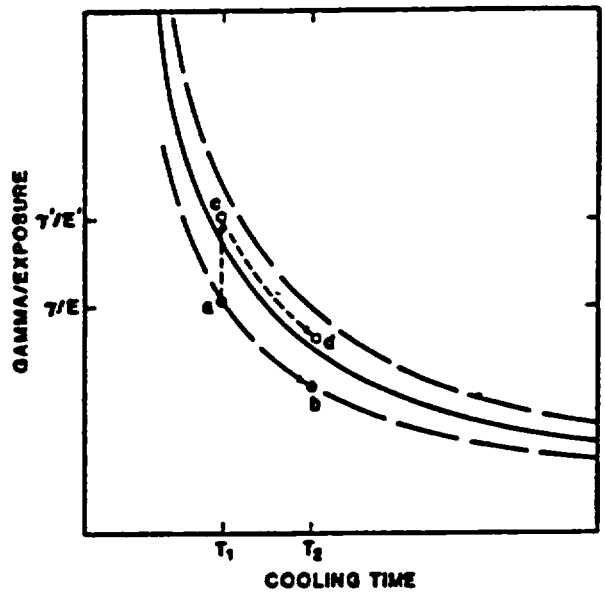

Fig. 33. For a diversion with a falsified exposure, a subsequent inspection will not reveal the diversion if the initial inspection also failed to find the diversion. The case of Fig. 32 is continued here to a later cooling time T_2. The true data point "a" would have produced "b"; the false point "c" moves to "d." The curve from "c" to "d" follows Eq. (6) and therefore stays within the tolerance limits. The diversion is never detected.

Fig. 34. After a diversion, both the exposure and cooling time could be falsely declared. In this drawing, the true data point "a" would have been on the lower limit, as in Figs. 32 and 33. After a diversion, the γ_1'/E' ratio increases (in this example) to "b_1" or "b_2." In either case a range of false cooling times T_1' is possible at "c_1" or "c_2," although point "b_1" would satisfy an inspection already and not be detectable at a later time. It would be difficult for a diverter to know whether T_1 should be falsified or not.

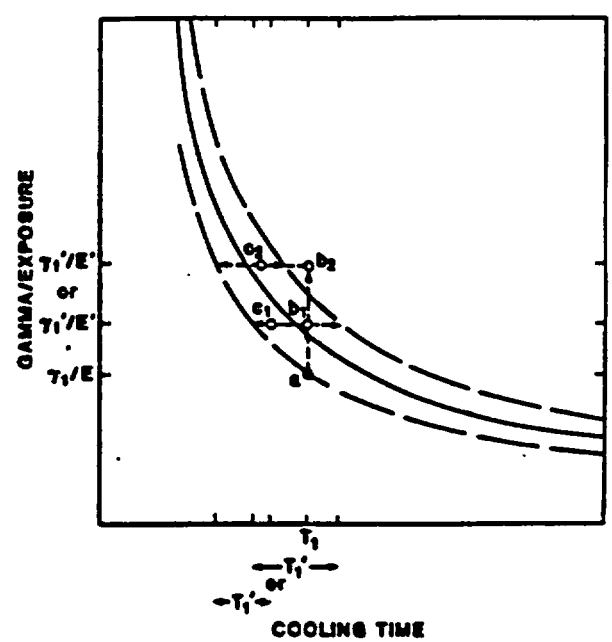

It is generous to assume that a diverter can know in advance which assemblies would produce data points on the appropriate tolerance limits and then select the desired combination of fuel removed and false values of exposure and cooling time. To consider the worst safeguards case, however, this is assumed.

a. Decreased n. The range of E' for the neutron data can be calculated in a manner that differs from Eqs. (45)-(49) only in that T_1' is not equal to T_1:

$$(E_{max}'/E)^{\beta} = (n_{m1}'/n_{m1})\ [f(E_{max}',T_1')/f(E,T_1)]\ [(1 + r_n)/(1 - r_n)]$$

$$e^{\lambda(T_1' - T_1)} \quad \text{and} \tag{57}$$

$$(E_{min}'/E)^{\beta} = (n_{m1}'/n_{m1})\ [f(E_{min}',T_1')/f(E,T_1)]\ e^{\lambda(T_1' - T_1)} \quad . \tag{58}$$

For $T_1' - T_1 = 365$ days, the exponential is 1.039. The values of E_{min}' and E_{max}' in Table VII are thus increased by about 4% by an additional year of declared cooling.

b. Increased γ/E. When γ/E increases after a diversion, the new cooling time T' can be assigned a range of values (Fig. 34). Generously assume the undiverted point would be on the lower tolerance limit:

$$\gamma_1/E = a\ T_1^{-b}\ (1 - r_\gamma) \quad , \tag{59}$$

$$(\gamma_1'/E'_{min}) = a\ T_1'^{-b}\ (1 - r_\gamma) \quad , \tag{60}$$

$$(\gamma_1'/E'_{max}) = a\ T_1'^{-b}\ (1 + r_\gamma) \quad , \tag{61}$$

TABLE VII

DIVERSIONS WITH FALSIFIED EXPOSURE AND COOLING TIME

$\beta = 3.33$, $b = 0.883$, $E = 30$ GWd/tU.

The subscript "1" has been suppressed on T, n, and γ.

The neutron and gamma-ray E' results are independent of each other.

T	T'	Neutrons				Gamma Rays			
(days)		n'/n	r_n	E_{min}'	E_{max}'	γ'/γ	r_γ	E_{min}'	E_{max}'
365	730	0.99	0.05	31.77	32.70	0.99	0.05	49.56	54.77
		0.10	31.77	33.64			0.10	44.81	54.77
		0.80	0.05	29.81	30.72	0.80	0.05	40.05	44.26
		0.10	29.81	31.65			0.10	36.21	44.26
365	1095	0.99	0.05	32.27	33.16	0.99	0.05	70.35	78.35
			0.10	32.27	34.06		0.10	64.11	78.35
		0.80	0.05	30.39	31.27	0.80	0.05	57.29	63.31
			0.10	30.39	32.16		0.10	51.80	63.31
365	1460	0.99	0.05	31.76	32.67	0.99	0.05	91.39	101.01
			0.10	31.76	33.58		0.10	82.65	101.01
		0.80	0.05	29.85	30.75	0.80	0.05	73.85	81.63
			0.10	29.85	31.65		0.10	66.69	81.63
730	1095	0.99	0.05	30.48	31.36	0.99	0.05	38.44	42.59
			0.10	30.48	32.25		0.10	34.76	42.49
		0.80	0.05	28.63	29.50	0.80	0.05	31.06	34.33
			0.10	28.63	30.37		0.10	28.09	34.33
1095	1460	0.99	0.05	29.37	30.26	0.99	0.05	34.64	38.29
			0.10	29.37	30.26		0.10	31.33	38.29
		0.80	0.05	27.50	28.37	0.80	0.05	27.99	30.94
			0.10	27.50	29.26		0.10	25.32	30.94

$$E'_{min}/E = (\gamma_1'/\gamma_1)\ (T_1'/T_1)^b \quad , \text{ and} \tag{62}$$

$$E'_{max}/E = (\gamma_1'/\gamma_1)\ (T_1'/T_1)^b\ (1 - r_\gamma)/(1 + r_\gamma) \quad . \tag{63}$$

c. Decreased γ/E. If γ/E decreases after a diversion, the range of declared cooling times can similarly be calculated for the initial data point on the upper tolerance limit:

$$\gamma_1/E = a\ T_1^{-b}\ (1 + r_\gamma) \quad , \tag{64}$$

$$(\gamma_1'/E'_{min}) = a\ T_1'^{-b}\ (1 - r_\gamma) \quad , \tag{65}$$

$$(\gamma_1'/E'_{max}) = a\ T_1'^{-b}\ (1 + r_\gamma) \quad , \tag{66}$$

$$E'_{min}/E = (\gamma_1'/\gamma_1)\ (T_1'/T_1)^b\ [(1 + r_\gamma)/(1 - r_\gamma)] \quad , \text{ and} \tag{67}$$

$$E'_{max}/E = (\gamma_1'/\gamma_1)\ (T_1'/T_1)^b \ . \tag{68}$$

d. Standard Assembly Examples. We evaluated Eqs. (57), (58), (62), and (63) for various ratios of data values and other parameters for the standard assembly. The results in Table VII indicate that the ranges of E'/E that correspond to plausible cooling times are very narrow (about 1 GWd/tU) and are determined by the neutron relations.

e. Subsequent Inspections. The diverter has gained flexibility by being able to alter both the exposure and cooling time. But altering the cooling time ensures that a diversion will eventually be detected, as developed in the next section.

(1) Neutron Data. Figure 30 can be used again to show the effect of a diversion and inspection at the declared time T_1'. The neutron data at point "c" is somewhere between the tolerance limits at the declared exposure E' and has this adjusted neutron count rate:

$$n_1' = n_{m1}' \; f(E',T_1') \; e^{\lambda T_1'} = p \; \alpha \; E'^{\beta} \quad , \tag{69}$$

with

$$(1 - r_n) < p < (1 + r_n) \quad . \tag{70}$$

At a later cooling time T_2', the adjusted count rate will be

$$n_2' = n_{m2}' \; f(E',T_2') \; e^{\lambda T_2'} = q \; \alpha \; E'^{\beta} \quad . \tag{71}$$

If detection is to be avoided, q must have the same restrictions shown for p in Eq. (70).

By taking the ratio of Eqs. (71) and (69), this relation is obtained:

$$(n_{m2}'/n_{m1}') \; [f(E',T_2')/f(E',T_1')] \; e^{\lambda(T_2' - T_1')} = (q/p) \quad . \tag{72}$$

For a diversion that removes proportionate amounts of all isotopes, as would the removal of whole pins, the ratio of measured count rates at different times is a constant (aside from multiplication effects that are small for a diversion of only a few pins):

$$(n_{m2}'/n_{m1}') \approx (n_{m2}/n_{m1}) \quad . \tag{73}$$

This relation can be connected to Eq. (72) with a similar relation for the case of no diversion:

$$1 = (n_{m2}/n_{m1})\ [f(E,T_2)/f(E,T_1)]\ e^{\lambda(T_2-T_1)} \quad . \tag{74}$$

This equation equals one because without a diversion, $n_2 = n_1$ (the cooling-time-adjusted count rate for ^{244}Cm is constant).

Solving Eq. (72) for (n_{m2}'/n_{m1}') and putting the expression into Eq. (74) for (n_{m2}/n_{m1}), an equation for T_2' is obtained; T_2 must be replaced by $T_1 + T_2' - T_1'$:

$$f(E',T_2')/f(E',T_1 + T_2' - T_1') = (q/p)\ f(E',T_1')/f(E,T_1) \quad . \tag{75}$$

The worst safeguards case has the data point at time T_1' on one tolerance limit, and detection is not possible until the data point drifts to the other limit. In Fig. 30 the data point would move along a vertical line at the exposure E'. The direction of the drift (increasing or decreasing n') depends on the nature of the assembly. From Eqs. (69) and (71),

$$(n_2'/n_1') = (n_{m2}'/n_{m1}')\ [f(E',T_2')/f(E',T_1')]\ e^{\lambda(T_2' - T_1')} \quad . \tag{76}$$

The ratio of the two f(E,T) functions and the exponential are both greater than one, but the ratio of measured count rates is less than one. If the product of these ratios is greater than one, then the data point drifts upward, and the worst safeguards case has $p = (1 - r_n)$ and $q = (1 + r_n)$. If the value of Eq. (76) is less than one, then the data point drifts downward, and the values of p and q are reversed for the worst case.

For the standard assembly, the data point will drift downward, so T_2' for the extreme case is found from this version of Eq. (75):

$$f(E',T_2')/f(E,T_1 + T_2' - T_1') = [(1 - r_n)/(1 + r_n)]\ f(E',T_1')/f(E,T_1) \quad . \tag{77}$$

Table VIII shows some time intervals during which a diversion from the standard assembly would be undetectable. The effect of E' is small within the range of 25 to 29 GWd/tU. The smallest plausible T_1' is 800 + 365 = 1165 days; with narrow tolerance intervals, a second inspection can detect a diversion after a few months. If T_1' is increased by a another year, the detection can occur more quickly (delay times are halved). The greater the falsification of the cooling time, the sooner detection is possible.

(2) Gamma-Ray Data. As the cooling time grows, a true gamma-ray data point will drift within the γ/E-vs-T plot along a line proportional to the average curve; the point will stay within the tolerance limits if it began there.

The study of a false gamma-ray data point closely mirrors the analysis in Sec. II.C.2, where only the cooling time was falsely declared. For the present case, E' replaces E of Sec. II.C.2; otherwise, the equations are unchanged.

A falsified data point from a "large" diversion will eventually drift out of the tolerance limits, but "small" diversions would be undetectable.

(3) Neutron-Gamma Equation. The exposure has only a small influence on Eq. (7) through the f(E,T) function, so the analysis of Sec. II.C.2 for Eq. (7) applies here also. If a diversion is not detected at the first inspection, it will not be detected later.

5. Summary of Problems for Diverters. Tolerance limits give a diverter some flexibility of action, but the freedom is constrained by the fork measurements, with the scatter of data about averages determining the tightness of the constraint. The declared exposures and cooling times must furthermore be reasonable for the operating history of the reactor.

TABLE VIII

DELAY TIME BETWEEN INSPECTIONS TO DETECT A DIVERSION WITH FALSE EXPOSURE AND COOLING TIME

$E = 30$ GWd/tU, $T_1 = 800$ days.

T_1' (days)	E' (Gwd/tU)	r_n	T_2' (days)	$T_2' - T_1'$ (days)
1165	25	0.01	1222	57
		0.05	1421	226
		0.10	1608	443
		0.20	1850	685
	29	0.01	1224	59
		0.05	1447	282
		0.10	1673	508
		0.20	1962	797
1530	25	0.01	1552	22
		0.05	1636	106
		0.10	1729	199
		0.20	1877	347
	29	0.01	1556	26
		0.05	1655	125
		0.10	1766	236
		0.20	1945	415

If the declared exposure and cooling time are not falsified after a diversion, the amount of material that can be removed from one assembly is simply related to the widths of the tolerance limits (and the measured values before the diversion; that is, how near to upper tolerance limits the data were).

With 5% tolerance limits, the diverter would be able to remove about 10% of the pins from an assembly without detection from the neutron data <u>if</u> the diverter knows that the true data point would be on the upper limit. The pins must be removed in such a way that the gamma-ray data point stays within the tolerance intervals for the gamma-ray curve.

All of the above conditions would have to be met successfully on 17 PWR assemblies to gain a significant amount of plutonium (while also outwitting

surveillance cameras, seals, and other safeguards instruments). In practice the diverter would surely assume that the undiverted assemblies' data points would fall below the upper tolerance limit; fewer than 10% of the pins would be removed to gain a margin of error. In reality, therefore, perhaps 35 or 50 assemblies would have a few pins removed to gain the significant quantity of plutonium. The diverter who wishes to escape detection by the fork is forced into a large effort, and the chances of detecting the fuel handling by other safeguards methods would be increased.

As long as the correct exposure and cooling time are declared, no detection advantage is gained by subsequent inspections.

A false declared cooling time gives the diverter more latitude in the size of the diversion but makes detection of the diversion more likely at a subsequent inspection. Diversion can be small enough to avoid detection, but again the diverter is forced to increase his efforts. The time gap between a larger diversion and its detection depends on the tolerance limit widths and the amount diverted. The declared cooling time must be consistent with known core unloading dates and restricts a diverter to making large changes in the time.

If only the declared exposure is falsified, only limited diversions can again be made without detection. For 5% tolerance intervals and E' within 2 GWd/tU of E, the number of pins that can be removed from an assembly is so small that dozens or even hundreds of assemblies would have to be handled.

Declaring false exposures and cooling times make small diversions possible, but with false cooling times, large diversions will eventually be detected.

Very small diversions can be undetected; whether or not a diverter would choose to remove small amounts from each of many assemblies cannot be known. A large diversion from an assembly could be detected quickly, whereas an intermediate-size diversion might not be detected until a second inspection some time after the first one.

What is meant by "small," "intermediate," and "large" diversions depends on the precisions of the fork measurements and the accuracy of the ^{244}Cm fraction correction. The data from the recent Tihange exercise have the ^{244}Cm correction applied. In that case a small, undetectable diversion seems to be about 10%; a large, easily detectable diversion is about 25%. A 50% diversion

would certainly be detected if the declared exposure and cooling time were correct. An attempt to disguise such a large diversion with falsely declared values would require about a 20% decrease in exposure along with a new cooling time that brings the gamma-ray data point very close to the average curve and yet matches the reactor operating history. The knowledge required of an operator to perform such a feat may be unattainable.

III. CONCLUSIONS

The use of the fork detector places severe limitations on the diversion of material from a spent fuel assembly.

The removal of large fractions (perhaps 20% or more) of assemblies is easily detected.

Taking small fractions (about 10% or less) of each of many assemblies might be done in such a way as to make detection difficult, but it forces the diverter to handle a large number of assemblies, and he must have expert knowledge of the assemblies and how data are generated by the fork.

Furthermore, the diverter must somehow overcome the other safeguards techniques (for example, records evaluations, surveillance cameras, underwater cameras, seals, and night-vision devices) used at the site. The probability of detection by these techniques is enhanced as a diverter handles more fuel assemblies to avoid detection by the fork.

A diverter has several strategic options with different consequences after fork measurements. For the present purpose of investigating the sensitivity of the fork detector, we assumed diversions remove whole pins without replacement with fuel or radioactive materials; the diverter may falsify the declared exposures, the cooling times, or both. The options within this scope have been examined in detail in this report using (where necessary) the best known approximate relations among neutron count rate, gamma-ray readings, and the mass of fuel in an assembly.

<u>Option 1</u>. Declare the correct exposure and cooling time.

If the amount diverted from a single assembly is small enough to keep the neutron and gamma-ray data points within the tolerance limits of the data analyses, the diversion will escape detection. However, the amount must

be very small (perhaps 10 pins from a 204-pin PWR assembly), so many assemblies (about 35) must be handled to gain a significant quantity of plutonium.

Option 2. Declare a false cooling time.
With the aid of an increased cooling time, a larger amount of material could be removed from an assembly without being detected initially. The selection of a false cooling time must match the operating history of the reactor. The diversion can be detected with a subsequent measurement; the time delay before this is possible can be days or months depending on the amount removed, the precision of the fork detector, and the nearness of the data point from the undiverted assembly to the lower tolerance limit.

Option 3. Declare a false exposure.
If done with great care, a small diversion can escape detection with a false exposure. But the interactions among the change in neutron count rate, the change in the gamma-ray readings, and the false declared exposure is very restrictive. If done without excellent estimates of the fork data to be collected in the future, detection is likely even with the false exposure.

Option 4. Declare both a false exposure and a false cooling time.
A diversion disguised by a combination of reduced exposure and increased cooling time is a very complex operation to perform. The scheme offers no real advantage over falsifying the exposure alone; the hazards to the diverter of using false cooling times arise again.

The informed diverter may choose option 1 because it is simple in principle and potentially undetectable, although the fork detector forces the diverter to modify many assemblies in the face of other surveillance and containment measures.

Option 3 is the next best choice because it allows somewhat larger diversions per assembly without detection, but the uncertain knowledge of what data an assembly will generate reduces the apparent flexibility. The uncertainty may even convince a diverter to use option 1 instead.

A crucial parameter in the detection of a diversion is the expected scatter in the data. Corrections for ^{242}Cm and other neutron-emitting isotopes are now being successfully applied and reduce the widths of the neutron tolerance limits. With tolerance limits whose widths are 5% to 10% of the average curve through the data, the diverter is generally forced into making small diversions from many assemblies to obtain a significant quantity of plutonium. Even a few small diversions should produce data points outside the tolerance limits because some of the genuine data points would have fallen near the lower tolerance limit.

The fork detector with the analyses of the data as outlined here can readily detect large diversions (20% or more of an assembly). A diverter is forced to make small diversions (less than 10%) from many assemblies to obtain a significant quantity of plutonium. As the number of assemblies needed for a significant quantity increases, the effectiveness of other safeguards systems are enhanced. This places a burden on the diverter that can (a) discourage him from making the large effort necessary to gain a significant quantity of plutonium or ^{235}U or (b) cause him to reveal his actions by simply denying access to the fuel for inspections.

APPENDIX A

"DIVFRAC.BAS"

This computer code in BASIC uses data from Refs. 11 and 17 to calculate effects of removing fuel pins on neutron count rates and gamma-ray values. The water surrounding the assembly of Fig. 1 may contain no boron or 2000 ppm boron.

The user specifies a rectangular region of pins to be "removed." The shape of any other region can be split into rectangular regions, each of which may be studied separately and their effects added.

```
 10   REM    DIVFRAC.BAS
 20   REM
 30   REM  IF A FRACTION OF AN ASSEMBLY IS DIVERTED,
 40   REM  WHAT IS THE EFFECT ON NEUTRON AND GAMMA DATA?
 50   REM
 60   REM   P.M. RINARD, JAN. 1987
 70   REM
 80   REM  NEUTRON CPS PER PIN, CD-WRAPPED
 90   REM  LA-10068-MS, PAGE 50
100   REM   (ROW  1, COL 1)  .  .  .  .  .  .  (ROW  1, COL 8)
110   REM   (ROW  2, COL 1)  .  .  .  .  .  .  (ROW  2, COL 8)
120   REM       .  .                              .
130   REM          .                              .
140   REM   (ROW 15, COL 1)  .  .  .  .  .  .  (ROW 15, COL 8)
150   REM
160   REM
165   REM  0 ppm Boron
170   DATA 119,115,108,103,105,103, 99, 97
180   DATA 146,134,127,121,119,116,111,112
190   DATA 168,155,  0,135,131,  0,127,122
200   DATA 187,170,156,148,140,138,135,  0
210   DATA 196,181,172,157,  0,149,144,142
220   DATA 216,191,  0,163,162,152,150,148
230   DATA 218,199,182,167,161,158,154,152
240   DATA 214,196,178,  0,158,156,152,  0
250   DATA 212,191,175,163,157,152,153,149
260   DATA 198,181,  0,160,152,146,146,143
270   DATA 185,168,159,152,  0,140,138,137
280   DATA 166,152,144,138,135,130,128,  0
290   DATA 140,133,  0,125,119,  0,113,117
300   DATA 122,113,112,110,108,104,102,104
310   DATA 103, 98, 93, 94, 93, 89 ,87, 90
311   REM
312   REM  2000 ppm Boron
313   DATA  79, 71, 61, 52, 47, 43, 42, 39
314   DATA  97, 84, 72, 63, 55, 52, 48, 47
315   DATA 118,101,  0, 72, 64,  0, 57, 54
316   DATA 134,112, 95, 79, 71, 63, 64,  0
317   DATA 148,122,105, 88,  0, 69, 65, 63
318   DATA 157,128,  0, 90, 82, 73, 68, 66
319   DATA 160,130,112, 93, 83, 76, 72, 71
320   DATA 160,131,111,  0, 82, 76, 71,  0
321   DATA 153,130,107, 96, 80, 74, 69, 69
322   DATA 140,121,  0, 87, 77, 71, 66, 66
323   DATA 127,107, 96, 81,  0, 67, 64, 61
324   DATA 116, 97, 85, 73, 65, 62, 59,  0
325   DATA  99, 88,  0, 66, 60,  0, 52, 51
326   DATA  81, 70, 63, 55, 51, 49, 45, 44
327   DATA  66, 58, 49, 48, 43, 40, 39, 38
328   REM
330   DEFINT X,Y,N
340   DIM N(15,15), G(15,15)
350   REM
352   CLS
354   PRINT: PRINT "What boron concetration?"
```

```
355   PRINT "1.    0 ppm"
356   PRINT "2. 2000 ppm"
357   PRINT
358   INPUT BCON
359   RESTORE 170
360   SUMN = 0 : NUMBER = 0
370   FOR Y = 1 TO 15
380     FOR X = 1 TO 8
390       READ N(X,Y)
400       N(16-X,Y)=N(X,Y)
410       SUMN = SUMN + 2 * N(X,Y)
420       IF N(X,Y) <> 0 THEN NUMBER = NUMBER + 2
430     NEXT X
440   NEXT Y
445   IF BCON = 2 THEN BCON = 0 : GOTO 360
450   FOR Y = 1 TO 15
460     SUMN = SUMN - N(8,Y)
470     IF N(8,Y) <> 0 THEN NUMBER = NUMBER - 1
480   NEXT Y
490   REM
500   REM  GAMMA FRACTIONAL CONTRIBUTIONS; SAME ARRAY AS FOR NEUTRONS
510   REM
520   DATA .316,.116,.043,.015,.009,.003,0,0
530   DATA .316,.116,.043,.015,.009,.003,0,0
540   DATA .633,.233,  0,.031,.018,   0,0,0
550   DATA .633,.233,.086,.031,.018,.005,0,0
560   DATA .633,.233,.086,   0,.018,.005,0,0
570   DATA .633,.233,   0,.031,.018,.005,0,0
580   DATA .633,.233,.086,.031,.018,.005,0,0
590   DATA .633,.233,.086,   0,.018,.005,0,0
600   DATA .633,.233,.086,.031,.018,.005,0,0
610   DATA .633,.233,   0,.031,.018,.005,0,0
620   DATA .633,.233,.086,   0,.018,.005,0,0
630   DATA .633,.233,.086,.031,.018,.005,0,0
640   DATA .633,.233,   0,.031,.018,   0,0,0
650   DATA .316,.116,.043,.015,.009,.003,0,0
660   DATA .316,.116,.043,.015,.009,.003,0,0
670   REM
680   SUMG = 0
685   RESTORE 520
690   FOR Y = 1 TO 15
700     FOR X = 1 TO 8
710       READ G(X,Y)
720       G(16-X,Y)=G(X,Y)
730       SUMG = SUMG + 2*G(X,Y)
740     NEXT X
750   NEXT Y
760   FOR Y = 1 TO 15
770     SUMG = SUMG - G(8,Y)
780   NEXT Y
790   REM
800   REM  ENTER ROWS AND COLUMNS OF DIVERSION
810   REM
820   CLS
830   PRINT "Terminate code with a negative 'Smallest Row'" : PRINT
```

```
 840   INPUT "Smallest row of diversion:  ";Y1
 850   IF Y1 < 0 THEN END
 860   INPUT " Largest row of diversion:  ";Y2
 870   PRINT
 880   INPUT "Smallest column of diversion:  ";X1
 890   INPUT " Largest column of diversion:  ";X2
 900   REM
 910   SMN = 0 : NUMBER1 = 0 : SMG = 0
 920   FOR Y = Y1 TO Y2
 930     FOR X = X1 TO X2
 940       SMN = SMN + N(X,Y)
 950       SMG = SMG + G(X,Y)
 960       IF N(X,Y) <> 0 THEN NUMBER1 = NUMBER1 + 1
 970     NEXT X
 980   NEXT Y
 990   REM
1000   CLS
1010   FMASS = (NUMBER - NUMBER1)/NUMBER
1020   PRINT "Rows = ";Y1;"-";Y2;"     COLS = ";X1;"-"X2"
1030   REM
1040   PRINT "  Mass fraction removed = ";NUMBER1/NUMBER
1050   PRINT "Mass fraction remaining = ";FMASS
1060   PRINT "  Fractional drop in neutron cps = ";SMN/SUMN
1070   PRINT "Fraction of original neutron cps = ";(SUMN-SMN)/SUMN
1080   REM
1090   PRINT "  Fractional drop in gammas = ";SMG/SUMG
1100   PRINT "Fraction of original gammas = ";(SUMG-SMG)/SUMG
1110   PRINT
1111   PRINT SUMN
1120   PRINT
1130   GOTO 840
```

APPENDIX B

UNCERTAINTIES OF PARAMETERS IN POWER-LAW RELATIONS

When a power-law relation, $y = ax^b$, is fit to data, it frequently seems that the uncertainty in the parameter a is very large and must be the dominant cause of the uncertainty in y when errors are propagated. With this function it is actually more likely that the uncertainties in a and b contribute nearly equally to the uncertainty in y.

From the variances in a and b, σ_a^2 and σ_b^2, and their covariance, σ_{ab}, the relative uncertainty in y can be calculated:

$$(\sigma_y/y)^2 = (\sigma_a/a)^2 + [\sigma_b \ln(x)]^2 + 2\,\sigma_{ab} \ln(x)/a \quad . \tag{B-1}$$

If the second term were $(\sigma_b/b)^2$, a large (σ_a/a) would indeed dominate the uncertainty in y. But in practice the value of $[\sigma_b \ln(x)]^2$ is rather similar to $(\sigma_a/a)^2$.

Consider the neutron data from Tihange (Refs. 8 and 9) applied to the power law $n = \alpha E^{\beta}$. Using the exposure E in GWd/tU and the neutron count rate in counts/s, it is found that $\alpha = (0.00377 \pm 0.0021)$ and $\beta = (3.327 \pm 0.17)$; the covariance is -3.518×10^{-4}. The relative uncertainty in α is much greater than that of β. Equation (B-1) yields this relative variance in count rate:

$$(\sigma_n/n)^2 = 0.308 + 0.02885\,[\ln(E)]^2 - 0.1866 \ln(E) \quad . \tag{B-2}$$

For an exposure of 30 GWd/tU,

$$(\sigma_n/n)^2 = 0.308 + 0.334 - 0.635 = 0.007 \quad . \tag{B-3}$$

The important point here is that the first two terms, with σ_α and σ_β, contribute very nearly equally. With E = 20 GWd/tU, their values are again quite close, namely 0.308 and 0.259, respectively.

For the gamma-ray case at Tihange, with the exposure still in gigawatt-days per ton of uranium and the cooling time in days, assume $(\gamma/E) = aT^{-b}$. The value of a is (9803 ± 1700), whereas b is (0.883 ± 0.026); the covariance is -43.42. Equation (B-1) takes on this form:

$$[\sigma_{\gamma/E}/(\gamma/E)]^2 = 0.0299 + 6.62 \times 10^{-4}\ [\ln(T)]^2 - 0.886\ \ln(T) \quad . \qquad \text{(B-4)}$$

For a cooling time of 1000 days,

$$[\sigma_{\gamma/E}/(\gamma/E)]^2 = 0.0299 + 0.0316 - 0.0612 = 0.0004 \quad . \qquad \text{(B-5)}$$

The values of the first two terms are again quite similar. This similarity exists over a wide range of cooling times because of the logarithmic function of T.

If the power-law relation is inverted to $x = (y/a)^{1/b}$ and errors are propagated, this relation is found:

$$b^2\ (\sigma_x/x)^2 = (\sigma_y/y)^2 + (\sigma_a/a)^2 + (\sigma_b/b)^2\ [\ln(y/a)]^2$$

$$+\ 2\ \sigma_{ab}\ \frac{\ln(y/a)}{ab} \quad . \qquad \text{(B-6)}$$

Typical magnitudes of the second and third terms are of interest here.

For Tihange neutron data, the second term is again 0.308; the third term is about 0.07 for neutron rates between 500 and 1000 counts/s. The α uncertainty contributes about four times the β uncertainty term, but this is much less than would be found had the third term been $(\sigma_\beta/\beta)^2$.

With Tihange gamma-ray data, the second term is 0.0299 and the third term with $\sigma/E = 30$ is 0.0285. The two terms are again nearly equal.

Although the uncertainty in the a factor of ax^b can appear unreasonably large, its effect on the overall uncertainty from propagation of errors is quite reasonable.

APPENDIX C

NEWTON-RAPHSON SOLUTION FOR A ROOT

The roots of a function may be found with the iterative process given by Newton and Raphson.[38] Some initial estimate of a root is needed, and this affects which root will be found and the number of iterations required.

The Newton-Raphson method calculates a new estimate x_{new} from the previous (old) estimate x_{old} with this formula:

$$x_{new} = x_{old} - f'(x_{old})/f(x_{old}) \quad , \tag{C-1}$$

where f is the function whose roots are to be found and f' is its derivative with respect to x.

A computer code is given below to assist the reader in applying this technique. It is written in a generic BASIC. The function f must be inserted at the place marked in the code. The derivative f' is not required because it is calculated numerically. The iterations are terminated when x_{new} and x_{old} differ by less than 0.01%; this criteria can be changed in the code if necessary.

```
 10   REM   NEWTON-RAPHSON SOLUTION FOR ROOT OF AN EQUATION
 20   REM
 30   REM   NEWRAP.BAS
 40   REM
 50   REM   PHILLIP M. RINARD
 60   REM   MARCH 23, 1987
 70   REM
 80   REM
 90   REM  PUT THE FUNCTION AFTER THE EQUAL SIGN IN THE LINE BELOW:
100   DEF FNFUNC = 10*X - 3
110   REM
120   CLS
130   LOCATE 10,10
140   PRINT "What is an estimate of the root?"
150   LOCATE 12,10
160   INPUT X
170   XOLD = X
180   REM
190   GOSUB 340
200   XNEW = XOLD - FNFUNC/DERIV
210   REM  ITERATIONS STOP AT 0.01% ACCURACY, AS SET IN THE LINE BELOW:
220   IF ABS((XNEW - XOLD)/XOLD) < .0001 THEN GOTO 290
230   XOLD = XNEW
240   X = XNEW
250   PRINT XNEW, DERIV
260   GOTO 190
270   REM
280   PRINT : PRINT : PRINT SPC(10);
290   PRINT : PRINT : PRINT SPC(10);
300   PRINT "Root = ";XNEW
310   END
320   REM
330   REM  CALCULATE THE DERIVATIVE NUMERICALLY
340   XSAVE = X
350   FRAC = .001
360   DIFF = FRAC * XSAVE
370   IF DIFF = 0 THEN DIFF = FRAC
380   X = X*(1+FRAC/2)
390   IF X = 0 THEN X=FRAC/2
400   VAL1 = FNFUNC
410   X = X*(1-FRAC/2)/(1+FRAC/2)
420   IF X=0 THEN X = -FRAC/2
430   VAL2 = FNFUNC
440   DERIV = (VAL1 - VAL2)/DIFF
450   X = XSAVE
460   RETURN
```

REFERENCES

1. "The Structure and Content of Agreements Between the Agency and States Required in Connection with the Treaty on the NonProliferation of Nuclear Weapons," International Atomic Energy Agency document INFCIRC/153 (corrected) (June 1972), p. 9.

2. "The Present Status of IAEA Safeguards on Nuclear Fuel Cycle Facilities," The IAEA Bulletin, Vol. 22, No. 3/4 (August 1980).

3. Safeguards Manual, Introduction and SMO, Department of Safeguards, International Atomic Energy Agency (November 30, 1984), Part SMO, Chap. 2, p. 2.

4. P. M. Tempus, "Problems and Progress in International Safeguards," Journal of the Institute of Nuclear Materials Management, Volume XV, Number 1, October 1986, page 32.

5. G. E. Bosler, H. O. Menlove, J. K. Halbig, N. Nicholson, L. Cowder, P. Ikonomou, J. D. Luoma, W. S. Wilkerson, H. Arvanitakis, and R. Tropasso, "Physical Inventory Verification Exercise at a Light-Water Reactor Facility," Los Alamos National Laboratory report LA-10695-MS (ISPO-248) (April 1986).

6. P. M. Rinard and G. E. Bosler, "BWR Spent-Fuel Measurements with ION-1/Fork Detector and a Calorimeter," Los Alamos National Laboratory report LA-10758-MS (August 1986).

7. R. Schenkel, G. Bosler, and S. Klosterbuer, "Demonstration of Spent-Fuel Measurement Equipment at KWO Obrigheim Facility," Commission of the European Communities Nuclear Science and Technology report EUR 9877 EN (1985).

8. R. Carchon, G. Smaers, G. P. D. Verrecchia, R. Arlt, I. Stoyanova, G. E. Bosler, and J. Satinet, "NDA Measurements on Spent Fuel Assemblies at Tihange 1 by Means of the ION 1/Fork," Studiecentrum Voor Kernenergie/Centre d'Etude de l'Energie Nucleaire-Mol report BLG 589 (June 1986).

9. R. Carchon, G. Smaers, G. P. D. Verrecchia, R. Arlt, I. Stoyanova, G. E. Bosler, and J. Satinet, "ION 1/Fork Measurements on PWR Spent Fuel Assemblies," International Atomic Energy Agency, Proceedings of an International Symposium on Nuclear Material Safeguards, Vienna, Austria, November 10-14, 1986, IAEA-SM-293/73, p. 599.

10. M. Tarvainen and M. Riihonen, "Spent Fuel Measurements at Loviisa Nuclear Power Station, May, 1982," Finnish Centre for Radiation and Nuclear Safety report STUK-A49 (February 1984).

11. P. M. Rinard, "Neutron Measurements in Borated Water for PWR Fuel Inspections," Los Alamos National Laboratory report LA-10068-MS (ISPO-223) (July 1984).

12. M. Tarvainen, G. af Ekenstam, R. Arlt, B. Barnes, J. Halbig, and J. Phillips, "NonDestructive Analysis of WWER-440 Spent Fuel Using Gamma and Neutron Measurements," International Atomic Energy Agency, Nuclear Safeguards Technology 1986, Proceedings of an International Symposium on Nuclear Material Safeguards, Vienna, Austria, November 10-14, 1986, IAEA-SM-293/110, p. 571.

13. J. R. Phillips, G. E. Bosler, J. K. Halbig, S. F. Klosterbuer, and H. O. Menlove, "Nondestructive Verification with Minimal Movement of Irradiated Light-Water Reactor Fuel Assemblies," Los Alamos National Laboratory report LA-9438-MS (ISPO-172) (October 1982).

14. J. R. Phillips, J. K. Halbig, D. M. Lee, S. E. Beach, T. R. Bement, E. Dermendjiev, C. R. Hatcher, K. Kaieda, and E. G. Medina, "Application of Nondestructive Gamma-Ray and Neutron Techniques for the Safeguarding of Irradiated Fuel Materials," Los Alamos National Laboratory report LA-8212 (ISPO-77) (May 1980).

15. G. E. Bosler, J. R. Phillips, W. B. Wilson, R. J. LaBauve, and T. R. England, "Production of Actinide Isotopes in Simulated PWR Fuel and Their Influence on Inherent Neutron Emission," Los Alamos National Laboratory report LA-9343 (July 1982).

16. P. M. Rinard, "A Spent-Fuel Cooling Curve for Safeguards Applications of Gross-Gamma Measurements," Los Alamos National Laboratory report LA-9757-MS (ISPO-195) (April 1983).

17. J. R. Phillips and G. E. Bosler, "Calculated Response Contributions of Gamma Rays Emitted From Fuel Pins in an Irradiated PWR Fuel Assembly," Los Alamos National Laboratory report LA-9837-MS (August 1983).

18. S. Salmenhaara and M. Tarvainen, "Nondestructive Measurements with a WWER-440 Fuel Assembly Model Using Neutron and Gamma Sources," Finnish Centre for Radiation and Nuclear Safety report STUK-A69 (February 1987).

19. S. Salmenhaara, P. Keikko, A. Ala-Ranta, T. Saarenpaa, and M. Tarvainen, "Gamma and Neutron Measurements with a WWER-440 Assembly Model," International Atomic Energy Agency, Nuclear Safeguards Technology 1986, Proceedings of an International Symposium on Nuclear Material Safeguards, Vienna, Austria, November 10-14, 1986, IAEA-SM-293/12, p. 537.

20. W. Moller, M. Burmester and R. Arlt, "Actinide Isotope Content and Associated Neutron Emission of WWER-440 Spent Fuel," International Atomic Energy Agency, Nuclear Safeguards Technology 1986, Proceedings of an International Symposium on Nuclear Material Safeguards, Vienna, Austria, November 10-14, 1986, IAEA-SM-293/87, p. 553.

21. S. Rohar, P. Liptak, V. Petenyi, R. Arlt and E. Dermendijev, "Procedure for Quantitative Evaluation of Passive Neutron Assay of WWER-440 Spent Fuel Assemblies," International Atomic Energy Agency, Nuclear Safeguards Technology 1986, Proceedings of an International Symposium on Nuclear Material Safeguards, Vienna, Austria, November 10-14, 1986, IAEA-SM-293/134, p. 585.

22. G. E. Bosler, Los Alamos National Laboratory memorandum N-1-87-611 to G. Tributsch, et al., June 30, 1987.

23. P. M. Rinard, "Gamma Doses from Irradiated Assemblies Under Water," Los Alamos Scientific Laboratory report LA-7914-MS (July 1979).

24. H. O. Menlove, "Description and Performance Characteristics for the Neutron Coincidence Collar for the Verification of Reactor Fuel Assemblies," Los Alamos National Laboratory report LA-8939-MS (ISPO-142) (August 1981).

25. H. O. Menlove and A. Keddar, "Field Test and Evaluation of the Passive Neutron Coincidence Collar for Prototype Fast Reactor Fuel Subassemblies," Los Alamos National Laboratory report LA-9449-MS (ISPO-176) (August 1982).

26. H. O. Menlove, "Passive/Active Coincidence Collar for Total Plutonium Measurement of MOX Fuel Assemblies," Los Alamos National Laboratory report LA-9288-MS (ISPO-170) (May 1982).

27. H. O. Menlove and A. Keddar, "Field Test and Evaluation of the IAEA Coincidence Collar for the Measurement of Unirradiated BWR Fuel Assemblies," Los Alamos National Laboratory report LA-9375-MS (ISPO-174) (December 1982).

28. R. Sher, "Active Neutron Coincidence Counting for the Assay of MTR Fuel Elements," Los Alamos National Laboratory report LA-9665-MS (ISPO-186) (February 1983).

29. H. O. Menlove, M. A. S. Marzo, S. G. de Almeida, M. C. de Almeida, L. P. M. Moitta, L. F. Conti, and J. R. T. de Paiva, "In-Plant Test and Evaluation of the Neutron Collar for Verification of PWR Fuel Assemblies at Resende, Brazil," Los Alamos National Laboratory report LA-10562-MS (November 1985).

30. H. O. Menlove and J. E. Pieper, "Neutron Collar Calibration for Assay of LWR Fuel Assemblies," Los Alamos National Laboratory report LA-10827-MS (March 1987).

31. T. R. England, W. B. Wilson, and M. G. Stamatelatos, "Fission Produce Data for Thermal Reactors, Part 2: Users Manual for EPRI-CINDER code and Data," Electric Power Research Institute report EPRI NP-356, Part 2 (December 1976). Also published as Los Alamos Scientific Laboratory report LA-6746-MS (December 1976).

32. T. R. England, "CINDER - A One-Point Depletion and Fission Product Program," Westinghouse Electric Corporation report WAPD-TM-334 (1962, Rev. 1964).

33. T. R. England, R. Wilczynski, and N. L. Whittemore, "CINDER-7: An Interim Report for Users," Los Alamos Scientific Laboratory report LA-5885-MS (April 1975).

SPENT FUEL MANAGEMENT

SEMINAR IX

SPECIAL BURNUP CREDIT SESSION

INSTITUTE OF NUCLEAR MATERIALS MANAGEMENT

JANUARY 15-17, 1992
WASHINGTON, D.C.

ENCLOSURE 5

Overview of Burnup Credit Issues*

SAND91-2841C
TTC-1157

T. L. Sanders
K. D. Seager
R. I. Ewing
Sandia National Laboratories**
Albuquerque, NM

Introduction

A traditional assumption used in evaluating the criticality safety of a spent fuel storage or transport cask is that the spent fuel is as reactive as fresh fuel. This is known as the "fresh fuel assumption." This assumption avoids a number of calculational and verification problems, but takes a heavy toll in decreased efficiency. An alternative to the fresh fuel assumption is called "burnup credit." That is, the reduced reactivity of spent fuel that occurs from the net depletion of fissile nuclides and the net increase in fission and activation product neutron absorbers (poisons) is considered.

Burnup credit has been successfully applied to spent fuel storage pools in the U.S., resulting in increased capacity and permitting the storage of spent fuel with higher initial enrichments. Both of the commercial transport cask designers supporting the Cask Systems Development Program (CSDP) of the U.S. Department of Energy's Office of Civilian Radioactive Waste Management (OCRWM) - General Atomic and Babcock & Wilcox - have cask designs incorporating burnup credit.

The implementation of burnup credit in the design of transport casks must be accomplished while still maintaining or enhancing individual cask safety and system safety. It is recognized that the use of burnup credit will increase the amount of unacceptable fuel available for misloading. To implement a burnup credit design and operational strategy, additional sources of uncertainties and issues must be identified and quantified, and steps taken to reduce those uncertainties.

---

*This work performed at Sandia National Laboratories, Albuquerque, New Mexico, supported by the United States Department of Energy under Contract No. DE-AC04-76DP00789.
**A United States Department of Energy Facility.

Criticality Safety

The criticality safety of a spent fuel system depends on the reactivity of that spent fuel. Spent fuel reactivity is a function of four variables: (1) the initial enrichment of the fuel, (2) the geometry of the fresh fuel, (3) the in-core burnup history of the fuel, and (4) the decay time since the fuel was discharged as "spent" from the operating reactor. From a design basis perspective, the reactivity of a given system can be held constant by varying the magnitudes of burnup and age requirements to compensate for changes in initial enrichment for a given fuel geometry.

The fresh fuel assumption essentially forces reactivity to be considered a function of a single variable, i.e., initial enrichment. The fresh fuel assumption results in a considerable criticality safety margin in individual casks. Requiring the cask criticality designs to be based on the maximum available initial enrichment of the fresh fuel provides sufficient excess design margin to preclude a criticality event from occurring under any foreseeable circumstance. This requirement implies that a misloading error is sufficiently probable to compromise criticality safety in transport. While the need for a criticality safety design margin is acknowledged, the actual margin provided by the fresh fuel assumption is not explicitly defined, and there are no explicit criticality safety controls on the fuel loading operation. The actual fuel loaded could range from fresh to high burnup fuel.

Criticality can only occur in an array of light-water reactor (LWR) fuel if (1) sufficient fissile material is available in a near optimum geometry, (2) a moderator is present, and (3) compromise of avialable engineered the criticality control features. No array of LWR fuel can achieve criticality without water present in the array.

One governing "ground rule" provides the basis for assuring criticality safety in all nuclear systems. No single event, loss, or failure, whether operational or component-related, should result in reduced criticality safety. Under the fresh fuel assumption, the cask criticality control system consists of a single "external" component that includes neutron absorbers (poisons) incorporated in the cask or basket web, void spaces or "flux traps" incorporated in the basket for moderator requirements, and structural support members. These features are "external" to the fuel. Flux traps are required to ensure that any neutron absorptions that occur do so in the external poison rather than the fuel. When a cask is flooded, the water contained in the flux traps will thermalize neutrons in the vicinity of the external absorbers, thus the probability is high they will be absorbed in the basket poison. These basket features are "hardware" subcomponents of the criticality control system. Loss of any hardware subcomponent could render the total system

ineffective or, at a minimum, result in reduced reliability. This can occur because under current practice, there are no controls placed on the moderator and fuel components.

An additional safety margin results from other aspects of the design basis. For example, the criticality design basis normally assumes maximum water moderation and reflection, though shipments are intended to be dry. This results in additional negative reactivity (30 to 40%) in the cask that is ignored in the criticality design. Also, the reactivity of the actual fuel loaded should be significantly less than the design basis fresh fuel values unless, of course, fresh fuel or slightly burned failed fuel is loaded into the cask. The reliability of the criticality safety margin associated with the fresh fuel assumption is generally assumed to be independent of the reliability of fuel loading operations. This is indeed true if future fuel is designed to the same reactivity limit over the life of the cask. If future fuel is made more reactive (higher initial enrichment), the system is no longer passive, and active operational requirements will be necessary to preclude loading nonspecification fuel into the cask. Nonspecification fuel is any fuel (fresh or irradiated) that exceeds the design basis reactivity. While the system can be thought of as passive with respect to fuel-loading errors, there remain numerous other design, development, fabrication, and operational activities with potential for human error. These error probabilities are very small; however, when combined, there remains a nonzero probability that the safety margin or the system reliability could be less than expected.

Regardless of the design basis, three individual events are required to result in a reduced subcritical margin or worse, a criticality accident during cask loading. The fuel reactivity margin could be less than expected if specification fresh or slightly burned fuel or nonspecification fresh fuel are loaded into the cask. Excessive fuel reactivity and inadequate criticality controls in a cask, combined with an absence of soluble poison in pool water, could result in reduced margin or a critical configuration as illustrated in Figure 1.

The likelihood of excessive fuel reactivity occurring for the fresh fuel design assumption is believed to be quite small, because the system criticality safety is virtually independent of fuel loading errors if fuel designs do not change (i.e., become more reactive) over the useful life of the cask. This situation already exists because current generation casks were designed for maximum fuel enrichments about 3.0 to 3.8 wt % U-235, and fresh fuel with enrichments up to 4.5 wt % U-235 are available at numerous reactor facilities. Future fuel designs are expected to be based on even higher enrichments and possibly varying enrichments within an assembly design.

Inadequate criticality controls can result from design error, defective fabrication processes, incorrect cask selection, or use of a damaged cask or basket, as illustrated by the fault tree in

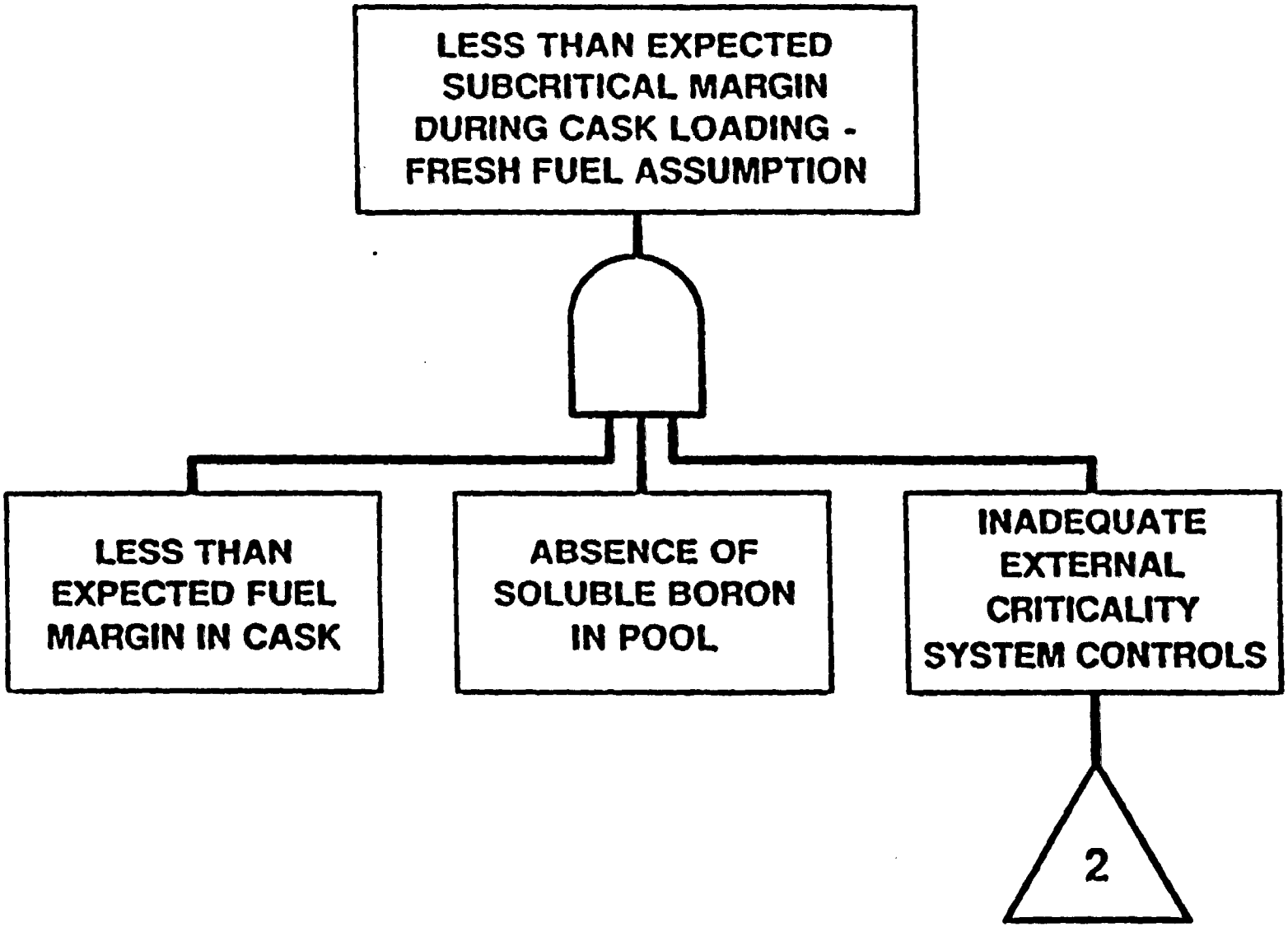

Figure 1. Factors Affecting the Criticality Safety Margin During Cask Loading for the Fresh-Fuel Assumption Case

Figure 2. Any of these could affect the criticality safety margin independently. While soluble poison is generally present in pool water at pressurized water reactor (PWR) plants, its reactivity effect may vary from site to site, and its concentration is not controlled. Soluble poison control is not used at boiling water reactor (BWR) plants.

Error sources which could lead to a defective cask design or fabrication are illustrated by the fault tree in Figure 3. A faulty component can result from incorrect fabrication procedures or errors during the fabrication process. An incorrect fabrication procedure may be developed because of design or analysis errors. These can occur because of analyst error, an error in the fuel enrichment chosen for the design basis, or errors associated with benchmark or experimental data or methodology. Fabrication errors can also result from inadequate material inspections or a procedural error in the inspection or forming processes. Finally, for a defective design or hardware to be placed in service, a faulty acceptance test must fail to detect the defects.

For criticality to occur during transport, a moderator and fissile material must be present in the cask in a criticality geometry. The dominating events that could result in a criticality accident during cask transport are independent of the particular fuel reactivity design basis. During normal transport, sufficient fuel reactivity, inadequate negative reactivity controls, and a water-flooded cask containing no soluble poison are required. Again, an LWR fuel array cannot achieve criticality unless a moderator is present. These conditions are identical to the minimum requirements during cask loading.

The fault tree in Figure 4 illustrates the conditions necessary for criticality to occur during a transport accident. Severe damage to external criticality control features such as the basket supports, absorbers, or flux traps could render any fuel design margin inadequate. Excessive fuel reactivity could result from either rearrangement during an accident or preshipment loading errors. Presence of a moderator could arise from two situations; an accident could occur that leaves a cask where a moderator is present (such as submerged in a river), or, the cask could begin transport in a moderated (flooded) condition. Similarly, moderator in-leakage can only occur in two ways. First, operator error during system assembly could result in an improper seal, or second, the containment could be severely ruptured during an accident. The net result of each path is a reduction in the subcritical margin of the cask/fuel system.

It should be noted that an accidental criticality event in transport requires at least two unlikely, independent, and concurrent or sequential changes in the conditions essential to criticality safety. Because LWR fuel must be moderated to achieve criticality, the most significant source of criticality safety comes from the requirement that the accident could result in a moderated

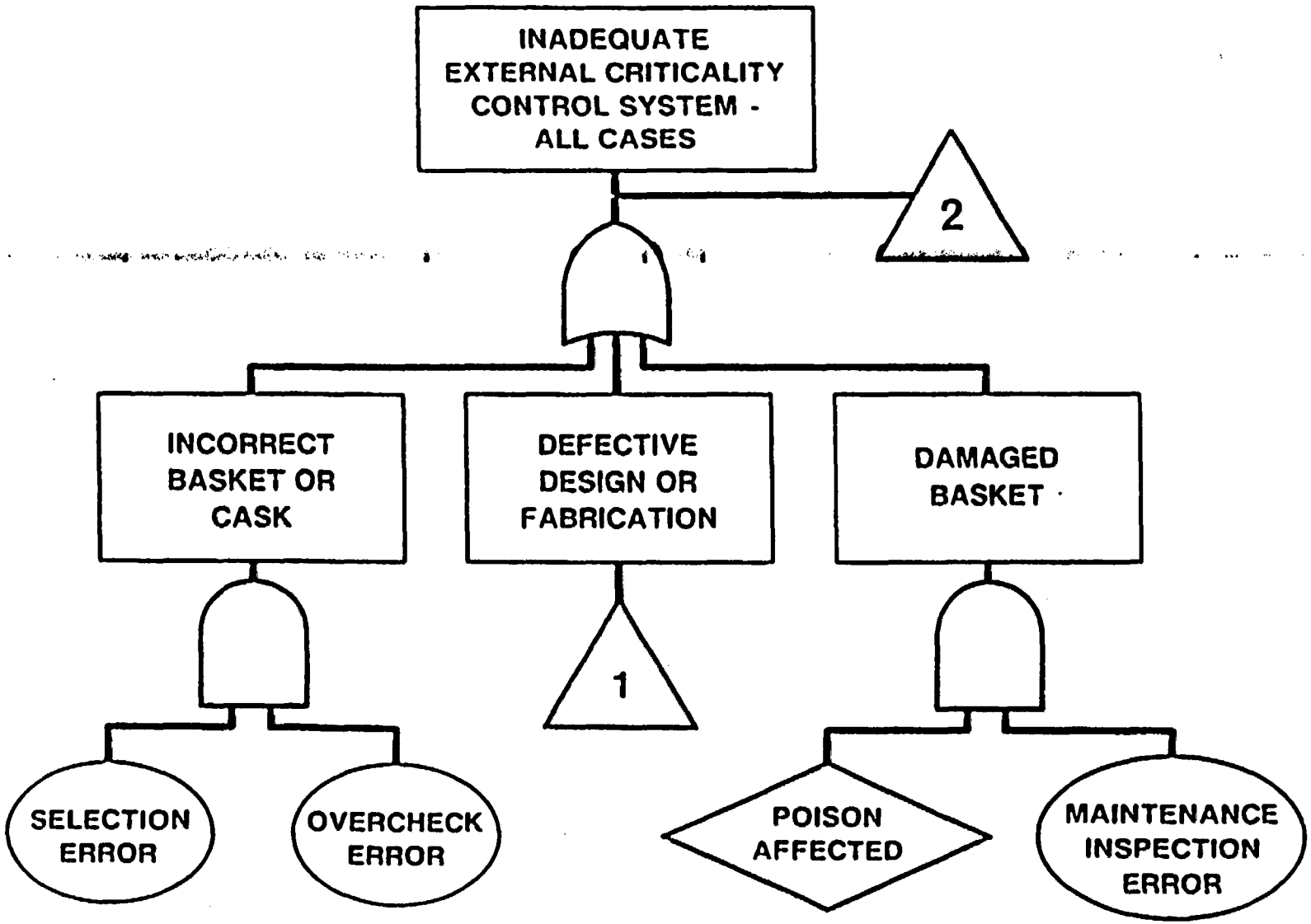

Figure 2. Factors Affecting the Reliability of the External Criticality Control System

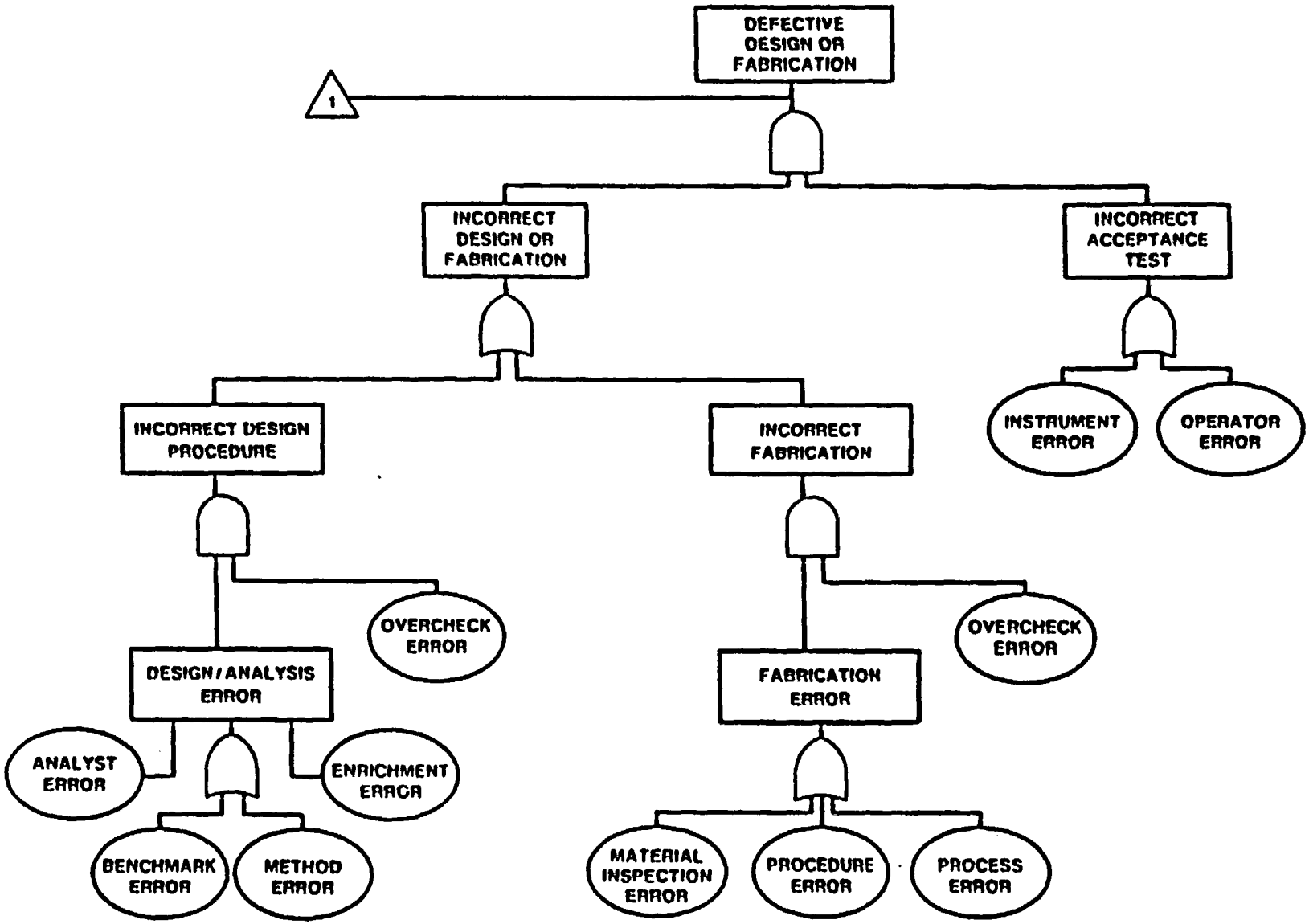

Figure 3. Failure Modes for a Defective Cask Design or Fabrication

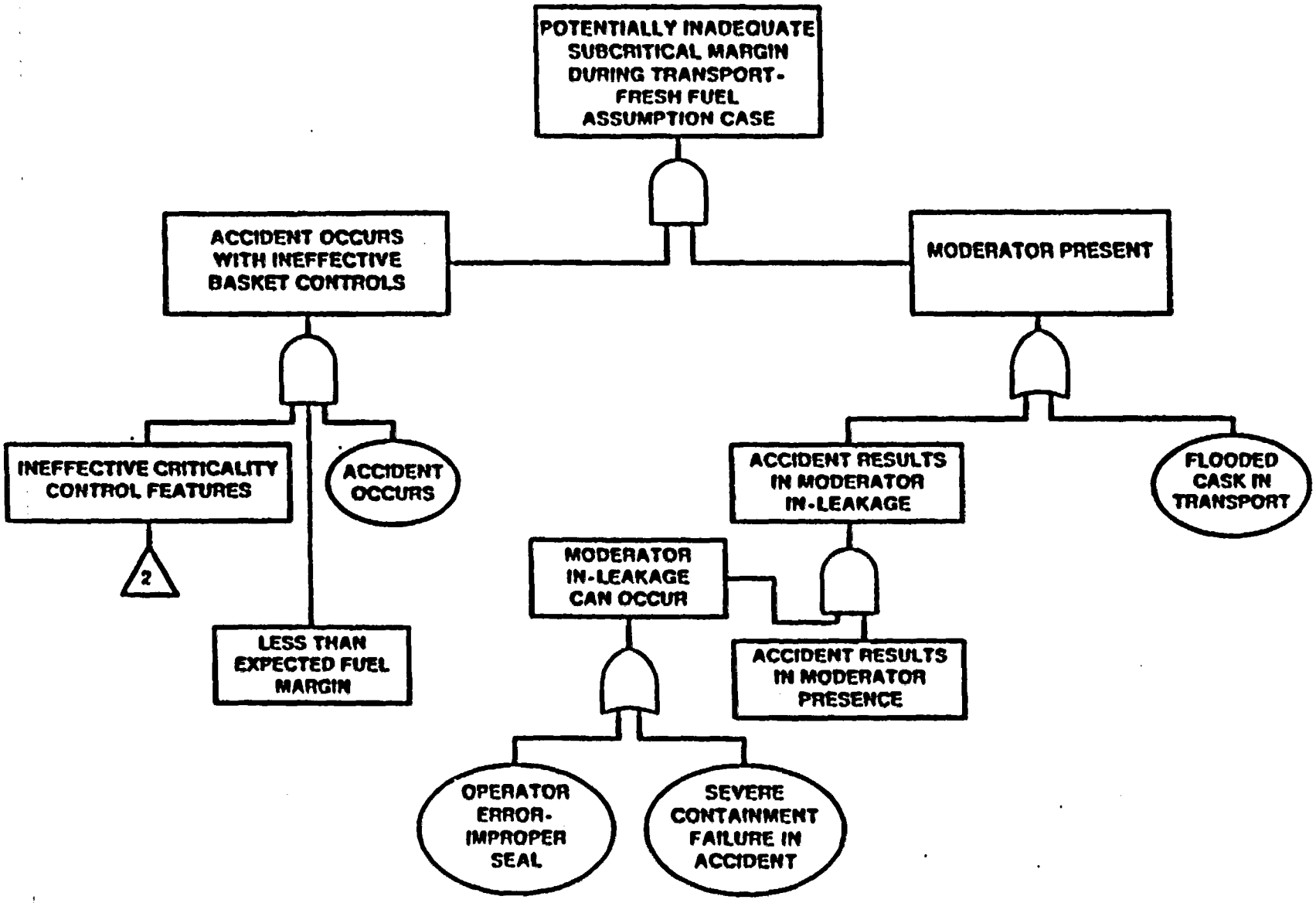

Figure 4. Factors Affecting Criticality Safety During Transport for the Fresh-Fuel Assumption Case

condition. If a cask in indeed "dry" and sealed properly before shipment, three independent events are required for criticality to be credible: first, an accident; second, severe containment failure; and third, moderator presence.

Burnup Credit Issues

In the case of burnup credit, the criticality control system consists of two separate components. The first is an "external" control component, similar to that used in a fresh fuel assumption design basis, that includes poisons in the cask or basket web and geometric spacing and support. The second is an "internal" control component - - the loaded spent fuel. Burned fuel reduces external criticality control requirements due to net depletion of the fissile material and the production of poisons.

From a broad perspective, the major events that could lead to reduced subcritical margin during cask loading or transport are unchanged with burnup credit. However, the number of opportunities for error leading to one of those events, excessive fuel reactivity, will increase because the populations of nonspecification fuel will be larger and the characteristics of spent fuel must be included in the cask design basis. These affect the error sources in Figure 2.

The isotopic composition of the spent fuel is the critical element in determining fuel reactivity. The capability of the calculational codes to predict accurately isotopic composition must be validated by comparison to experimental isotope assays - chemical and radiochemical - of spent fuel rods. The fissile and dominant actinide isotopes have well-characterized yields and cross-sections because of their importance to reactor control. Only a few fission products need to be considered because of their dominance of neutron absorption.

As illustrated in Figure 5, exceeding fuel reactivity limits could result from a fuel-loading error, an error in the analysis used to develop fuel-loading procedures, or an error in the burnup characterization of the spent fuel (from error in in-core measurements or subsequent analyses). Events that can lead to in-core analysis error are illustrated in Figure 6. An erroneous loading procedure (Figure 7) could occur if nonspecification fuel is included in the spent fuel inventory. Such an error must be repeated several times (i.e., several wrong assemblies must be chosen) to achieve sufficient excessive fuel reactivity for criticality to occur. For example, analyses indicated that at least 3 to 4 misloadings of highly enriched fresh PWR fuel are required to approach critical in a burnup credit spent fuel cask. A system assembly error (Figure 8) could result if incorrect fuel is loaded, or an incorrect cask or basket is used. Loading errors affect criticality safety only if

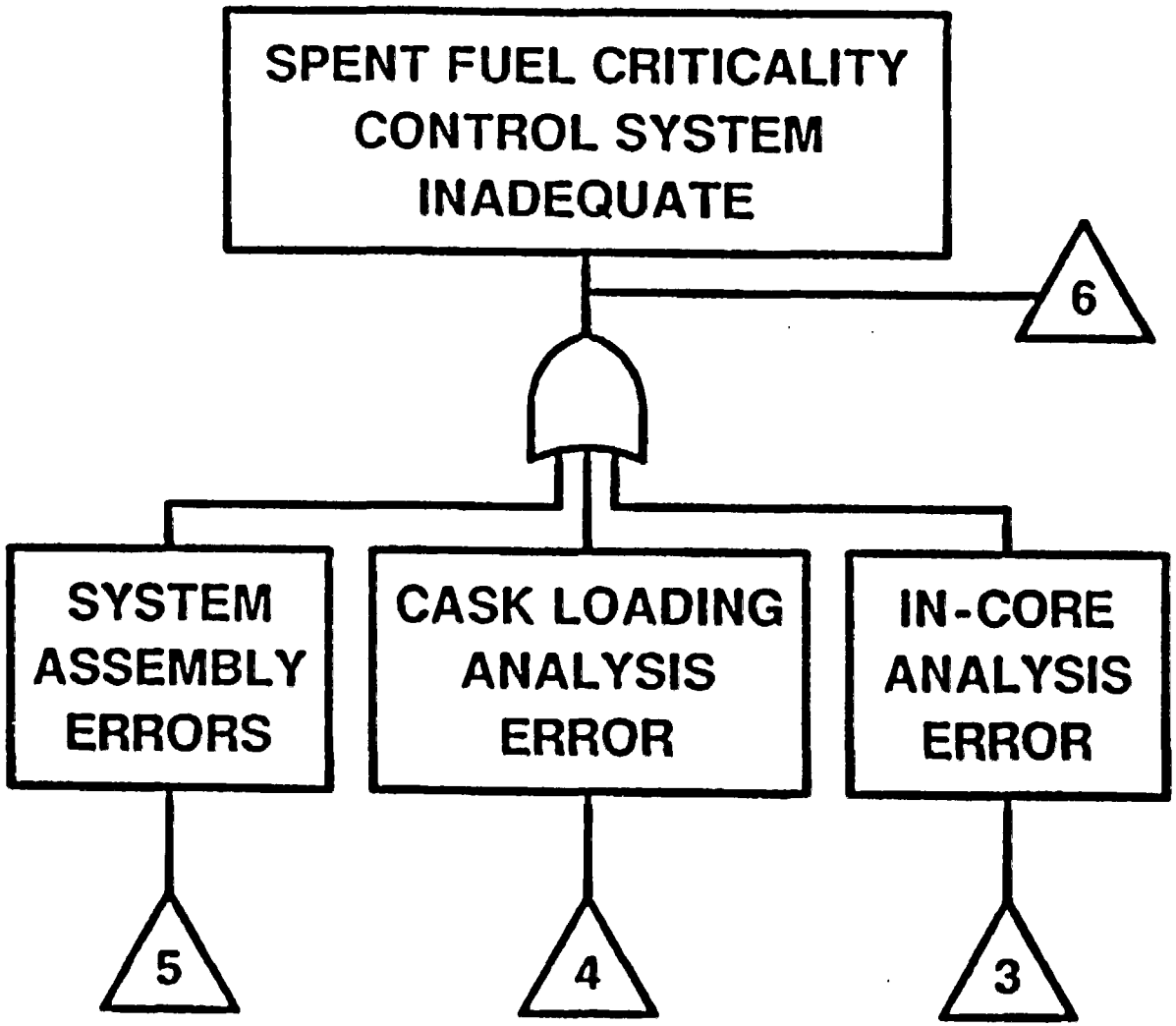

Figure 5. Failure Modes Affecting the Reliability of the Spent-Fuel Criticality Control System

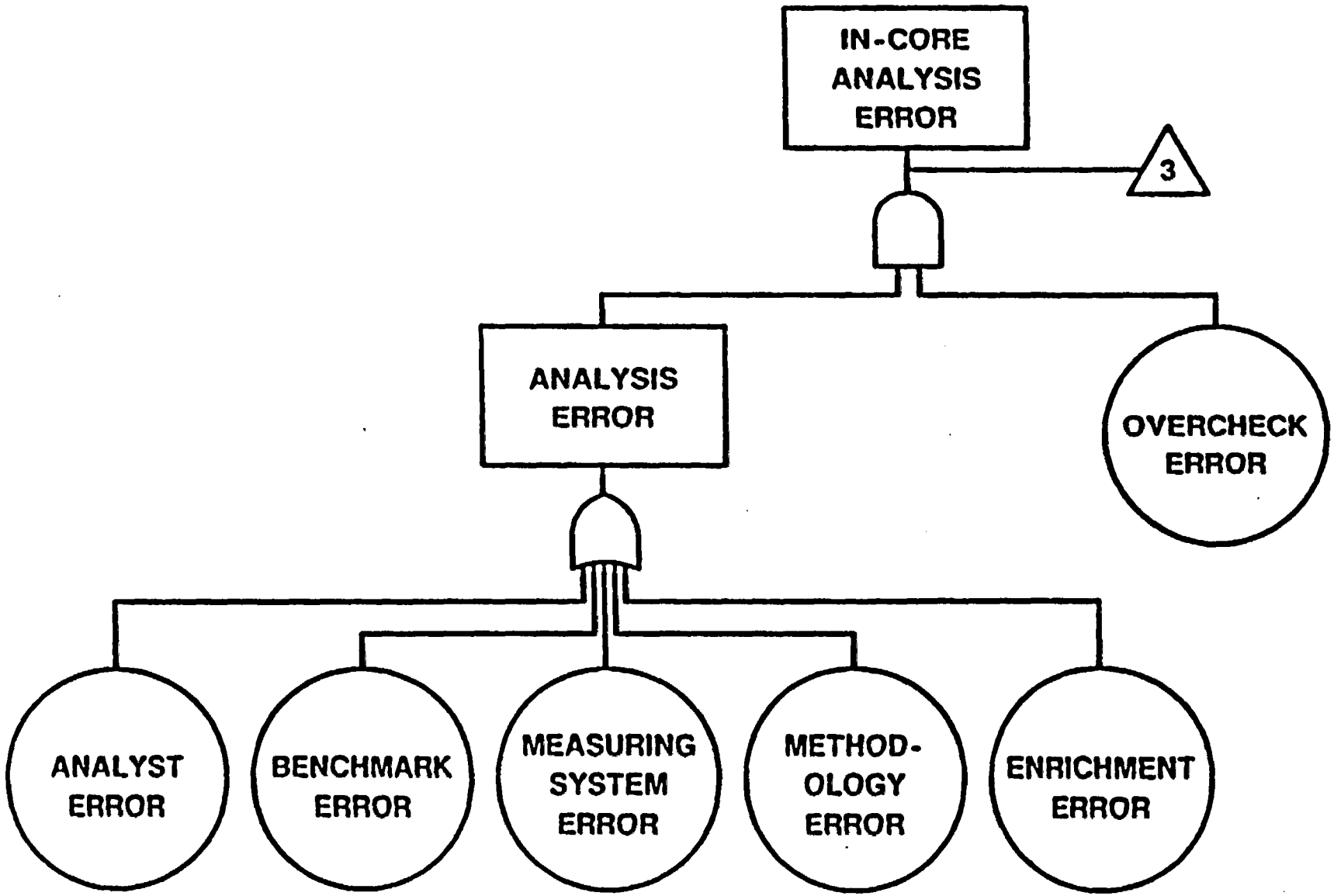

Figure 6. Failure Modes Affecting Spent-Fuel Characterization

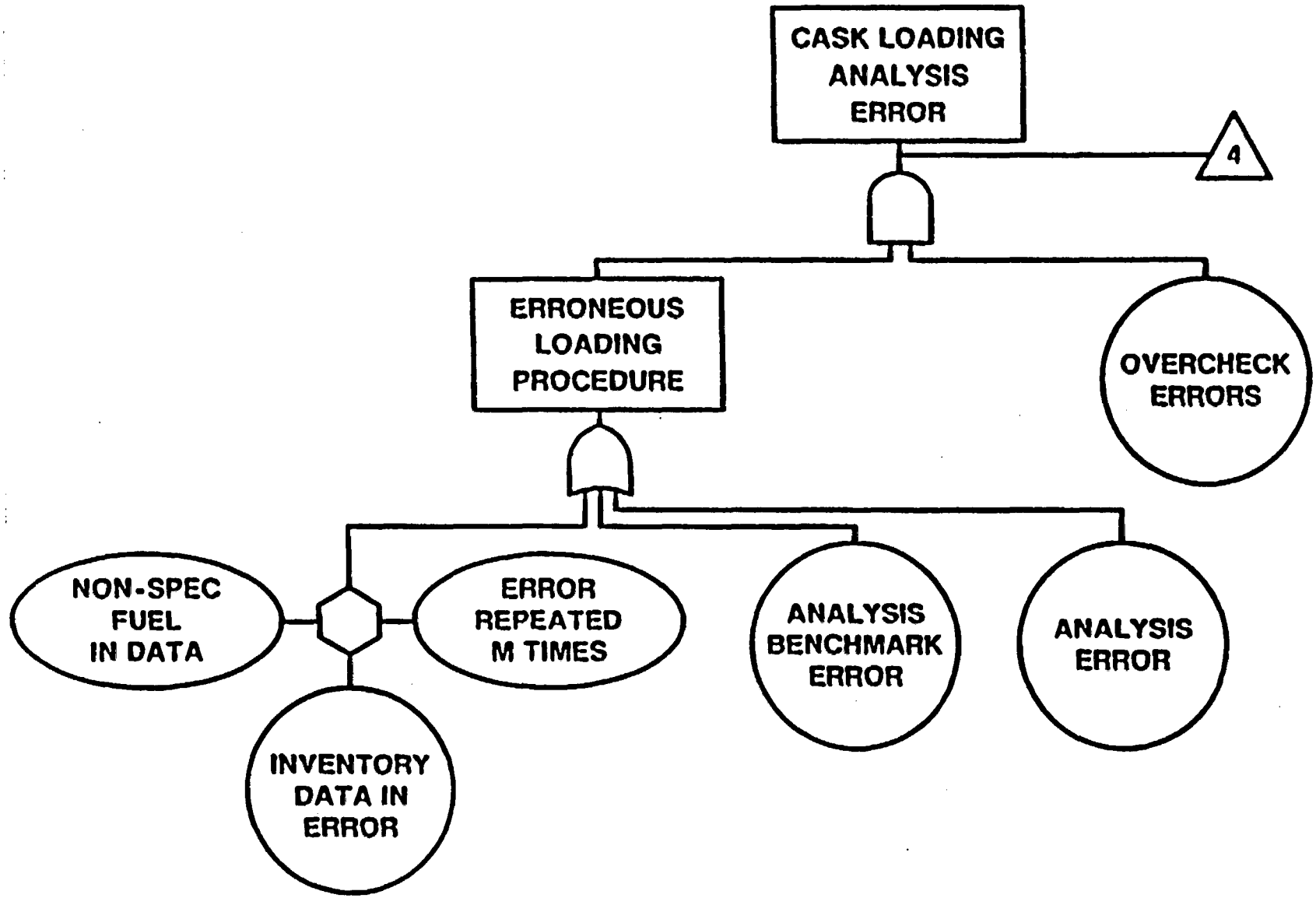

Figure 7. Failure Modes Affecting Fuel-Loading Procedures

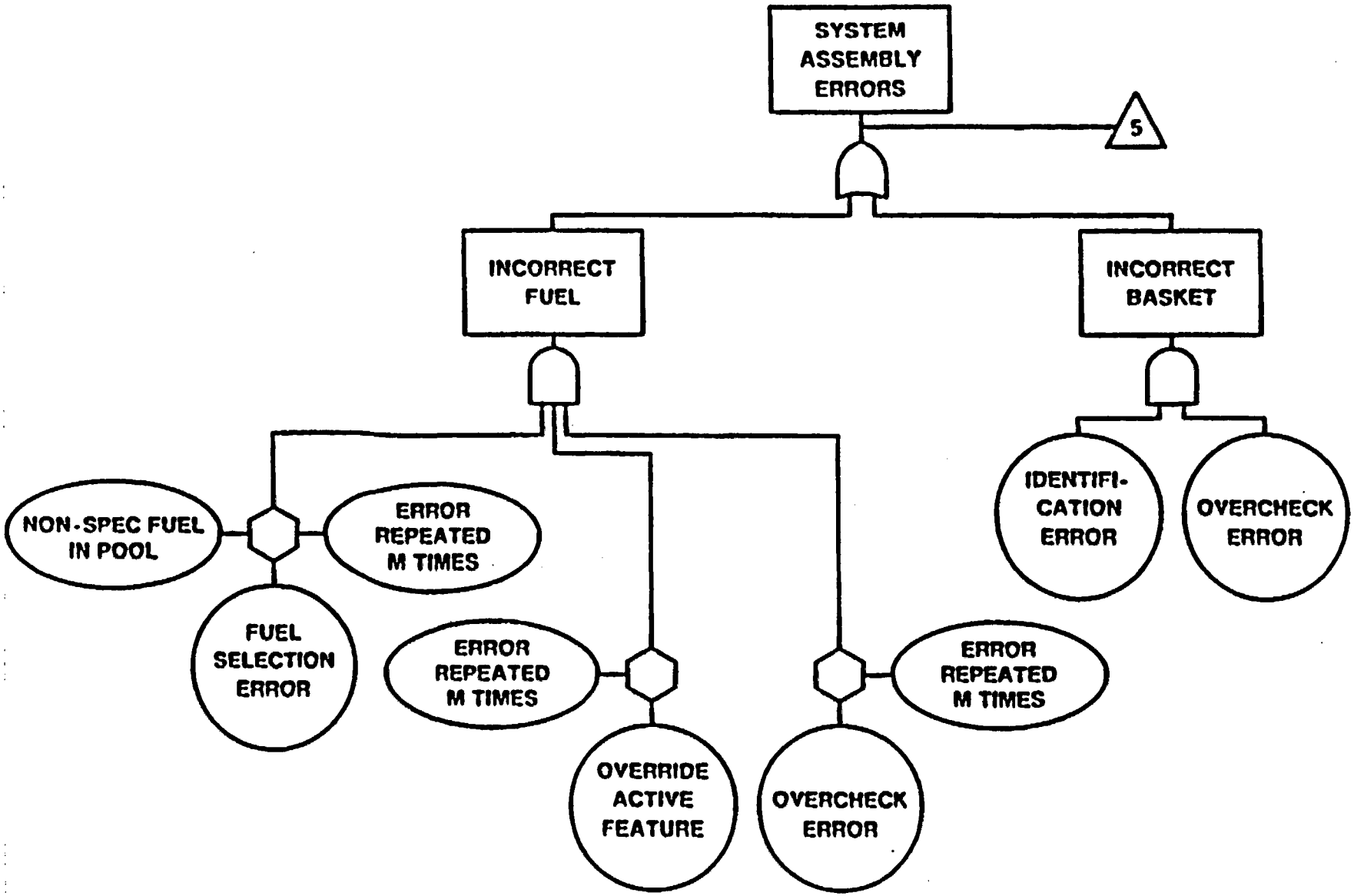

Figure 8. Failure Modes Affecting the Reliability of Fuel-Loading Operations and System Assembly

there is nonspecification fuel in the pool. Each error must be identically repeated if an independent overcheck of each loading operation is required.

The effect of fuel-related failure modes on criticality safety depends on the nonspecification fuel inventory available for misloading. The size of this inventory depends on the burnup and enrichment specifications used as the reactivity design basis for a cask. Analyses indicate that the minimum burnup necessary for a given enrichment will be significantly lower than the design burnup value for that enrichment, for any fuel type, because there is an upper limit on the potential benefits of burnup credit for a given cask design. As more assemblies are added to the cask, weight or shielding restrictions will become the capacity limiting factor rather than criticality. For this reason, it is not necessary to take full credit for the design burnup of a given assembly before sufficient negative reactivity is present to reduce the need for external criticality control features in a cask design. This is particularly true for legal and overweight truck casks. Model analyses indicate that burnups as low as 5 to 10 GWD/MTU (at 5.5 wt % U-235 initial enrichment) are sufficient to reduce the reactivity of a 3 to 4 PWR assembly array such that truck cask capacities can be increased from 2 to 4 PWR assemblies. For rail casks, burnups in the range of 25 GWD/MTU (5.5 wt % U-235) appear to be necessary to achieve a benefit from burnup credit. For a given cask design, lower enrichments and burnup combinations yield lower reactivities and thus can also be accommodated. In fact, the reactivities associated with fresh fuels of much lower enrichments could also be accommodated.

Spent Fuel Inventory

Statistical analyses of the existing spent fuel inventory have been completed that indicate several important points. First, less than about 2% of the existing spent fuel inventory appears to consist of fresh or irradiated fuel that would have reactivity in excess of a typical maximum enrichment/minimum burnup specification for a rail cask. Second, as few as 50 individual assemblies appear to be available in the current inventory that could not be shipped in a four PWR assembly truck cask. Third, a significant fraction of the existing inventory of nonspecification spent fuel consists of older-generation stainless-steel-clad fuel with high enrichment-to-design burnup ratios. Much of this fuel was prematurely discharged because of in-core failures or other reasons that may require special handling and transport conditions. Fourth, the majority of the existing inventory of nonspecification spent fuel appears to be located at a small number of older reactor facilities.

A trend analysis of historical premature fuel discharges from reactors was conducted to investigate the reasons for those discharges. The results indicate that the sciences of fuel

management and plant chemistry controls have matured considerably. Standardization and improvements in fuel designs, operational efficiencies, and chemistry management practices have occurred during the intervening years, resulting in fewer projected premature fuel discharges. The nonspecification spent fuel inventory of the future could still be dominated by older spent fuel discharged during the late 1960s and early 1970s. This fuel will compromise a very small fraction of the future inventory, even if it is not removed first.

The only difference between the fresh fuel and burnup credit cases is the addition of the spent fuel criticality control component as illustrated in Figure 9. It is important to recognize that this component is also a "system," consisting of many design, development, fabrication, and operational activities that are very similar to those that result in the external criticality control features of a cask. The external features are also affected by the spent fuel characteristics. Some minimal acceptance criteria for demonstrating the reliability of spent fuel analysis and operational activities is needed. This does not mean that the reliability or quality of current spent fuel operations is questionable; however, the reliability associated with those operations needs to be defined. The fact that the subsystem activities in both the fresh fuel and burnup credit cases are similar indicates that the root cause error probabilities are likely of similar magnitude.

Conclusions

The regulatory acceptance of cask design incorporating burnup credit depends on the identification and resolution of uncertainties that affect the determination of criticality safety margins, and on operational safety issues. The factors contributing to uncertainties in the determination of burnup credit criticality safety have been independently assessed by several methodologies. These uncertainties include cooling time, reactor operating history, non-uniformity of burnup, variations in assembly design, and low density moderation.

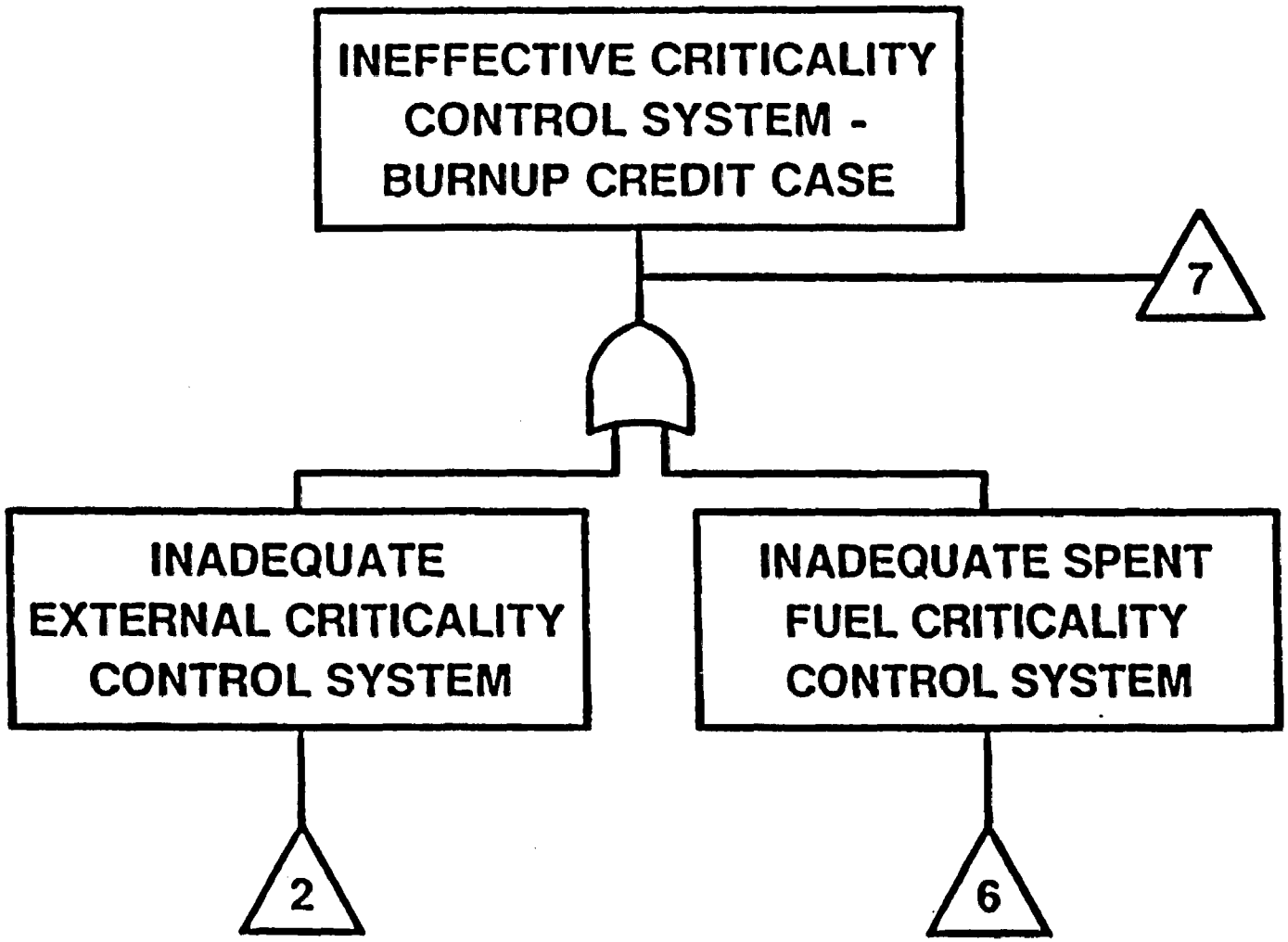

Figure 9. Failure Modes Affecting the Reliability of a Burnup Credit Criticality Control System

SPENT FUEL MANAGEMENT

SEMINAR IX

SPECIAL BURNUP CREDIT SESSION

INSTITUTE OF NUCLEAR MATERIALS MANAGEMENT

JANUARY 15-17, 1992
WASHINGTON, D.C.

ENCLOSURE 6

MEASUREMENT TECHNIQUES FOR VERIFYING BURNUP

Ronald I. Ewing, Sandia National Laboratories[1], Albuquerque NM 87185
and S.R. Bierman, Battelle-Pacific Northwest Laboratories[2], Richland WA

INTRODUCTION

Radiation measurements have been used for many years to aid in the characterization, handling, and processing of spent nuclear fuel. Applications have included radiation protection, international safeguards, fissile content estimation for reprocessing, and verification of records and calculations. The application of radiation measurements to support the identification of spent fuel assemblies for loading into "burnup credit" transport casks is an outstanding issue in the cask development program. Transport casks are being designed to accept assemblies that meet certain restrictions as to burnup, initial enrichment, and cooling time. Previous studies have concluded that the utility-supplied data on burnup, age, and initial enrichment is of greater accuracy and reliability than could be provided by additional radiation measurements on spent fuel assemblies [Ref. 1]. A possible role for measurements in burnup credit operations is to help prevent misloading of unacceptable fuel assemblies, either by confirming reactor records prior to cask loading, or by detecting operator error at the time of loading.

A possible alternative to measurements is to use the administrative controls and operational procedures that have been used at reactor sites that make use of burnup credit for spent fuel storage. Experience at such sites needs to be carefully analyzed for its applicability to the misloading and mis-identification probabilities.

Since there are over 40,000 spent fuel assemblies stored at more than one hundred locations in the U.S., it is important to carefully determine the necessity for and applicability of any measurement requirement. It is imperative that any measurement system selected be as simple, inexpensive, quick, and non-intrusive as possible.

In this report we will consider how radiation measurements on spent fuel can contribute to verifying the loading of burnup credit casks.

1. A U.S. Department of Energy Facility, work supported under contract DE-AC04-76DP00789
2. Work supported under U.S. DOE contract DE-AC06-76RLO1830

BURNUP CREDIT CASKS

The characteristics of fuel acceptable for loading into a burnup credit cask are determined by the design of the cask, and can be specified by a loading curve, as shown in Figure 1. The cask to which this Figure applies is designed to accomodate four assemblies of the Westinghouse 17 X 17 pressurized water reactor (PWR) fuel design. The criticality (k_{eff}) of the cask was calculated using computer programs and cross section data contained in the Standardized Computer Analyses for Licensing Evaluation (SCALE) system [Ref. 2]. This system was developed for the NRC by Oak Ridge National Laboratory to perform standardized criticality, shielding, and heat transfer analyses. In this example, the acceptable assemblies (cooled for a minimum of two years) are configured in the cask so that, under flooded conditions, the system is less than 95% of critical ($k_{eff} < 0.95$). The curve separating the "acceptable fuel region" from the "unacceptable fuel region" is determined by $k_{eff} = 0.95$. Fuel for which the combination of initial enrichment and burnup place it in the acceptable fuel region will result in $k_{eff} < 0.95$ when loaded into the cask, assuming the cask is filled with pure water. The curve also delineates the minimum burnup credit required for a particular initial enrichment. In Figure 1, the cask can accomodate spent fuel of initial enrichment 4.5 wt% U-235 with burnup greater than 7 GWD/MTU and maintain $k_{eff} < 0.95$. This cask design can accomodate fresh fuel (burnup = zero) for initial enrichments less than 3.5 wt% U-235. One interesting result of the calculations is that, over the range of burnup values of interest, a 25% variation in burnup produces a change of less than 3% in k_{eff} for this cask.

RADIATION FROM SPENT FUEL

The spent fuel assemblies of initial interest in burnup credit loading operations are those that have been cooling for the longest period of time. Most assemblies that are likely to be loaded into burnup credit casks in the first years of transport cask operations will have cooling times greater than 10 years. This long cooling time results in simplified radiation spectra from the spent fuel. Some important gamma-ray and neutron emitting nuclides for aged assemblies are listed in Table 1. For shorter cooling times, many more isotopes are significant emitters, but most have decayed to insignificance after 10 years because of the predominance of short half-lives in the fission and activation products.

TABLE 1.

NUCLIDE	HALF-LIFE (yr)	RADIATION
^{242}Cm	0.45	n, spontaneous fission
^{244}Cm	18.1	n, spontaneous fission
^{238}Pu	87.8	n, spontaneous fission
^{134}Cs	2.06	γ, 605, 796 keV
^{137}Cs	30.0	γ, 662 keV

The cesium isotopes are produced as fission products while in the reactor, so their production is essentially proportional to burnup. After the fuel is removed from the reactor, the isotopes decay with the indicated half-lives. The spontaneously fissioning isotopes are produced by successive neutron capture, beginning with uranium. ^{244}Cm production initially proceeds as the sixth power of the integrated flux. Initially, burnup is directly related to the flux times the initial enrichment. For higher burnups, ^{244}Cm production is found to be proportional to the fourth power of burnup, still a very strong function. ^{242}Cm and ^{238}Pu are less sensitive, but also very strong functions of burnup. This strong dependence of neutron emission on burnup means that uncertainties in measuring the neutron emission result in even smaller uncertainties in the burnup, identifying neutron emission as a very sensitive and accurate means of inferring burnup. At ten years cooling, for low burnups, the Pu isotopes dominate the neutron emission. For higher burnups, ^{244}Cm dominates, and the decay follows the 18.1 year half-life. Gross gamma emission follows a similar function of cooling time that is complicated for short cooling times, with many isotopes contributing, but after ten years, ^{137}Cs dominates. For cooling times out to about 8 years, the ratio of ^{134}Cs to ^{137}Cs gamma-rays provides a means of detemining cooling time, but after 10 years, the technique is no longer viable due to the decay of ^{134}Cs.

The information that can be inferred from passive neutron measurements on spent fuel that has cooled for more than ten years is limited to burnup/ enrichment ratios, with some dependence on the absolute burnup, but only weakly dependent on age. Gamma-ray measurements provide a less sensitive indication of burnup, also weakly dependent on age.

MEASUREMENT SYSTEMS

Neutron sources, such as ^{252}Cf, can be used to induce fissions in the fissile material remaining in spent fuel. The neutron multiplication can be measured and related to cask criticality by calculations, independent of initial enrichment, burnup, or age. This active interrogation technique is complicated by complexities in operation and interpretation that would restrict its use to applications for which passive measurements are inadequate.

A number of measurement systems have been examined for applicability to burnup credit cask operations. Those systems that have been emplaced at spent fuel locations and have generated useful data and operational experience were analyzed in greater detail. Included were both passive and active systems used in Japan, France, the Soviet Union, as well as the U.S.

It should be emphasized that all of these systems produce only relative values for their measurements, and all are dependent on the availability of a standard calibration assembly of the same design as the assemblies to be examined. The pertinent characteristics of the calibration assembly are assumed to be known. In the measurements under consideration , an assembly or group of assemblies of well-documented characteristics could be selected as the reference standard, and all measurements are referred to the chosen standard.

Only one measurement system will be considered in detail here, because it combines the features considered most desireable in this application.

THE "FORK" SYSTEM

The spent fuel measurement system designated "Fork" because of its shape, was developed at Los Alamos National Laboratory for use in safeguards applications for the IAEA[Ref. 3]. The system is diagrammed in an operational arrangement in Figure 2. It is portable, and can be moved in the storage pool to the spent fuel assembly to be examined. It requires that the assembly be raised in the storage rack so that the midpoint is about 50 cm above the top of the rack. The detector head is located at the midpoint of the assembly for the measurement. A cadmium-covered fission chamber is used to measure neutrons from the assembly, and an ion chamber is used to measure gammas. An additional fission chamber, without a cadmium cover, is used to infer boron content in the storage pool, since the value of that parameter could vary widely in the safeguards application. The detector head is made of polyethylene and has identical three-detector arrays in each of the two tines of the fork, for redundancy, in case of a detector failure. A battery-powered electronics unit and microprocessor are used to supply all power to the detectors, collect and analyze the detector outputs, and perform necessary calculations and documentation. The unit has been used to examine spent fuel assemblies at storage facilities in the U.S., Finland, Germany, France, Bulgaria, and

Czechoslovakia. The measurements have required less than 100 seconds measuring time per assembly, and a considerable database has been established. The users state that with proper calibration standard assemblies, burnup has been determined to an average accuracy of about 5%, for burnup in excess of 10 GWD/MTU. The gross gamma-ray measurements have been shown to be consistent with operator-declared values for burnup and age to about 10%. This result has proved to be adequate to eliminate the need for more complex active or high-resolution measurement techniques[Ref. 4].

The safeguard measurement requirement, the validation of reactor records, is similar to the requirements for measurements in burnup credit operations, so it is likely that the Fork system, or a similar design, would be adequate for the burnup application. The Fork system has apparently not been used for fuel aged in excess of 10 years, so some additional measurements may be useful. Other modifications possibly useful in the burnup application include elimination of the second fission chamber, replacement of the detectors with simpler, more sensitive, less expensive, or more reliable detectors. A "corner" arrangement rather than the "fork" may also be desireable.

PLANS

The database generated to date using the "Fork" system will be examined for applicability to ten-year-plus fuel, and to determine if additional measurements are needed. The desireability of modifications will be further investigated. Operatonal requirements and restrictions will be more clearly defined by obtaining utility input, and applying the experience of operators using burnup credit in storage facilities.

CONCLUSIONS

Measurements can be used in burnup credit operations to help prevent misloading of fuel that does not meet the minimum specifications for a particular cask design. Passive neutron and gross gamma-ray measurements are proposed as a means of qualifying spent fuel assemblies. Active systems to measure reactivity or fissile content are necessarily more complex and appear to offer no obvious advantage to burnup credit applications over simpler systems. Plans are underway to produce a prototype measurement system and generate a database of spent fuel measurements, making use of experience with the "Fork" design used by the IAEA for safeguards inspections.

REFERENCES

1. "The Incentives and Feasibility for Direct Measurement of Spent Nuclear Fuel Characteristics in the Federal Waste Management System", ORNL/Sub/86-SA094/3, JAI-296, report prepared by E. R. Johnson Assoc. for Oak Ridge National Laboratory, 1988.

2. "SCALE: A Modular Code System for Performing Standardized Computer Analyses for Licensing Evaluation." Rev. 3, Vols.1-3, NUREG/CR-0200, Parks, C.V., ed.; Oak Ridge National Laboratory, Oak Ridge, Tennessee.

3. "Safeguarding LWR Spent Fuel with the Fork Detector", P.M. Rinard, and G.E. Bosler, Los Alamos National Laboratory report LA-11096-MS (March 1988).

4. "Experience Using a Spent-Fuel Measurement System", J.R. Phillips, et al, Institute of Nuclear Materials Management Annual Meeting 1983, Vol. 12, p. 175.

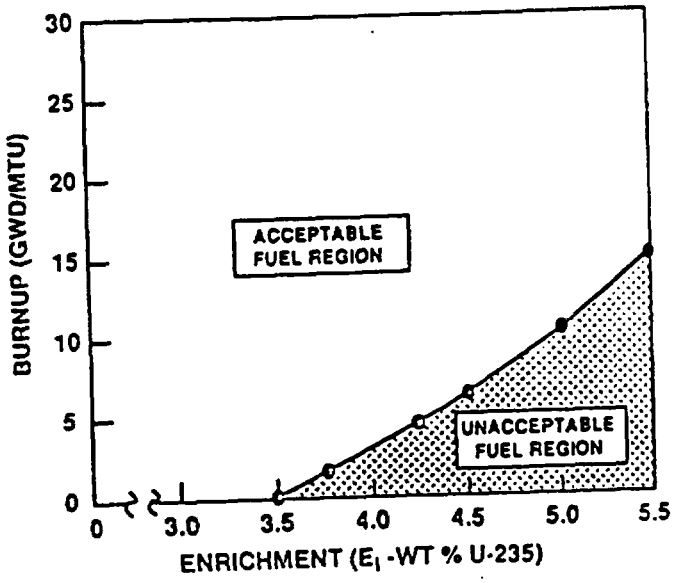

FIG. 1 LOADING CURVE FOR A BURNUP CREDIT CASK

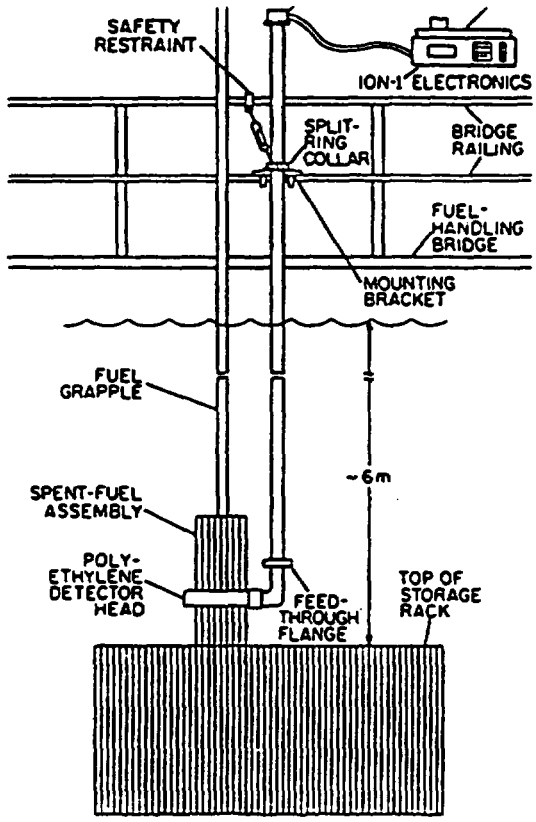

FIG. 2 SKETCH OF FORK DETECTOR IN OPERATION

SPENT FUEL MANAGEMENT

SEMINAR IX

SPECIAL BURNUP CREDIT SESSION

INSTITUTE OF NUCLEAR MATERIALS MANAGEMENT

JANUARY 15-17, 1992
WASHINGTON, D.C.

ENCLOSURE 7

VALIDATING ANALYSIS METHODOLOGIES USED IN BURNUP CREDIT CRITICALITY CALCULATIONS*

M. C. Brady
Oak Ridge National Laboratory**
P.O. Box 2008
Oak Ridge, Tennessee 37831-6370

D. G. Napolitano
Yankee Atomic Electric Company
580 Main Street
Bolton, Massachusetts 01740-1398

To be presented at
Spent Fuel Management Seminar IX
Loew's L'Enfant Plaza
Washington, DC USA
January 15-17, 1992

Sponsored by
Institute of Nuclear
Materials Management

"The submitted manuscript has been authored by a contractor of the U.S. Government under contract No. DE-AC05-84OR21400. Accordingly, the U.S. Government retains a nonexclusive, royalty-free license to publish or reproduce the published form of this contribution, or allow others to do so, for U.S. Government purposes."

*Research performed under Sandia National Laboratories contract 66-0162 with Oak Ridge National Laboratory and Sandia National Laboratories contract 75-0590 with Yankee Atomic Electric Company.

**Managed by Martin Marietta Energy Systems, Inc., under contract DE-AC05-84OR21400 with the U.S. Department of Energy.

VALIDATING ANALYSIS METHODOLOGIES USED IN BURNUP CREDIT CRITICALITY CALCULATIONS

M. C. Brady
Oak Ridge National Laboratory
P.O. Box 2008
Oak Ridge, Tennessee 37831-6370

D. G. Napolitano
Yankee Atomic Electric Company
580 Main Street
Bolton, Massachusetts 01740-1398

ABSTRACT

The concept of allowing reactivity credit for the depleted (or burned) state of pressurized-water-reactor fuel in the licensing of spent fuel facilities introduces a new challenge to members of the nuclear criticality community. The primary difference in this analysis approach is the technical ability to calculate spent fuel compositions (or inventories) and to predict their effect on the system multiplication factor. Isotopic prediction codes are used routinely for in-core physics calculations and the prediction of radiation source terms for both thermal and shielding analyses, but represent an innovation for criticality specialists. This paper discusses two methodologies currently being developed to specifically evaluate isotopic composition and reactivity for the burnup credit concept. A comprehensive approach to benchmarking and validating the methods is also presented. This approach involves the analysis of commercial reactor critical data, fuel storage critical experiments, chemical assay isotopic data, and numerical benchmark calculations.

INTRODUCTION

In the past, criticality analysis of pressurized-water-reactor (PWR) fuel stored in racks and casks has assumed that the fuel is fresh and of the highest conceivable enrichment. This assumption has led to the design of widely spaced and/or highly poisoned storage and transport arrays. If credit is assumed for fuel burnup, compact and economical arrays can be designed. In addition, if burnup credit casks are used in the transport of spent light-water-reactor (LWR) fuel to a repository, a significant reduction both in the cost of transport and in the risk to the public can be realized.[1]

The ANSI/ANS 8.1 criticality safety standard[2] requires validation and benchmarking of the calculational methods used in evaluating criticality safety limits for away-from-reactor (AFR) applications. Numerous critical experiments for PWR fuel in storage configurations exist and can be used as a validation data base.[3-7] There are no published critical experiments with burned PWR fuel in storage configurations. However, two sources of experimental data for spent fuel have been identified: fuel assembly chemical assay data[8-10] and commercial reactor cycle performance data including hot zero-power and hot full-power criticals.[11-13] Chemical assay data can be used to validate

and benchmark a method's depletion performance, and commercial reactor criticals can be used to validate and benchmark a method's criticality performance with burned fuel. By breaking down the burnup credit validation problem into various parts, conclusions can be drawn about the validity and uncertainty of a method used in calculating criticality safety limits for burned fuel in storage and transport arrays.

ANALYSIS METHODOLOGIES

Two methodologies currently being developed as part of the U.S. Department of Energy (DOE) Burnup Credit Program are discussed in this paper. One is based on the SCALE code system,[14] which is comprised of computational tools widely accepted for use in AFR applications.[15,16] The second methodology utilizes the CASMO-3/SIMULATE-3 code package,[17-19] which is typically accepted for use in a variety of in-core applications.

Oak Ridge National Laboratory (ORNL) has developed and validated the SCALE-based methodology. This approach uses the KENO V.a Monte Carlo code to calculate the multiplication factor for spent fuel storage and transport geometries. KENO V.a has a large degree of flexibility in its geometrical modeling capabilities which is essential for modeling a large variety of storage and transportation casks. Spent fuel arrays and container geometries can be modeled in explicit detail by KENO V.a. The isotopic composition of the spent fuel is derived from a SAS2H/ORIGEN-S calculation that simulates two-dimensional (2-D) effects in a one-dimensional (1-D) model of an LWR fuel assembly. The depletion model is a simple point model using cross sections and neutron flux parameters derived from the 1-D fuel assembly model. Computational tools have been developed to facilitate processing the isotopic data generated for spent fuel into the criticality calculations.[16]

Yankee Atomic Electric Company (YAEC) has developed and validated a burnup credit methodology based on SIMULATE-3 nodal diffusion theory with cross sections and isotopics from CASMO-3. Criticality calculations using CASMO-3/SIMULATE-3 can only be performed on arrays that are square and nodalizable. However, a large number of storage and transport arrays satisfy this geometric constraint. In this methodology, detailed isotopic data are implicit in the two-group macroscopic cross sections obtained from the CASMO-3 integral transport analysis. Burned fuel assemblies are characterized by nodal variables, such as exposure and moderator density history. These assemblies can be directly shuffled from in-core models to out-of-core storage or transport arrays models.

COMMERCIAL REACTOR CORE CRITICALS

Nuclear reactor core criticals are relevant benchmarks to burnup credit cask and storage criticality analysis because these types of criticals test the ability of a methodology to perform depletion and to handle the reactivity effects of heterogeneities and strong absorbers. Commercial reactors offer an excellent and inexhaustible source of critical configurations against which criticality analyses can be validated for burned fuel configurations.[11-13] Analyses can be performed for precise state points at beginning of cycle (BOC) and end of cycle (EOC), or throughout the cycle depletion.

The SCALE methodology has been used to evaluate BOC and EOC core configurations for several PWRs: North Anna and Surry (Virginia Power Company); and Sequoyah (Tennessee Valley Authority).[15,16] Isotopics produced by Virginia Power using three-dimensional (3-D) PDQ analysis techniques were utilized in a computation involving the SCALE criticality methodology (KENO V.a and SCALE cross sections) for the North Anna and Surry reactors. These results have been compared with those obtained using the complete SCALE burnup credit methodology to indicate the uncertainty due to the method chosen for the calculation of spent fuel isotopics. Results indicated that the SCALE methodology underpredicted k_{eff} by 1 to 1.5% relative to the PDQ/KENO V.a calculations. The PDQ/KENO V.a calculations underpredicted k_{eff} by 1 to 1.5% for BOC configurations and overpredicted k_{eff} by 1 to 1.5% for EOC configurations. The SCALE results were very good for the EOC configurations, within 0.5% Δk.

YAEC has used the CASMO-based methodology to perform core follow calculations for cycles 1 and 2 of the Surry Unit 1 reactor.[19] The CASMO-based methodology explicitly models the power level, soluble boron, system pressure, coolant temperatures, and control rod bank D height. Twenty-six state points were calculated for cycle 1, with an average k_{eff} of 0.99965 $\pm$ 0.00198. The average k_{eff} calculated for 11 exposure state points in cycle 2 was 0.99982 $\pm$ 0.00106. Thus, the calculated results are considered to be in excellent agreement with the utility data.

The CASMO-3/SIMULATE-3 methodology is designed for in-core calculations and performs in an exemplary fashion for the reactor-critical configurations. Results obtained using the SCALE-based system demonstrate that a simple AFR calculational system can be used to predict k_{eff} for spent fuel in a reactor with an uncertainty of about 1.5%.

ISOTOPIC EVALUATIONS

Reactor criticals provide an indication of the integral validity of the ability of a method to predict isotopics and evaluate k_{eff}, but chemical assay data for spent fuel provide a unique means for an explicit validation of actinide behavior and fission-product buildup. Since burnup credit assumes fuel depletion and fission-product buildup, validation of the details of a method's isotopic calculation is important. Numerous determinations of the actinide content in LWR fuel have been performed.[8-10] A limited quantity of experimental data for fission-product inventories in LWR spent fuel is also available.

In the mid-1980s, the Office of Civilian Radioactive Waste Management (OCRWM) assigned the Materials Characterization Center at the Pacific Northwest Laboratory (PNL) the responsibility of procuring and characterizing a representative selection of LWR spent fuel. Several fuel elements in the U.S. spent fuel inventory were identified and obtained for characterization as approved testing materials (ATMs). Data for six fuel samples from one of these test assemblies (ATM-103) and data for two fuel assemblies from the German Obrigheim PWR have been used by the group at ORNL in validation analyses for the point-depletion sequence (SAS2H) used to calculate spent fuel inventories.[15] The measured data spanned a range of burnups from 25,930 to 44,340 megawatt days per metric tonne initial uranium (MWd/MTU). The computed percentage differences between the measured and calculated concentrations were on the order of 1 to 6% for uranium isotopes and slightly higher (1.2 to 6.3%) for the plutonium isotopes and Americium-241. One exception is that the predicted concentrations for ^{242}Pu were nearly 10% less than the measured values. Only three fission products of interest to the burnup credit program have been explicitly measured by the PNL

group: ^{99}Tc, ^{133}Cs, and ^{135}Cs. On the average, the fission-product number densities calculated by SAS2H were overpredicted by 8.2, 2.5, and 18.8% for ^{99}Tc, ^{133}Cs, and ^{135}Cs, respectively. The Obrigheim results reported measurements of fission-product ratios which included the neodymium isotopes, 143 and 145, measured relative to ^{148}Nd. Calculations of these two fission-product ratios were in very good agreement with the measured values (-0.4 and 2.3%, respectively).

The significance of the comparisons of isotopic concentrations relative to their impact on criticality calculations is the key issue for the application of burnup credit. This analysis was performed by computing the reactivity sensitivity coefficient (defined as the percentage change in k_∞ divided by the percentage change in isotopic concentration) for each of the isotopes of interest. This parameter indicates the importance of an individual nuclide in the overall criticality calculations. The results indicate that ^{238}U had the largest negative effect on reactivity, and ^{239}Pu had the largest positive effect (not including the obvious importance of ^{235}U). The concentration of ^{235}U was generally underpredicted by SAS2H by about 4.2%, whereas the ^{239}Pu concentration was conservatively overpredicted by 4.8%. The ^{238}U number densities are overpredicted by 1.2% on the average. All other nuclides have calculated reactivity sensitivity coefficients that are an order of magnitude smaller than for these three important nuclides. Note that important fission products, such as the samarium isotopes, were not included in this study because no measured concentration data were available. A calculation that modified number densities for all nuclides by the average percentage difference indicated that the overall effect in terms of the multiplication factor was very small (0.66% $\Delta k/k$) in the negative direction.[15] Conservative assumptions used by cask designers involve neglecting differences that would result in a lower k_{eff} and modifying number densities for nuclides that cause reactivity to increase.

YAEC has performed comparisons of the CASMO-3 actinide isotopic calculations with Yankee Rowe Core I (ref. 8) and with selected high burnup fuel pins from a fuel assembly that resided in Zion Cores 1 through 4 (ref. 9). Yankee Core I isotopics were measured over a broad range: approximately 12,000 to 31,000 MWd/MTU. The Yankee data were segregated into batches of fuel rods occupying fuel assembly positions in asymptotic, intermediate and perturbed neutron spectra. These spectra corresponded to fuel rods from the assembly interior, between the interior and water slots, and next to water slots to represent a range of conditions. Comparisons of calculated and measured uranium and plutonium isotopics showed relatively good agreement as a function of burnup.

The Zion data provided benchmark isotopics for contemporary Westinghouse PWR 15 x 15 assemblies and for extended burnup ranges. The data included uranium and plutonium atom percents, and americium and curium isotopic ratios to ^{239}Pu for five different pin locations within an assembly. The burnups range from 23,471 to 51,753 MWd/MTU. Generally, the CASMO-based methodology tended to underpredict uranium and plutonium concentrations. The exception to this was that the concentrations of ^{238}U and ^{241}Pu were slightly overpredicted (<1% and <5%, respectively). The concentration of ^{239}Pu also tended to be overpredicted (on the average of 1.3%) for higher burnups (>40,000 MWd/MTU). As noted in an earlier discussion, ^{235}U, ^{238}U, and ^{239}Pu concentrations have the most significant effect on k_{eff}. The results for ^{238}U and ^{239}Pu are in excellent agreement with the SCALE-based results. The Zion data cover a wider range in burnup than did the data used in the SCALE comparison. Neglecting the Zion sample with the highest burnup, the average percentage difference in the results for ^{235}U is about 6%, which is again consistent with the SCALE results. The average percentage difference for the highest burnup samples (49 and 51 GWd/MTU) is approximately 10% for ^{235}U. A slight positive trend in the magnitude of the differences with increasing burnup was also observed. However, one must use caution in drawing

conclusions based on small differences because the measurement uncertainties and the difficulty in measuring small concentrations must also be considered.

Overall, the isotopic prediction schemes used by each of the two analysis methodologies perform very well. Preliminary indications are that the fission-product concentrations are overpredicted by 10 to 20% and that corrections no larger than 10% are necessary for any of the actinide nuclides. Specific results are dependent on the methodology used to predict the isotopics.

FUEL STORAGE CRITICALS

Fuel storage criticals provide an evaluation of the validity of a method's ability to handle neutron interactions between fuel assemblies with: water gaps, poison sheets, poison loadings, dissolved soluble boron, flux trap geometries, and shielding materials. Numerous benchmarks of this type exist to validate the performance of the calculation methodologies.[3-7]

ORNL modeled 15 critical experiments[20] using the SCALE-based methodology in order to examine seven different criticality aspects related to LWR fuel in transportation and storage casks:

1. neutron interaction between fuel assemblies,
2. effectiveness of neutron flux traps between fuel assemblies to reduce reactivity,
3. effect of voiding on the effectiveness of neutron flux traps,
4. effectiveness of neutron absorber plates and rods to reduce interaction between fuel assemblies,
5. reactivity effect of commonly used biological shielding materials,
6. neutron spectra shift or relative neutron moderation caused by dissolved boron, and
7. plutonium buildup and uranium depletion.

All experiments used in the validation study were water moderated. The mean k_{eff} for the 15 critical experiments was 0.9927. Mean values of k_{eff} were calculated by category: UO_2 reflected by water, 0.9923; UO_2 reflected by metal, 0.9984; and mixed-oxide (MOX) criticals, 0.9801.

These comparisons indicated that for the SCALE-based methodology a bias of approximately 2% would be required to account for cross-section bias and for the bias in the computational method. Comparisons with additional MOX critical experiments are to be performed. These additional calculations could have a potential effect on the overall bias for the methodology and would definitely impact the uncertainty in that bias by increasing the number of data points from which it is derived.

YAEC modeled 33 LWR fuel storage critical experiments using CASMO-3/SIMULATE-3 nodal diffusion techniques. These included: 10 B&W 3 x 3 array fuel storage criticals,[3] 9 PNL single-lattice criticals,[4] 4 PNL two lattice cluster flux trap criticals,[4] and 10 PNL 2 x 2 cluster cruciform flux trap criticals.[6] The mean k_{eff} and standard deviation for all critical experiments was 0.9993 $\pm$ 0.0063. These statistics show a low bias and a low standard deviation, which indicates that the CASMO-3/SIMULATE-3 method is valid and accurate for LWR fuel storage criticality analyses.

NUMERICAL BENCHMARK PROBLEMS

In addition to standard benchmark criticals, numerical benchmark problems can be formulated which address isotopic and storage array reactivity evaluations. These benchmark problems can be used to intercompare methods and quantify differences in results. A PWR fuel assembly isotopic benchmark has been described and evaluated by ORNL and YAEC.[21] A hypothetical 31-assembly burnup credit cask design has been described and evaluated by ORNL and YAEC. These results provide independent verification of criticality trends with cooling time, water level and water density.[22,23]

CONCLUSIONS

By breaking down the burnup credit validation problem into various parts, conclusions can be drawn about the validity and uncertainty of a method in calculating criticality safety limits with burned fuel in storage and transport arrays. Commercial reactor criticals, isotopic evaluations, fuel storage criticals, and numerical benchmark problems can be used to evaluate the performance of a method used in calculating criticality safety limits for burned fuel in storage and transport arrays.

ACKNOWLEDGEMENTS

The U.S. burnup credit program is dependent on a range of expertise, and the authors would like to acknowledge S. M. Bowman, O. W. Hermann, C. V. Parks, J.-P. Renier, and R. M. Westfall of ORNL for their substantial contributions to the different phases of the project. We would also like to express our appreciation for the technical expertise, assistance, and advice from D. G. Adli (Yankee Atomic Energy Company), S. R. Bierman (Pacific Northwest Laboratory), W. H. Lake (U.S. Department of Energy), C. R. Marotta (Marotta Consulting), O. Ozer (Electric Power Research Institute), T. L. Sanders (Sandia National Laboratories), and M. L. Smith (Virginia Power Company).

This work is supported by the Office of Civilian Radioactive Waste Management of the U.S. Department of Energy and the Electric Power Research Institute, and is managed by Sandia National Laboratories.

REFERENCES

1. T. L. Sanders and R. M. Westfall, "Feasibility and Incentives for Burnup Credit in Spent Fuel Transport Casks," *Nucl. Sci. Eng.* 104 (1990).

2. "American National Standard for Nuclear Criticality Safety in Operations with Fissionable Materials Outside Reactors," ANSI/ANS-8.1-1983.

3. N. M. Baldwin, G. S. Hoovler, R. L. Eng, and F. G. Welfare, *Critical Experiments Supporting Close Proximity Water Storage of Power Reactor Fuel*, B&W-1484-7 (July 1979).

4. S. R. Bierman and E. D. Clayton, *Criticality Experiments with Subcritical Clusters of 2.35 w/o and 4.31 w/o ^{235}U Enriched UO_2 Rods in Water at a Water to Fuel Volume Ratio of 1.6*, NUREG/CR-1547, PNL-3314 (July 1980).

5. S. R. Bierman and E. D. Clayton, "Criticality Experiments with Subcritical Clusters of 2.35 w/o and 4.31 w/o ^{235}U Enriched UO_2 Rods in Water with Steel and Reflecting Walls," *Nucl. Tech.* 132-133, 54 (1981).

6. S. R. Bierman, *Criticality Experiments to Provide Benchmark Data on Neutron Flux Traps*," PNL-6205 (June 1988).

7. S. R. Bierman, *Reactivity Measurements on an Experimental Assembly of 4.31 w/o ^{235}U Enriched UO_2 Fuel Rods Arranged in a Shipping Cask Geometry*, PNL-6838 (October 1989).

8. R. Nodvik, *Supplementary Report on Evaluation of Mass Spectrometric and Radiochemical Analysis of Yankee Core I*, WCAP-6086 (August 1969).

9. M. Balfour et al., *Final Report EP80-16, Hot Cell Examination of Zion Fuel Cycles 1 Through 4*, WCAP-10473 (April 1985).

10. U. Fischer and H. W. Wiese, *Improved and Consistent Determination of the Nuclear Inventory of Spent PWR Fuel on the Basis of Cell Burnup Methods Using KORIGEN*, KFK 3014 (ORNL-tr-5043), Karlsruhe Nuclear Research Center (January 1983); available from Radiation Shielding Information Center as CCC-457.

11. *Reactor Core Physics Design and Operating Data for Cycles 1, 2, and 3 of the Surry Unit 1 PWR Power Plant*, EPRI NP-79-2-LD (March 1979).

12. *Reactor Core Physics Design and Operating Data for Cycles 1 and 2 of TMI Unit 1 Power Plant*, EPRI NP-1410 (August 1980).

13. *NSSS Design and Cycle 1 Operating History Data For Arkansas Nuclear One, Unit 2*, EPRI NP-1385-1 (March 1981).

14. *SCALE: A Modular Code System for Performing Standardized Computer Analyses for Licensing Evaluation*, NUREG/CR-0200, Rev. 4 (ORNL/NUREG/CSD-2/R4), Vols. I, II, and III (draft February 1990). Available from Radiation Shielding Information Center as CCC-545.

15. M. C. Brady and T. L. Sanders, "A Validated Methodology for Evaluating Burnup Credit in Spent Fuel Casks," *Proceedings of International Conference on Nuclear Criticality Safety*, Christ Church, Oxford, United Kingdom, September 9-13, 1991.

16. J.-P. Renier et al., *Analysis of Reactor Critical Configurations for Burnup Credit Verification*, ORNL/CSD/TM-280 (to be published).

17. M. Edenius, A. Ahlin, and B. Forssen, *CASMO-3G, A Fuel Assembly Burnup Program*, User's Manual, STUDSVIK/NFA-86/7 (November 1986).

18. D. M. Ver Planck, K. S. Smith, and J. A. Umbarger, *SIMULATE-3P Advanced Three-Dimensional Two Group Reactor Analysis Code*, STUDSVIK/SOA-88/01 (February 1988).

19. D. G. Napolitano and D. G. Adli, "Burnup Credit Using Advance Nodal Techniques," *Topical Meeting on Advances in Mathematics, Computations, and Reactor Physics*, Pittsburgh, Pa. (April 1991).

20. S. M. Bowman, *Validation of SCALE-4 for a Reference Problem Set*, ORNL/M-1332 (July 1991).

21. Personal communication from D. G. Napolitano, Yankee Atomic Electric Company to M. C. Brady, Oak Ridge National Laboratory, August 1989.

22. M. C. Brady, C. V. Parks, and C. R. Marotta, "End Effects in the Criticality Analysis of Burnup Credit Casks," *Trans. Am. Nucl. Soc.* 62 (November 1990).

23. D. G. Napolitano and D. G. Adli, "Burnup Credit Analysis of a 31-Assembly Cask," *Trans. Am. Nucl. Soc.* 62 (November 1990).

SPENT FUEL MANAGEMENT

SEMINAR IX

SPECIAL BURNUP CREDIT SESSION

INSTITUTE OF NUCLEAR MATERIALS MANAGEMENT

JANUARY 15-17, 1992
WASHINGTON, D.C.

ENCLOSURE 8

STRATEGIES FOR CERTIFYING A BURNUP CREDIT CASK

William H. Lake, U.S. Department of Energy, Washington, DC
Jack K. Boshoven, General Atomics, San Diego, CA
Lawrence A. Hassler, Babcock & Wilcox, Lynchburg, VA

ABSTRACT

A new generation of high capacity spent fuel transport casks is being developed by the Department of Energy (DOE) as part of the Federal Waste Management System (FWMS). Burnup credit, which recognizes the reduced reactivity of spent fuel is being used for these casks. Both cask designs being developed for DOE by Babcock & Wilcox and General Atomics use burnup credit. The cask designs must be certified by the Nuclear Regulatory Commission (NRC) if they are to be used in the FWMS. Certification of these casks by the NRC would not require any change in transport regulations, and would be consistent with past practices. To support certification, DOE has identified the technical issues related to burnup credit, and embarked on a development program to resolve them. Following a background discussion of criticality safety for spent fuel transport, an approach to design and use of a burnup credit cask is presented. It is concluded that an adequate technical basis is being developed for spent fuel casks to demonstrate compliance with the NRC criticality safety requirements.

INTRODUCTION

The Department of Energy's (DOE's) Office of Civilian Radioactive Waste Management (OCRWM) is in the process of developing a new generation of high capacity casks to transport spent fuel from commercial nuclear reactor facilities to federal waste facilities. The DOE's role in the Federal Waste Management System (FWMS) is defined in the 1982 Nuclear Waste Policy Act (NWPA) and its 1987 amendment (NWPAA). The NWPAA requires DOE to use spent fuel and high level radioactive waste casks certified by the Nuclear Regulatory Commission (NRC). Because of the high shipping rates anticipated, and since cooling times of spent fuel that will be shipped significantly exceed the design cooling times of existing casks, a decision was made to develop new higher capacity casks. The potential benefit of higher cask capacities, is fewer shipments. Fewer shipments result in health and safety benefits as well as cost benefits. In evaluating the needs of the cask development program a number of technical issues were identified that would further support improved cask capacities. Burnup credit is one of these technical issues.[1]

Burnup credit is the practice of accounting for the reduced reactivity of spent fuel in evaluating criticality safety. The NRC transportation regulations[2] (10 CFR 71) require

subcriticality of transport systems. The regulations do not elaborate on how subcriticality should be assured, nor do they prohibit the use of burnup credit for criticality safety. The NRC has, in the past, approved one cask which uses burnup credit. It is the Model NLI-6502[3] (NRC certificate of compliance no. 9103) which is used to ship highly enriched research reactor fuel. However, in the case of commercial light water reactor (LWR) spent fuel, the NRC has established a long standing precedent of assuming that fuel is unburned or fresh (i.e., the fresh fuel assumption) for the purpose of evaluating criticality safety.

Since burnup credit has not been considered in the past for criticality safety analysis of spent LWR fuel, it has been necessary to develop additional technical data to supplement the data used for the fresh fuel assumption. Other areas of interest being pursued are verification of analytic methods and verification of procedures to assure proper loading for casks using burnup credit.

THE DOE/OCRWM BURNUP CREDIT PROGRAM

The OCRWM burnup credit activities are performed cooperatively by two separate groups. The base technology for burnup credit is being developed by the Burnup Credit Task Group (BCTG), lead by Sandia National Laboratories (SNL). The implementation of burnup credit for use in spent fuel cask design is the responsibility of the second group, consisting of the OCRWM cask contractors.

The BCTG activities include identifying and resolving generic technical issues associated with the design of burnup credit casks. The issues which have been identified by SNL and others within the OCRWM transportation program,[1] have also been identified more recently by an independent group of experts.[4]

Both of the OCRWM Initiative 1 cask contractors are planning to use burnup credit for criticality safety. Both of the contractors, General Atomics (GA) and Babcock & Wilcox (B&W), are using burnup credit for their pressurized water reactor (PWR) spent fuel cask designs. Neither contractor is currently using burnup credit for their boiling water reactor (BWR) spent fuel cask designs. Both contractors have met with the NRC on several occasions to discuss their approaches to using burnup credit. The BCTG has met with the NRC separately, and has supported the cask contractors in their efforts to gain NRC approval for the use of burnup credit.

CRITICALITY AND CRITICALITY SAFETY

Criticality is the achievement of a self-sustaining nuclear chain

reaction. The chain reaction proceeds as atoms of a fissile material absorb thermal (rather than fast) neutrons, fission (i.e., split) into new lighter atoms (i.e., fission products), and additional neutrons which interact with more fissile atoms. When the process continues on its own, the system of atoms of fissile material is said to be critical. The measure of criticality is the multiplication factor, k. The multiplication factor is the ratio of the rates of neutron production to neutron loss. When $k < 1$, we say the system is subcritical. Criticality is achieved when $k = 1$, and a system is said to be supercritical if $k > 1$. In theory we may consider an unbounded system of fissile material (i.e., infinite system), in which case k_{inf} is used as the measure of criticality. In practice we are interested in real systems which have finite size, in which case k_{eff} is used as the measure of criticality.

Nuclear reactors are designed to achieve criticality. The results of a reactor's operation include the conversion of fissile material to its lighter elements called fission products and heat which is used to generate electric power. About once a year, 1/3 of the fuel in a reactor is replaced (i.e., an average assembly spends about three years in a reactor before it's replaced). The spent fuel is removed because its reactivity is too low to effectively contribute to power generation in the reactor environment.

Spent fuel casks are designed to be subcritical (i.e., they must not achieve criticality). This is accomplished by using one or more of the following approaches: 1) limit the quantity of fissile material in the system, 2) remove thermal neutrons by using neutron absorbers (poisons), 3) control the population of thermal neutrons by moderator and/or reflector materials, and 4) control the spacing of the fissile elements of the system to reduce reactivity. Although the spent fuel is no longer very effective for power generation it is still somewhat reactive. Furthermore, under the assumed worst case flooded conditions of 10 CFR 71, and under transport conditions which are cooler and lack the boron control of PWR water, the spent fuel would be somewhat more reactive.

To obtain an NRC certificate of compliance the cask designer must demonstrate subcriticality of the spent fuel cask under the requirements of 10 CFR 71. Criticality safety must be demonstrated for a single package assumed to contain water, and be surrounded by water (this provides moderation and reflection of neutrons). Criticality safety must also be demonstrated for arrays of casks in their most reactive credible condition following both normal and hypothetical accident damage conditions of 10 CFR 71. For dry spent fuel casks which are water tight under normal and hypothetical accident conditions, the single package which assumes a water flooded cask is most reactive. Furthermore, since water is necessary for criticality in a LWR

system only the single package case can achieve criticality for such a dry cask system. The analytic conditions described above represents a worst case approach to assuring criticality safety. In addition, it has become a customary practice to design transport casks to a 5% criticality safety margin. That is, the cask under its most reactive circumstance must be shown to have a $k_{eff} \leq 0.95$. For OCRWM casks which will be used to transport spent fuel to a repository that will be licensed by NRC under 10 CFR 60 a cask $k_{eff} \leq 0.95$ is required by those regulations.[5]

CASK DESIGN FOR CRITICALITY SAFETY

Casks are designed and used to specific limits of fissile content and internal configuration. For multi-assembly PWR casks fuel baskets are used to limit neutron interaction between assemblies by controlling geometry and by the use of external (i.e., outside the fuel) poisons. Baskets may also use flux traps to control neutron interaction between adjacent fuel assemblies. A flux trap is basically a gap built into a basket which is activated for a water flooded cask by forming a sandwich of water surrounded by neutron poisons to separate adjacent fuel assemblies. The flux trap configuration traps neutrons travelling between fuel assemblies.

Under the fresh fuel assumption for criticality safety analysis, the fissile content of the fuel is assumed to be the same as the unused levels, and fission products that may act as internal poisons are ignored. For casks designed using burnup credit for criticality safety, the reduced fissile content of the fuel is considered along with the internal poisons present in the burned fuel.

A substantial amount of data and experience exists for criticality safety in transportation under the fresh fuel assumption. This information is directly applicable to criticality safety design for burnup credit casks. However, the use of burnup credit introduces several new variables and issues that require additional information and resolution. These include: 1) fuel characteristics and criticality analysis methods, 2) effects of fuel in-core burnup history on average and local characteristics (e.g., the so-called end effects), 3) assurance of loading burnup casks with fuel having sufficient minimum burnup characteristics, and 4) uncertainties associated with the new variables.

The predictability of spent fuel characteristics and criticality by analysis is being addressed by the BCTG headed by SNL. This activity is referred to as benchmarking.[6] Once the basic benchmarking efforts are completed by the BCTG, the cask contractors will be able to incorporate the information into their specific cask designs. Similarly the end-effects issue is being addressed by the BCTG,[7] and will be incorporated into the

specific cask design activities by the cask contractors. Finally, the issue of assuring proper cask loading will be primarily addressed by the cask contractor, with support from the BCTG who will develop loading verification measurement methods.[8]

Figure 1 presents a graphical description of an approach to criticality design safety. The graph provides a useful quantitative description of criticality safety design for a cask using either the fresh fuel assumption or burnup credit.

Curve A represents k_{inf} for an infinite array (or perfectly reflected finite array) of spent fuel assemblies having various initial enrichments, no external criticality controls, and no burnup (i.e., fresh fuel assumption). Curve B represents the k_{eff} for essentially the same system, but of finite size. The difference in k between curves A and B is due to neutron leakage. For very large arrays the leakage is small, and for small arrays the leakage would be larger (e.g., a R/B cask vs. a LWT cask).

Curve C_0 is the k_{eff} for an externally controlled version of the system represented by curve B. The external criticality controls may include poisons as well as flux traps which are part of the fuel basket. The k_{eff}s represented by curves C_1 through C_5 correspond to the system represented by C_0, but with increasing burnup credit assumed, and corresponding reduced reactivity.

The multiplication factor for our hypothetical cask design, $k_{eff,D}$, is represented by curve C_0 up to initial enrichment e_0, and curve D between e_0 and e_m. The increasing $k_{eff,D}$ (up to e_0) is the fresh fuel portion of the criticality safety design curve. The decreasing portion between e_0 and e_m is the burnup credit portion. If there were no uncertainties associated with burnup credit the burnup portion of the curve would coincide with a design multiplication factor $k_{eff,D} = 0.95$ throughout its range. The difference in k_{eff} between curve D and 0.95 represents the increase in uncertainty as more burnup credit is taken. Basically, we see that for a cask designed using the fresh fuel assumption or burnup credit the peak k_{eff} occurs at the maximum enrichment under the fresh fuel assumption. Although uncertainties can be reduced for burnup credit, they can never be reduced to zero; furthermore, they tend to increase with increased burnup credit. These factors are reflected by curve D.

USE OF A BURNUP CREDIT CASK

Operation and use of a burnup credit cask is nearly the same as operation and use of a cask designed using the fresh fuel assumption. The difference is that for fuel falling into the region where criticality safety relies on burnup credit, the loading process must assure that the additional burnup conditions are met. For proper loading of a burnup credit cask we need to know the amount of burnup the fuel has undergone, its age, and

initial enrichment. Of those, only the initial enrichment is needed for a fresh fuel cask loading. Figure 1 provides a design curve for a specific fuel type in a specific cask design along with specific age, initial enrichments, and burnups. The curve representing the cask design k_{eff} in Figure 1 can be used to develop the spent fuel loading curves shown in Figure 2. The family of loading curves, designated L_0, ... L_3, represent loading curves for different fuel types with different reactivities. Curve L_0 represents the most reactive of those considered. Curve L_3 represents the least reactive.

Spent fuel with burnup and initial enrichment above and to the left of the curve representing (or bounding) its fuel type in Figure 2, may be loaded to full capacity. Spent fuel with initial enrichment less than the enrichment designated $e_{0,i}$ (where i = 1, 2, 3, or 4) for its fuel type is loaded as a fresh fuel array, and minimum burnup is not a concern. Spent fuel with burnup and initial enrichment below and to the right of the curve representing (or bounding) its fuel type cannot be loaded without additional evaluation and possibly additional actions to control reactivity, and assure a $k_{eff} \leq 0.95$. Additional control could include reduced capacity (less fissile mass) or use of additional neutron poisons (increased external control).

OCRWM CASK DESIGNS USING BURNUP CREDIT

The two spent fuel casks currently being designed for OCRWM are the GA LWT casks and the B&W R/B cask. Both GA and B&W use burnup credit in addition to external poisons in the fuel baskets for criticality safety of their PWR loadings. Both use external poisons alone for their BWR loadings (i.e., fresh fuel assumption). Neither GA nor B&W use flux traps in their basket designs. Both GA and B&W will use loading curves similar to that shown in Figure 2. The loading operations for the OCRWM casks will rely on utility fuel management practices which are regulated by the NRC, and verification of cask loading through physical measurements.

The GA-4 Legal Weight Truck Cask

GA uses two separate cask bodies for their LWT cask system. The GA-4 is used for spent PWR fuel. The GA-9 is used for spent BWR fuel. The GA-4 has a capacity of up to four PWR assemblies with initial enrichments of up to 4.5 wt% U-235. The GA-4 uses a cruciform stainless steel fuel support structure (FSS or basket) which has boron carbide (B_4C) rods held in the FSS plates to provide external criticality control. GA takes credit for only a small portion of the available fission products for demonstrating criticality safety. Those fission products used have been well characterized, and represent about 80% of the control available from fission products.

GA is currently considering a single curve for use in assuring safe loading of a burnup credit cask. The single curve is conservatively based on the most reactive fuel types to be approved for the GA-4 cask design. The GA-4 fuel loading curve is convex outward rather than a straight line as shown in Figure 2. For the GA-4 cask, burnup credit is taken for spent PWR fuel with initial enrichments between 3 wt% U-235 and the maximum initial enrichment for the cask, 4.5 wt% U-235. At the maximum enrichment, the minimum burnup is 25 gigawatt-day/metric ton uranium (GWD/MTU). The loading curve is based on a $k_{eff} \leq 0.95$ with all calculational biases and uncertainties due to the use of burnup credit taken into account.

The B&W Rail/Barge Cask

B&W uses a single cask body for their BR-100 R/B cask. Separate interchangeable baskets are used for PWR or BWR spent fuel in the BR-100. Only the PWR configuration of the BR-100 uses burnup credit. The BR-100 has a capacity of up to 21 PWR assemblies with initial enrichments of up to 4.5 wt% U-235. The BR-100 basket is a stainless steel structure with Boral (borated aluminum) plates to provide external criticality control. The basket also includes copper plates to enhance heat transfer. Like GA, B&W takes credit for only a small portion of the available fission products for demonstrating criticality safety. Those fission products used have been well characterized, and represent about 80% of the control available from fission products.

B&W is currently considering a single curve for use in assuring safe loading of a burnup credit cask. The single curve is conservatively based on the most reactive PWR fuel types to be approved for the BR-100 cask design. The BR-100 fuel loading curve has a slightly convex outward shape rather than the straight line shown in Figure 2. For the BR-100 cask, burnup credit is taken for spent PWR fuel with initial enrichments between 2.2 wt% U-235 and the maximum initial enrichment for the cask, 4.5 wt% U-235. At the maximum enrichment, the minimum burnup is 30 GWD/MTU. The loading curve is based on a $k_{eff} \leq 0.95$ with all calculational biases and uncertainties due to the use of burnup credit taken into account.

CONCLUSIONS

Although no LWR spent fuel casks using burnup credit have been certified by the NRC, the regulations do not prohibit such an action. Furthermore, the NRC has certified a cask for burnup credit under the condition of verification of the loaded cask by measurement. It is clear that the use of burnup credit as part of the criticality control for a spent fuel cask introduces new variables in evaluating criticality safety. It is also clear that for burnup credit casks, loading is somewhat more important

for criticality safety than loading of a cask that is designed used based on the fresh fuel assumption. For the loading of a fresh fuel cask, only initial enrichment needs to be considered to assure criticality control. For a burnup credit cask, initial enrichment, age, and burnup must be considered to assure criticality control.

The uncertainties associated with the introduction of burnup credit for criticality control of spent LWR fuel in transportation casks have been identified. Furthermore, these uncertainties are being addressed adequately, and technical issues are being resolved in a manner that will assure criticality safety for burnup credit cask designs. In addition, the use of utility fuel management practices coupled with verification measurements will assure proper loading of burnup credit casks. It is believed that a strong basis is being developed for NRC's eventual approval of spent LWR fuel casks that use burnup credit as part of their criticality safety design.

REFERENCES

1. Sanders, T.L., R.M. Westfall, and R.H. Jones, 1987, "Feasibility and Incentives for the Consideration of Spent Fuel Operating Histories in the Criticality Analysis of Spent Fuel Shipping Casks," SAND87-0151, Sandia National Laboratories, Albuquerque, NM.

2. U.S. Nuclear Regulatory Commission, 1983, "Packaging and Transportation of Radioactive Materials," Code of Federal Regulations, Title 10, Part 71, Washington, DC.

3. U.S. Nuclear Regulatory Commission, October 1991, "Directory of Certificates of Compliance for Radioactive Materials Packages," NUREG-0383, V2, Rev. 14.

4. Carlson, R.W., and L.E. Fischer, July 1990, "Safety Implications of Burnup Effects in Criticality Safety Margins for Spent Pressurized Water Reactor Fuel Transport and Storage," UCRL-ID-104572, Lawrence Livermore National Laboratory, Livermore, CA.

5. U.S. Nuclear Regulatory Commission, 1988, "General Design Criteria for the Geological Repository Operations Area," Code of Federal Regulations, Title 10, Part 60.131, Washington, DC.

6. Brady, M.C., D. Napolitano, "Code Benchmarking," INMM Spent Fuel Seminar IX, Jan. 15-17, 1992, Washington, DC.

7. Marotta, C.R., M.C. Brady, D. Napolitano, "End Effects and Uncertainties," INMM Spent Fuel Seminar IX, Jan. 15-17, 1992, Washington, DC.

8. Ewing, R., and S. Bierman, "Scoping Analysis of Spent Fuel Measurement Techniques," INMM Spent Fuel Seminar IX, Jan. 15-17, 1992, Washington, DC.

Criticality Safety Design Curves for a Spent Fuel Cask

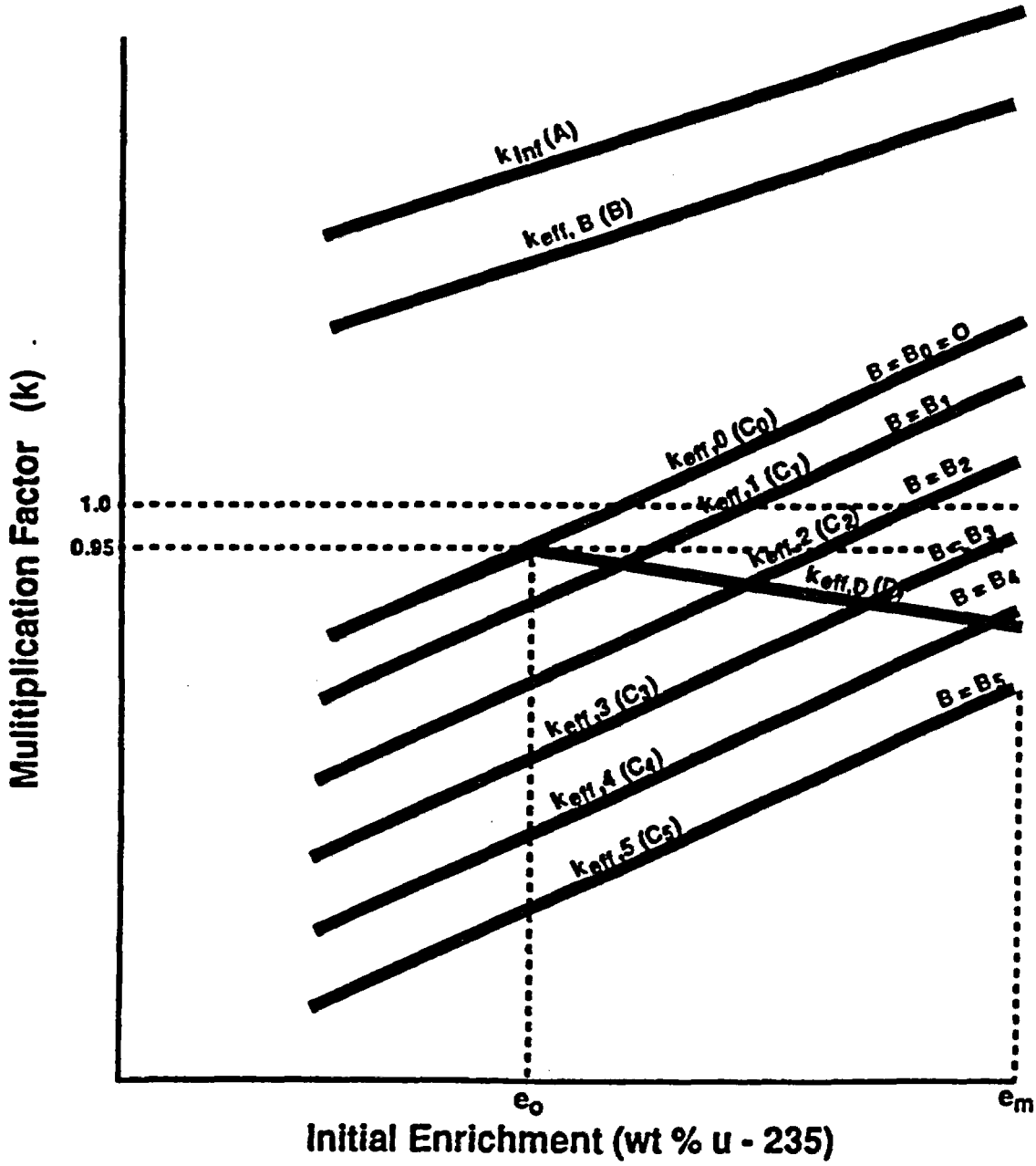

Figure 1. Criticality safety design curve.

Curves are for a worst case (criticality safety) condition (water filled cask with full water reflection).

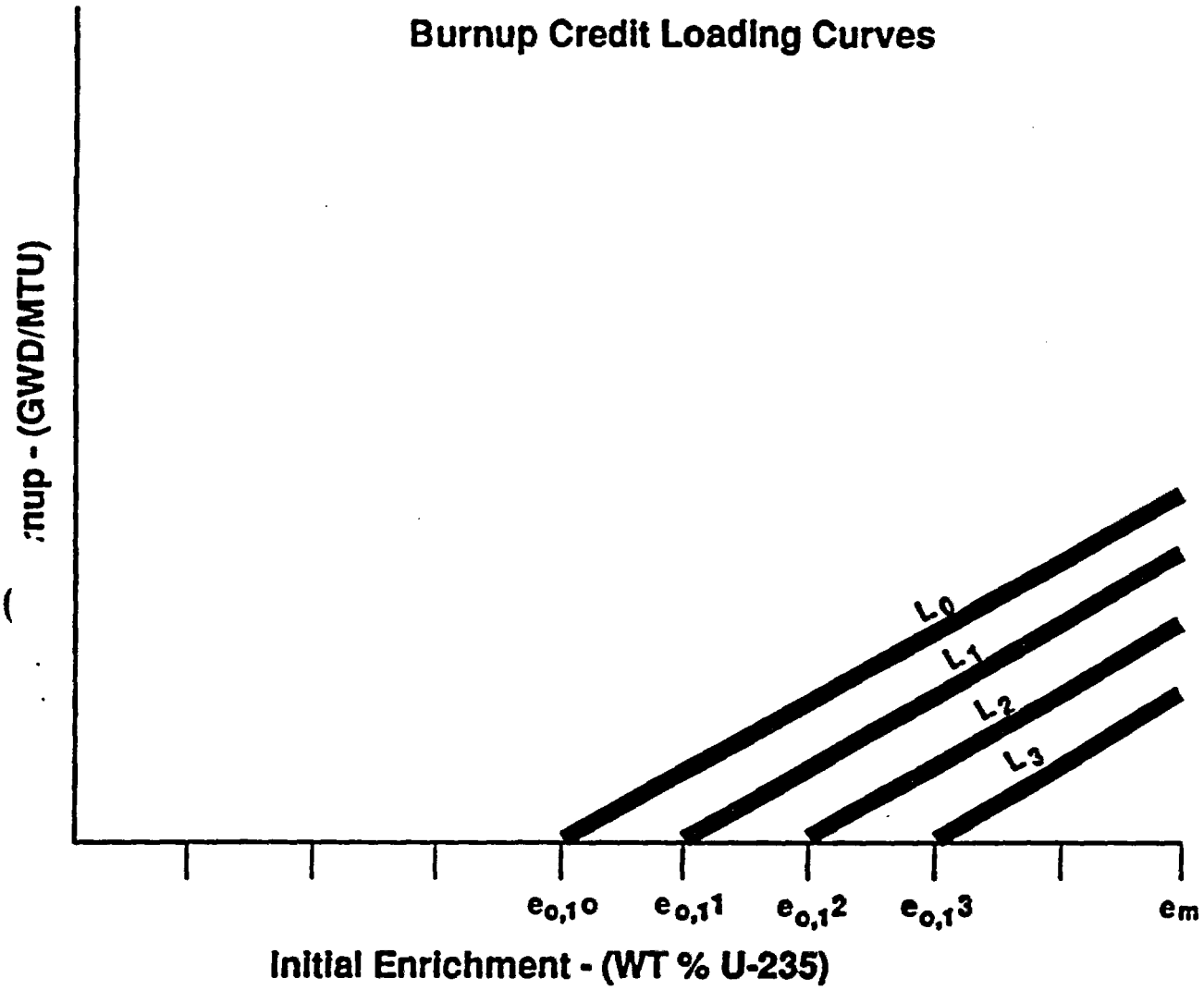

Figure 2. Burnup credit loading curve.

Loading curves meet $k_{eff} \leq 0.95$ with calculational biases and burnup credit uncertainties included. Curves are for a worst case (criticality safety) condition (water filled cask with full water reflection).

SPENT FUEL MANAGEMENT

SEMINAR IX

SPECIAL BURNUP CREDIT SESSION

INSTITUTE OF NUCLEAR MATERIALS MANAGEMENT

JANUARY 15-17, 1992
WASHINGTON, D.C.

ENCLOSURE 9

EFFECT OF AXIAL EXPOSURE DISTRIBUTIONS IN BURNUP CREDIT CRITICALITY ANALYSES*

Charles R. Marotta
Consultant
Sandia National Laboratories**
P.O. Box 5800
Albuquerque, New Mexico 87185

M. C. Brady
Oak Ridge National Laboratory***
P.O. Box 2008
Oak Ridge, Tennessee 37831-6370

D. G. Napolitano
Yankee Atomic Electric Company
580 Main Street
Bolton, Massachusetts 01740-1398

To be presented at
Spent Fuel Management Seminar IX
Loew's L'Enfant Plaza
Washington, DC USA
January 15-17, 1992

Sponsored by
Institute of Nuclear
Materials Management

"The submitted manuscript has been authored by a contractor of the U.S. Government under contract No. DE-AC05-84OR21400. Accordingly, the U.S. Government retains a nonexclusive, royalty-free license to publish or reproduce the published form of this contribution, or allow others to do so, for U.S. Government purposes."

---

*Research performed under Sandia National Laboratories contract 66-0162 with Oak Ridge National Laboratory and Sandia National Laboratories contract 75-0590 with Yankee Atomic Electric Company.

**A U.S. Department of Energy facility operated under contract DE-AC04-76DP00789.

***Managed by Martin Marietta Energy Systems, Inc., under contract DE-AC05-84OR21400 with the U.S. Department of Energy.

EFFECT OF AXIAL EXPOSURE DISTRIBUTIONS IN BURNUP CREDIT CRITICALITY ANALYSES*

Charles R. Marotta
Consultant
Sandia National Laboratories
P.O. Box 5800
Albuquerque, New Mexico 87185

M. C. Brady
Oak Ridge National Laboratory
P.O. Box 2008
Oak Ridge, Tennessee 37831-6370

D. G. Napolitano
Yankee Atomic Electric Company
580 Main Street
Bolton, Massachusetts 01740-1398

ABSTRACT

Burnup credit is the application of the effects of fuel exposure or burnup to nuclear criticality considerations in the design of spent fuel transport and storage facilities. One unique issue in this design approach is the proper treatment of the axial variation in burnup experienced by pressurized-water-reactor fuel assemblies. This paper describes calculations and results quantifying this effect in the criticality analysis of spent fuel array geometries. Recommendations are made to provide guidance in evaluating these effects via three different approaches. Final selection of the analysis methodology would be dependent on the specific application and the degree of accuracy required.

INTRODUCTION

Reactivity effects due to the axial exposure distribution in pressurized-water-reactor (PWR) fuel assemblies resulting from the uneven axial power distribution experienced by PWRs is referred to as the axial or "end effects." As burnup proceeds in-core, the central fuel regions become more burned than the top and bottom of the fuel assembly because of the buckled shape of the axial flux distribution. This phenomenon results in more reactive fuel at the top and bottom. In a typical PWR, the top is usually less exposed than the bottom because of a slight bottom peaking in the power distribution due to moderator density effects. As a result, the top becomes more reactive relative to the bottom, which, in turn, is more reactive than the higher burned central fuel region. Generally, when the reactor is at power, these effects are not pronounced. When core power is reduced to zero and/or coolant temperature is reduced, there can be a positive effect in reactivity

from the redistribution of flux to the top of the fuel. From this discussion, one may conclude that the operating history of the reactor will have a direct effect on the axial exposure distribution and, thus, the reactivity of the spent fuel.

In the past, conservative criticality analyses of PWR fuel in storage and transport arrays have been done in two spatial dimensions (2-D), typically modeling the radial extent of an array. This traditional approach, which uses the fresh fuel assumption, neglects axial leakage and gives a higher k_{eff} than that which would be calculated for a three-dimensional (3-D) model. In the fresh fuel assumption, fuel is assumed to be unburned and of the highest conceivable enrichment. If the depleted state of the fuel is represented, a 2-D model may no longer yield conservative results due to the increased worth of the underburned fuel ends. However, experience must be accumulated to determine what level of detail is required for the 3-D representation of the axial exposure distribution. Earlier scoping calculations to evaluate the feasibility of burnup credit represented the entire active fuel length as a single composition of fuel at a burnup equal to 82% of the assembly average (based on an estimate of the power generation rate in the upper axial 2 ft).[1] Since that time, many different approaches to evaluating burnup credit in the criticality analyses of spent fuel storage arrays[2-8] and transport casks[9-16] have been utilized and reported.

The methods reported in refs. 7 and 8 are unique in their approach to evaluating end effects. Reference 7 reports using diffusion theory constants edited from CASMO-2E calculations in 1-D diffusion theory calculations to estimate k_{eff} for the axially distributed burnup case. The end effect was then derived as the difference between this value and the k_∞ value corresponding to the assembly-average burnup. The potential reactivity worth of the fuel tips was demonstrated in ref. 8 based on an infinite array of shortened fuel pins with an assumed average discharge enrichment of 2.0 wt % ^{235}U. Criticality calculations for this case were performed using the 3-D Monte Carlo code, KENO IV. Most of the other references address the issue of end effects using one of three general approaches: (1) 2-D arrays with a penalty for burnup determined from comparisons with 3-D calculations; (2) 3-D calculations with uniform axial burnup representing the assembly-average, and using a post-calculational bias derived from multiaxial-zone 3-D calculations to account for end effects; and (3) use of explicit 3-D calculations.

All of these approaches to evaluating the end effect have a common element. In order to quantify these end effects, a 3-D representation of the PWR exposure distributions and corresponding isotopics must be used. This method is generically difficult because of the diversity of PWR assembly designs and operating conditions. However, considerable data exist on measured and calculated exposure distributions within the nuclear utility industry, and validated codes to calculate the corresponding isotopics are readily available in both the public and private software domains. Specific experiments have been performed[17] to measure both the axial exposure distribution and isotopic content of spent fuel in a U.S. Department of Energy Office of Civilian Radioactive Waste Management (OCRWM) program. The proper characterization of these reactivity effects is essential to the acceptance of burnup credit in spent fuel transport and storage arrays. Various fuel and operating characteristics that influence the relative reactivity worth of the fuel tips will be noted. This paper will also discuss the qualitative and quantitative results reported in refs. 2, 8, and 11-13 and will make recommendations regarding several alternative approaches to evaluating end effects.

DEPENDENCE ON FUEL AND OPERATING CHARACTERISTICS

Fuel characteristics such as the initial ^{235}U enrichment, burnup and post-discharge cooling time have been used to parameterize k_∞.[18] The general trends are for k_∞ to increase with initial

enrichment and to decrease with burnup and cooling time. Studies have also been performed to evaluate trends in the magnitude of the end effect with these fuel characteristics.[6,7,9,12]

INITIAL ENRICHMENT

Generally, one would not expect to see a change in the reactivity worth of the fuel tips as a function of the initial enrichment of the fuel. Recall that the end effect represents the difference in the relative worth of the fuel tips to the central fuel region. The initial enrichment of the fuel assembly is uniform in the length of the assembly and, therefore, would not be expected to contribute directly to the end effect. The influence of initial enrichment on the central region of the fuel would be nearly the same as at the fuel tips. Calculations have been performed that demonstrate the changes in the end effect with enrichment are within the statistics of the Monte Carlo codes used to evaluate the end effect or suggest a slight decrease with increasing enrichment at higher burnups.[6,12]

ASSEMBLY BURNUP

The equation derived for k_∞ in ref. 18 illustrates that the infinite multiplication factor will decrease at a rate slightly less than 0.01 times the burnup (neglecting the small positive quadratic term with burnup). Assume that the axial burnup distribution (or profile) is held constant. For example, the burnup at the 1-ft tips is one-half that of the central region, the burnup in the central region may be taken to be approximately equal to 1.1 times the assembly-average burnup. As the assembly-average burnup increases, the magnitude of the difference in burnup between the fuel tips and the central region increases. This implies that the difference in reactivity between the two regions will also increase. The multiplication factor representing the reactivity worth of the central region will decrease faster than that of the fuel tips. This leads to the expectation that the end effect, defined as the difference in the relative worth of the fuel center versus the tips, will increase with increasing burnup. This supposition is supported by analyses reported in refs. 6, 8, 9, 12, and 13, among others. In general, these results are in good agreement for cases with similar assumptions in cooling time and with similar assumed axial burnup distributions. These results indicate that at low burnups, the end effect is actually a negative effect (i.e., representing the average burnup is more conservative than explicitly modeling the axially distributed burnup). As burnup increases, the end effect will increase and the end effect becomes positive. The burnup value at which this occurs is dependent on many factors, including the burnup profile and the array geometry itself, but generally has been found to be between 15 and 25 GWd/MTU.

COOLING TIME

The dependence of the end effect with discharge or cooling time cannot be deduced from the equation presented in ref. 18 because, as was the case with initial enrichment, cooling time is constant for a given fuel assembly. However, the influence of cooling time is directly related to the difference in burnup between central fuel region and the fuel tips. A review of the nuclear characteristics of the major absorber nuclides in spent fuel reveals that only three nuclides (^{241}Pu, ^{241}Am, and ^{155}Gd) show a strong dependence on cooling time. (Plutonium-238, a fissionable nuclide, has an 87.7-y half-life, causing its contribution to k_{eff} to decrease slowly with cooling time. However, its overall contribution to k_{eff} is small. The fission product ^{151}Sm ($t_{1/2}$ = 90 y) is an absorber whose concentration also decreases slowly with cooling time.) All other important nuclides are effectively stable (some of the actinides have extremely long half-lives, e.g. ^{235}U). The decay of ^{241}Pu ($t_{1/2}$ = 14.4 y), a fissile nuclide, with a positive effect on k, leads to the production of ^{241}Am. This actinide has a small fission cross section at thermal energies and a high parasitic absorption cross section and, therefore, a negative effect on k. Production of the fission product absorber ^{155}Gd results from the

decay of ^{155}Eu ($t_{1/2}$ = 4.71 y). The net effect of the production of the absorbers, ^{241}Am and ^{155}Gd, and the decay of the fissile ^{241}Pu is that k decreases with cooling time as indicated in ref. 18. However, the quantities of both ^{241}Pu and ^{155}Eu increase with burnup,[18] therefore increasing the quantities of ^{241}Am and ^{155}Gd in the cooled fuel. Regions of higher burnup with higher concentrations of these important absorber nuclides which vary with cooling time will show a greater dependence on cooling time than the lower-burn regions. As such, the worth of the higher-burned central fuel region will decrease with cooling time more than the lower-burned fuel tips. Therefore, the relative worth of the fuel tips will increase with cooling time (i.e., the end effect will increase with cooling time).

REACTOR OPERATING HISTORY AND AXIAL BURNUP PROFILE

Uncertainties in predicting the multiplication factor for a spent fuel system must include reactor operation effects. Reference 9 describes these as effects due to (1) partial control rod insertion during the operating cycle, (2) presence of burnable poisons [including both burnable poison rods (BPRs) and fuel designs that include burnable poisons as an integral part of the fuel], (3) extended low-power operation (i.e., power density), and (4) the fuel assembly position during operation (i.e., near the periphery of the core surrounded by other fuel assemblies). Other authors have included additional parameters, such as the moderator density history.[2] The influence of these operating history effects have generally been taken to represent uncertainties in the calculations. However, these parameters directly affect the axial burnup distribution or profile. Selection of a "conservative" profile based on a study of a large number of utilities reported would compensate for the range of values these parameters typically experience. The "design basis profile," chosen from the careful study of actual profiles, could be used to represent a worst-case situation, thereby relieving the necessity to add an uncertainty to the calculation in order to account for these operational uncertainties. Most of the work to date has assumed a typical burnup profile and, using results from sensitivity studies, added a Δk uncertainty (or criticality safety margin) to the calculated multiplication factor to conservatively account for any variation in these parameters. Calculations have been performed to compare the results from these typical profiles with an assumed conservative profile. In these calculations, performed at Oak Ridge National Laboratory, burnup profiles representative of operating cycle burnups were taken from utility data. Additional calculations were performed assuming a conservative "2-to-1" profile in which the 1-ft end regions are given an average burnup equal to one-half of that in the central 10-ft region of the fuel assembly model. Calculations were performed to quantify the end effect as a function of burnup (assuming 4.2 wt % initial ^{235}U) for a mock rail cask (36 fuel assemblies with a borated stainless steel basket). The results using the profiles extracted from the reactor data showed a slowly increasing trend, with burnup turning from negative to positive at ~30 GWd/MTU. The magnitude of the end effect for this case was small (on the order of 1% at 40 GWd/MTU). Use of the conservative 2-to-1 profile yielded much higher Δk values (~5% at 40 GWd/MTU) increasing at a faster rate with burnup. The turnover under these assumptions was near 20 GWd/MTU. These results illustrate that the magnitude of the end effect is dependent on the assumed axial burnup distribution. Recall that the final Δk for the case with the reactor cycle profiles would need to include an additional bias to compensate for the uncertainty in operating history effects, whereas the use of the conservative profile inherently compensates for these effects.

GEOMETRY

The magnitude of the end effect will also depend on both the size and axial distribution of neutron absorbers in the specific storage or transport array, both on its size and the corresponding

axial distribution of neutron absorbers. Depending on the axial distribution of neutron poison, the end effect can be exaggerated or diminished relative to uniform neutron poison distribution. A specific example will be cited in a later section of this paper. As one might expect, the size of the fuel storage array or shipping cask will influence the end effect due to differences in leakage rates. Smaller systems will generally have higher leakage. Depending on the specific geometry, this effect can be particularly significant at the fuel tips where the reactivity is higher but the cask body is generally less shielded. The end effects for larger systems (on the order of 31 to 36 fuel assemblies) exhibit trends similar to those observed for infinite systems.

Quantitative examples of the influence of the parameters described above are discussed in the following sections.[2,8, 11-13]

FUEL STORAGE ARRAYS

Criticality analyses of the Seabrook Station spent fuel storage racks were performed with CASMO-3/SIMULATE-3 nodal analysis to determine the end effects. Axial burnup distributions used in the rack analysis came from a validated in-core model. Batch average exposure characteristics from Cycles 1 and 2 were used with fuel assemblies of 3.1 wt % ^{235}U initial enrichment. The calculations show that at 0 burnup, neglecting axial leakage is indeed conservative by 0.002 k. However, as burnup increases, there is an initial decrease in reactivity due to increased leakage, and then a turnover and steady increase in reactivity in the 3-D analysis relative to the 2-D model. At 25.5 GWd/MTU, this difference is 0.0116 Δk.

FUEL TRANSPORT CASKS

Criticality analyses of a hypothetical 31-fuel-assembly cask were also performed with the CASMO-3/SIMULATE-3 in two and three dimensions. The cask basket was composed of borated steel canisters that fully cover the fuel assembly active fuel region. The fuel assemblies modeled in the calculation were Westinghouse 15 x 15 lattices (2.573 initial wt % ^{235}U) which had been discharged from Surry Unit 1, Cycle 2, with an average burnup of 22.60 GWd/MTU. The k_{eff} for the 2-D model was 0.8105, and 0.8270 for the 3-D model (including axial exposure and moderator history effects), an increase of 0.0165 Δk. This result is consistent with fuel storage rack analysis for fuel of approximately the same burnup.

End effects are not only a result of the axial distribution of fuel exposure, but are also influenced by the axial distribution of neutron absorbing materials (poisons) surrounding the spent fuel. Foreshortened or nonuniform neutron absorbers can exaggerate or diminish the reactivity effects caused by the unburned ends of the fuel assemblies. This situation is illustrated in the GA-4 transport cask model. In this design, a central steel support structure with horizontal tubes containing B_4C pellets is used for criticality control. Two sizes of pellets are used in the central cross that separates the four PWR fuel assemblies: 0.278-in.-diam pellets are used at the top and bottom 12 to 15 in. of the case, and 0.426-in.-diam pellets are used in the central region. Because of the positioning of the active fuel region in the cask (i.e., only the bottom of the fuel assembly is exposed to the region of small B_4C pins), the bottom of the fuel assembly is less poisoned and therefore more reactive than the top. Criticality analyses of the GA-4 transport cask suggest that the end effects are diminished because of the influence of the nonuniform distribution of neutron poisons. In some

exposure cases, the flux distribution is bottom peaked rather than top peaked, as in the case of uniform poison.

The 31-element hypothetical transport cask was also modeled with the KENO V.a Monte Carlo transport code. Cross-section processing and fuel-depletion calculations were necessary to prepare material specifications for the KENO V.a model. The SCALE code system[19] was used to perform these calculations. Predictions of both the effective multiplication factor and the magnitude of the end effect, for cases with similar fuel characteristics and axial burnup distributions, were in good agreement with the CASMO-3/SIMULATE-3 results.[20]

DISCUSSION AND RECOMMENDATIONS

The purpose of this paper is not to recommend or to compare analysis methodologies such as KENO V.a and CASMO-3/SIMULATE-3. The issue of the proper analysis of the reactivity worth of the fuel tips is addressed more generically than from that point of view. Any calculational methodology used to quantify end effects should be validated against existing experimental data for spent fuel systems[20]. In general, it is recommended that a constant cooling time of 5 years be used to evaluate burnup credit; although the end effect is smaller for 5 years than for 10 years, the overall k_{eff} will be higher. Since the majority of the spent fuel currently on inventory at U.S. nuclear power facilities exceeds the 5-year limit, this will result in a conservative approximation. Each individual spent fuel facility will need to determine a range of burnup and corresponding initial enrichments that can be safely accommodated in their facility. Scoping studies to determine these parameters should rely on either a conservative burnup profile derived from a large data base of utility data, or from a typical profile with a post-calculation bias to account for operating history effects. The evaluation of the end effect should be performed for the limiting burnup and corresponding enrichment. This section discusses three approaches to evaluating the end effect: explicit 3-D calculations, approximate 2-D calculations, and simplified hand calculations based on perturbation theory.

EXPLICIT 3-D CALCULATIONS

Results from a limited study to evaluate the effect of the number of axial intervals used in the 3-D model on k_{eff} are given in ref. 11. The burnup profile is generally quite flat across the central 8 ft of the fuel assembly, and, thus, this region does not require any detailed modeling. However, the burnup profiles change rapidly in the upper and lower 2 ft of the assembly. A statistical Monte Carlo code was used to evaluate k_{eff} as a function of the number of regions used to model the tips. An increase in calculated k_{eff} was observed when the fuel tips were subdivided into three regions; however, no statistically significant differences were observed when each of the tips further divided into seven finer groups. Therefore, the use of seven axial intervals with the finer divisions concentrated at the upper and lower 2 ft of the fuel should be sufficient to model the axial effect.

The use of a 3-D model with only one axial material (or burnup) zone may be used if the user applies a correction factor or bias. Figure 1 is an illustration of how the end effect might vary with burnup for large and small arrays. A figure such as this could be used as a general guide for evaluating the change in end effect with increasing burnup for fuel of a given initial enrichment.

APPROXIMATE 2-D CALCULATIONS

Two-dimensional calculations are adequate when a comparison with a detailed 3-D calculation verifies that, for the particular spent fuel facility, they produce conservative results. This

determination will depend on the geometry and the distribution of neutron poisons for a specific design. The use of a generalized 2-D bias derived from a detailed 3-D calculation may also be considered for designs for which the 2-D result is nonconservative. Care should be taken in 2-D models to explicitly represent the radial extent of the model.

HAND CALCULATIONS

The additional reactivity, $\Delta k/k$, incurred from the relatively underburned tips of a PWR spent fuel assembly is estimated in this calculational approach by a simplified one-group perturbation theory. This is completely analogous to the reactor-control method in which the worth of a system's localized poison is compared with the worth of that poison uniformly spread throughout the system. The perturbation in this instance is the ^{235}U enrichment increase in the assembly (~1 ft) tips compared with the discharge enrichment residing in the assembly's central 10 ft. The system is represented by an infinite (in the x-y direction) array of 12-ft-tall (finite in the z direction) PWR fuel assemblies with infinite water reflectors (top and bottom) at a given ^{235}U enrichment. KENO IV, 27-groups generated a clean-fresh k_∞ versus ^{235}U enrichment curve to establish $\Delta k_\infty/k_\infty$ from natural to 5 wt % ^{235}U for conservative responses of an infinite system to enrichment perturbations.

Estimates of these end effects are performed by simple k_∞ enrichment perturbation calculations based solely on the estimated ^{235}U enrichment difference between the tip (1 ft) and the central (10 ft) portions of the assembly. This difference is established from the utility's quoted average ^{235}U discharge enrichment for the assembly and a measured (or conservatively calculated) ratio, R, which is the axial burnup (or gross gamma activity) averaged over the central 10 ft to the axial burnup averaged over the 1-ft tip regions considered identical. It is assumed that the regional residual ^{235}U enrichment is inverse to the region burnup. This latter observation establishes the tip enrichment to be R multiplied by the "quoted" discharge ^{235}U enrichment. Neglecting all the accumulated plutonium isotopes turns out to be conservative in calculating the end effects in this approach. R, as defined and interpreted, gives proper dependence of the end-effect reactivity with burnup and cooling time.

The method is independent of size, internals, and shield materials of transport and storage casks containing such spent fuel, and predicts $\Delta k_\infty/k_\infty$ in the range of 2.5 to 4.5% for a realistic R of 1.75 and discharge enrichments between 2.0 to 0.8 wt % ^{235}U. For a mixture of assemblies, a linear prorating of $\Delta k_\infty/k_\infty$ assembly is recommended. Figure 2 gives the estimated end effects (for two tips) for PWR discharge enrichments 0.8, 1.0, 1.25, 1.5, 1.75, and 2.0 wt % ^{235}U as a function of R for an unlimited array of spent fuel assemblies.

CONCLUSIONS

Several alternative methods for evaluating the increased reactivity at the underexposed tips of spent PWR fuel have been discussed. The most sensitive parameter in quantifying the reactivity worth of the underburned tips is the axial exposure profile assumed in the detailed 3-D calculations. Operating uncertainties, such as the presence of burnable poisons, the position of control rods during irradiation, the position of the fuel assembly in-core, the axial distribution in water density, etc., must be incorporated in the selection of a conservative profile. The large quantity of commercial reactor data that are available should be utilized in a data base from which a typical or conservative profile could be determined. Based on the selection of this design basis profile, any of the methodologies outlined in this paper may be utilized to estimate the end effect for the spent fuel facility of interest.

Note, however, that a 3-D model will be required to determine the bias and uncertainty in the simpler calculational approaches. With good judgement, a set of generic biases could be determined as a function of burnup and array size that could be applied in many cases.

ACKNOWLEDGMENTS

The U.S. burnup credit program is dependent on a range of expertise, and the authors would like to acknowledge S. M. Bowman, O. W. Hermann, C. V. Parks, J.-P. Renier, and R. M. Westfall of ORNL for their substantial contributions to the different phases of the project. We would also like to express our appreciation for the technical expertise, assistance, and advice from D. G. Adli (Yankee Atomic Energy Company), S. R. Bierman (Pacific Northwest Laboratory), W. H. Lake (U.S. Department of Energy), O. Ozer (Electric Power Research Institute), T. L. Sanders (Sandia National Laboratories), and M. L. Smith (Virginia Power Company).

This work is supported by the Office of Civilian Radioactive Waste Management of the U.S. Department of Energy and managed by Sandia National Laboratories.

REFERENCES

1. T. L. Sanders and R. M. Westfall, "Feasibility and Incentives for Burnup Credit in Spent Fuel Transport Cask," *Nucl. Sci. Eng.* 104 (1990).

2. D. G. Napolitano and D. G. Adli, *Criticality Analysis of Seabrook Station's New and Spent Fuel Storage Racks*, YAEC-1778 (February 1991).

3. J. R. Thornton, "Burnup Credit in a Dry Storage Module," *Proc. of a Workshop on the Use of Burnup Credit in Spent Fuel Transport Casks*, Washington, D.C., February 21-22, 1988, pp. 91-107.

4. R. W. Rasmussen, "Verification of Criticality Safety in On-Site Spent Fuel Storage Systems," *Proc. of a Workshop on the Use of Burnup Credit in Spent Fuel Transport Casks*, Washington, D.C., February 21-22, 1988, pp. 237-247.

5. William A. Boyd and Mark W. Fecteau, "Effect of Axial Burnup on Fuel Storage Rack Burnup Credit Reactivity," *Trans. Am. Nucl. Soc.* 62, 328 (1990).

6. M. Takano and F. Masukawa, "Effect of Fuel Burnup Distribution on Criticality Safety," *Proc. of International Conference on Nuclear Criticality Safety*, 9-13 September 1991, Oxford, U.K., Vol. 1, p. II-107.

7. S. E. Turner, "An Uncertainty Analysis - Axial Burnup Distribution Effects," *Proc. of a Workshop on the Use of Burnup Credit in Spent Fuel Transport Casks*, Washington, D.C., February 21-22, 1988, pp. 167-177.

8. C. R. Marotta, "Bounding Estimates of Criticality Effects of Unburned LWR Fuel Assembly Tips for Casks Assuming Burnup Credit," *Proc. 9th International Symposium on the Packaging and Transportation of Radioactive Materials*, June 11-16, 1989, Washington, D.C., CONF-890631, Vol. 2, p. 793.

9. R. W. Carlson and L. E. Fischer, "Burnup in Criticality Safety for Spent Fuel Casks," *RAMTRANS* 1, 3, pp. 187-199 (1990).

10. M. Smith, *Evaluation of Burnup Credit for Dry Storage Casks*, EPRI NP-6494 (August 1989).

11. M. C. Brady, C. V. Parks, and C. R. Marotta, "End Effects in the Criticality Analysis of Burnup Credit Casks," *Trans. Am Nucl. Soc.* 62, 317 (1990).

12. M. C. Brady and T. L. Sanders, "A Validated Methodology for Evaluating Burnup Credit in Spent Fuel Casks," *Proc. of International Conference on Nuclear Criticality Safety*, 9-13 September 1991, Oxford, U.K., Vol. 1, p. II-68 (1991).

13. Dominic G. Napolitano and Dariush G. Adli, "Burnup Credit Criticality Analysis Using Advanced Nodal Techniques," *Proc. International Topical Meeting of Advances in Mathematics, Computations, and Reactor Physics*, April 28-May 2, 1991, Pittsburgh, Pa., Vol. 1, p. 5.2 3-1.

14. Jack K. Boshoven and Shiaw-Der Su, "Burnup Credit Application for GA-4 Transportation Casks," *Trans. Am. Nucl. Soc.* 62, 318 (1990).

15. E. J. McGuinn, P. C. Childress, and C. M. Bochard, "BR-100 Spent Fuel Shipping Cask," *Proc. 9th International Symposium on the Packaging and Transportation of Radioactive Materials*, June 11-16, 1989, Washington, D.C., CONF-890631, Vol. 3, p. 1796.

16. N. R. Smith and M. H. Watmough, "Progress in the Development of a Validated Method for Assessing the Reactivity Effects Associated with Fuel Burnup," *Proc. of International Conference on Nuclear Criticality Safety*, 9-13 September 1991, Oxford, U.K., Vol. 1, p. II-83 (1991).

17. S. R. Bierman, "Spent Reactor Fuel Benchmark Composition Data for Code Validation, *Proc. of International Conference on Nuclear Criticality Safety*, 9-13 September 1991, Oxford, U.K., Vol. 1, p. II-113 (1991).

18. S. P. Cerne, O. W. Hermann, and R. M. Westfall, *Reactivity and Isotopic Composition of Spent PWR Fuel as a Function of Initial Enrichment, Burnup, and Cooling Time*, ORNL/CSD/TM-244, Martin Marietta Energy Systems, Inc., Oak Ridge Natl. Lab. (October 1987).

19. *SCALE: A Modular Code System for Performing Standardized Computer Analyses for Licensing Evaluation*, NUREG/CR-0200, Rev. 4 (ORNL/NUREG/CSD-2/R4), Vols. I, II, and III (draft February 1990). Available from Radiation Shielding Information Center as CCC-545.

20. M. C. Brady and D. G. Napolitano, "Validating Analysis Methodologies Used in Burnup Credit Criticality Calculations," to be presented at Spent Fuel Management Seminar IX, Washington, D.C., January 15-17, 1992.

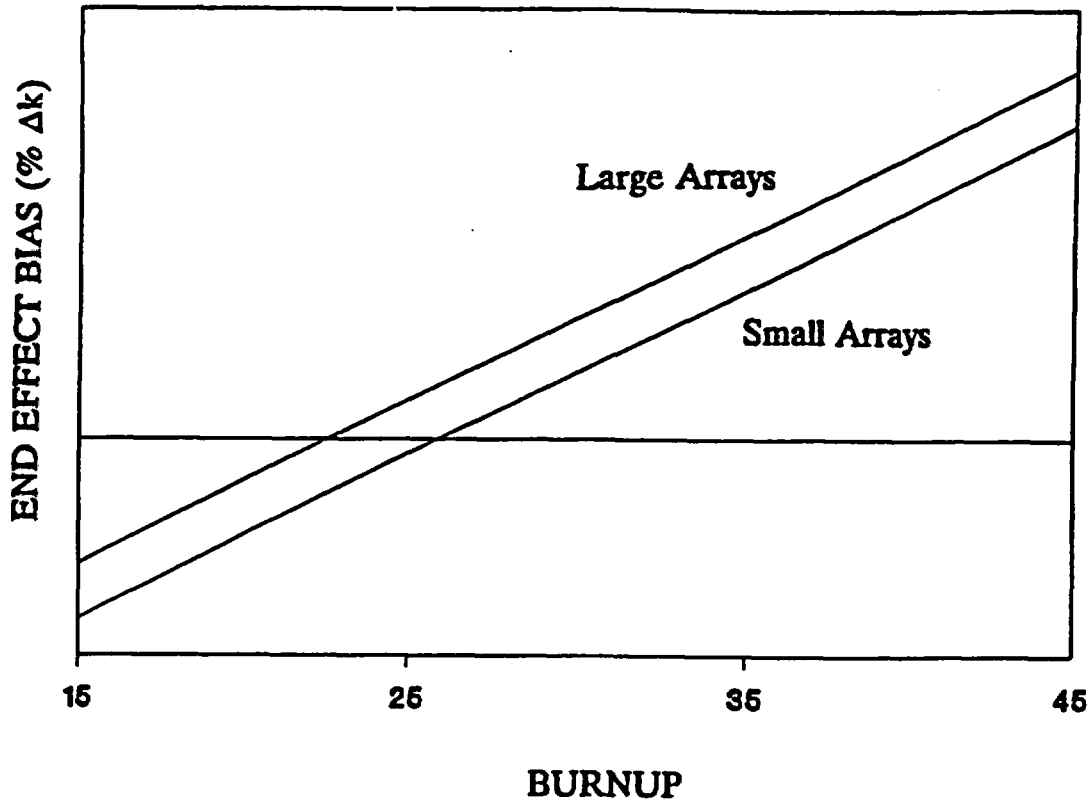

Fig. 1. Illustration of end effect bias (% Δk) with increasing burnup for large and small array assuming a constant initial enrichment and cooling time and a conservative axial profile.

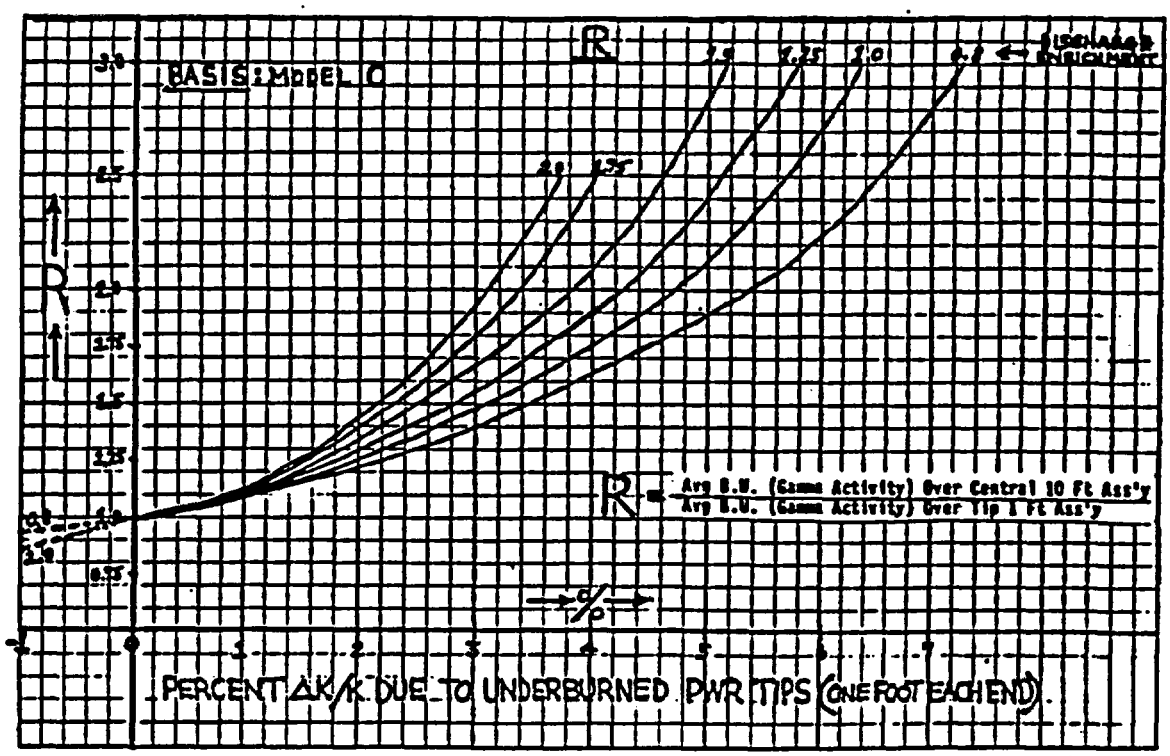

Fig. 2. End effect (Δk/k) for six ^{235}U discharge enrichments as a function of R.